RUTGERS
THE STATE UNIVERSITY
OF NEW JERSEY

Department of Electrical and Computer Engineering

14:332:428 Capstone Design- Communication Systems Spring 2014

Vision Based Free Space Optical Communication

Final Project Design Report

Group Members:
Kyle Cavorley
Wayne Chang
Jonathan Giordano
Taichi Hirao

Project Director: Dr. David G. Daut

May 14, 2014

Table of Contents

1. Design Project Overview ……1
2. Technical Specifications ……2
3. Final Project Summary ……...3
3.1 System Design - Final Version ……...….3
3.2 System Implementation ……...4
3.3 System Performance ……....6
3.4 System Design Iterations ……..…8
4. Task List and Work Distribution ……10
5. Design Project Details ……12
5.1 Computer Vision: ……...12
5.1.1 Theoretical Considerations……...12
5.1.2 Design Procedure……...12
5.1.3 Simulation Results ……...…13
5.1.4 Observed and Measured Results ……13
5.2 Computer/Embedded System Interface:……..…13
5.2.2 Design Procedure ……14
5.2.3 Simulation Results ……..…14
5.2.4 Observed and Measured Results ……....15
5.3 Transmit Section: ……16
5.3.1 Theoretical Considerations ……16
5.3.2 Design Procedure ……17
5.4 Receiver: ……...33
5.4.1 Theoretical Considerations ……33
5.4.2 Design Procedure ……39
5.4.3 Simulation Results ……..49
5.5.4 Observed and Measured Results ……...50
5.5 Sub-system Retro Optical Chopper: ……...56
5.5.1 Theoretical Considerations ……....56
5.5.2 Design Procedure ……....57
5.5.3 Simulation Results ……..58
5.5.4 Observed and Measured Results ……....59
6. Sub-system Integration Considerations ……....65
7. Economic Considerations ……..……...……66
7.1 Cost Analysis – Prototype……...…….…...……....66
7.2 Cost, Manufacturability and Marketability...……...……....67
8. Individual Team Member Discussions ……..……69
Kyle Cavorley's Discussion ……..…….……69
Jonathan Giordano's Discussion ……..…….....71
Wayne Chang's Discussion ……..…….....72
Taichi Hirao's Discussion ……..…….....73
9. **Future Work**……78
10. **APPENDICES ……..…...……....81**
Appendix 1: List of Equipment ……..…….…81
Appendix 2: Simulations and Program Code..……..…….……83
Appendix 3: Datasheets ……..……...…….…...87

1. Design Project Overview

This paper involves the implementation of a free-space optical (FSO) communications system capable of interfacing with moving receivers such as unmanned ground or aerial vehicles. The systems serves as a two-way communication system with only one end of the link required to have a laser and LED source while the other end has photodiode receiver architecture and the ability to communicate back via a reflected signal source. The transmit component can receive data from any computer with a USB port and calibrates the data for optical transmission through a schmitt trigger before the signal enters the LED driver circuit. Inexpensive light emitting diodes (LEDs) are used to transmit data at rates up to 700 Kbps. On the receive side, a transimpedance amplifier is used to receive the signal from a reverse biased photodiode. The signal is amplified and sent to a comparator circuit so the data can be recognized by the computer at the receiver. The final system implementation successfully streams audio files of a few megabytes. A computer vision tracking system integrated into the transmitter controls a pan-tilt platform for target acquisition and tracking. Due to time limitations we were unable to reach the ultimate design goal of 1 Mbps. Due to time constraints not all parts of the system are compactly integrated together, in particular, the Retro Optical chopper and computer vision features of the initial design project scope were not fully integrated into the final implementation. However, these parts were successfully project and characterized. Video documentation of the experimentation of the system can be found by following the YouTube link:

<https://www.youtube.com/channel/UCLcOockgnsydlnRXT7J9wwg>

2. Technical Specifications

The Vision Based Free Space Optical Communication system is composed of four major sub systems. These include the transmitter, receiver, Reflective Optical Chopper (ROC) and data processors which take place in the form of PCs or Raspberry Pis.

The transmitter requires a power source of +5 V rated for at least 1 A. Recorded transmission rates have reached 1 MHz, and observed recoverable data rates up to 700 kbps. If the Engin 5W LZ1-00R100 LED is used for transmission, the dominant wavelengths emitted are between 618-630 and maximum luminous flux not greater than 228 lm. If lasers are used for transmission they will be either 5mW at 670nm, 10 mW at 650nm, or 5 mW at 830nm. Input to the transmitter system requires TTL voltage levels.

The receiver requires two power supplies at ± 5 V, ±18 V, +2.5V, +3.3 V. The final prototype of the communication system utilizes the SFH213 photodiode which is sensitive to wavelengths between 600-1000 nm. The diode is reversed biased at 18 V. The receiver is theoretically capable of reception of signals at 1.3 Mhz, and recorded transmission rates were 700 kHz. The output of the receiver is in the form of TTL compatible voltage levels.

The ROC has a dimension of 2.5" lengthwise with a diameter of 1.1875". There is an active aperture of 8.5mm dimension used for the modulation of the input light. Operational wavelengths for use in this communication system are set to 650nm – 1050nm by use of filter. The modulation frequency range of the ROC is stated to be up to 100 kHz, although higher frequencies have been observed. Contrast ratio at 100 kHz is 80.0%

The last major subsystem, the data processors, consists of a computer capable of a Python interface. The final prototype utilized two different PC's, one running Windows 7 the other running Linux. Operating systems are irrelevant so long as scripting language Python can run. Transmission rates are predetermined and are adjustable in the Python code. The output, and receiver for the computer is the USB port through a serial TTL connection which is capable of 6 MHz transmission speeds. Power supplies for the computer are dependent on model.

3. Final Project Summary

3.1 System Design - Final Version

Below is the system block diagram. Note that this represents the working system to date. The ROC and Computer Vision is not integrated, but are working components.

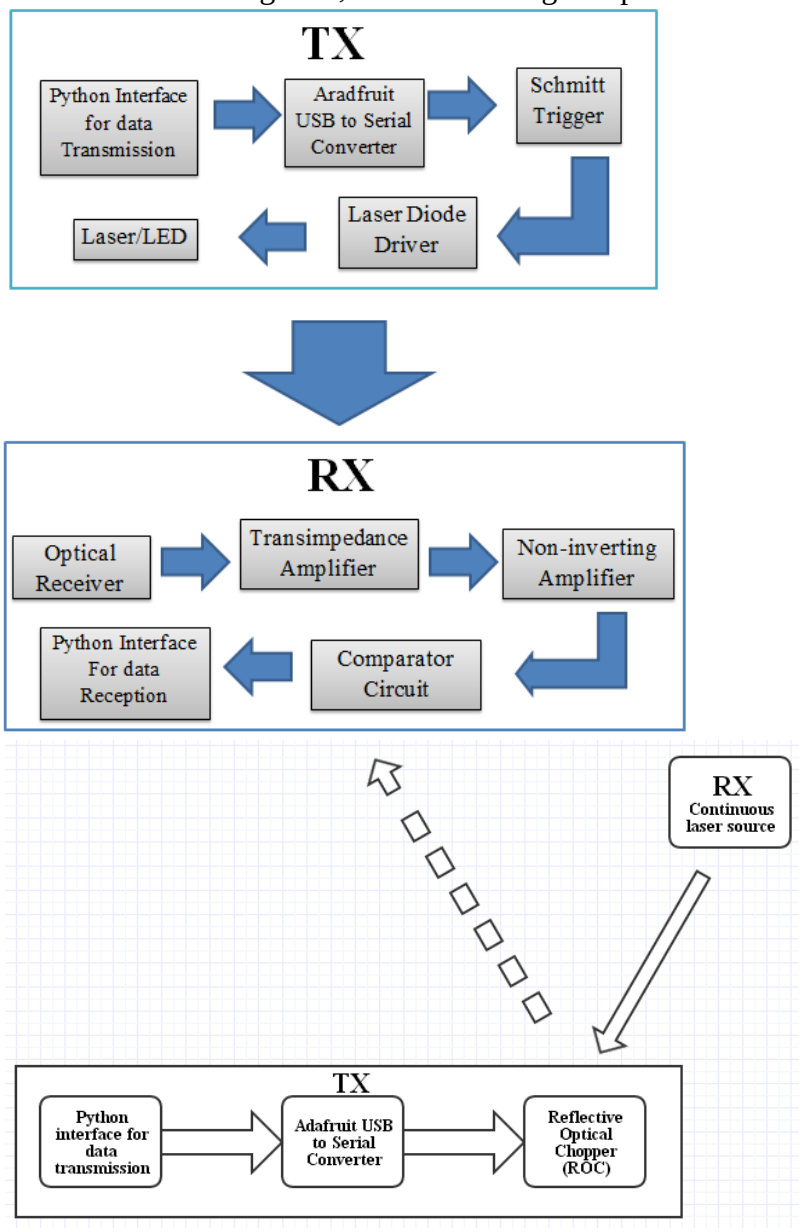

Final prototype establishes a two-way FSO direct line-of-sight communication link and requires the ability to transceive a 3.3V TTL signal up to 700 kHz. For our purposes, Linux and Python programming was used as an interfacing means to process and transceive data via a USB-TTL adapter.

The single-ended TTL transmission signal is inputted into Schmitt Trigger & LED Driver

system. This architecture relays the on-off keying protocol to the LED for it to emit light according to the binary data bits. The light is received by a photodiode receiver architecture, which incorporates a transimpedance amplifier, voltage amplifier and a comparator circuit.

The system ultimately outputs a 3.3V TTL signal (the same signal that was initially inputted). This TTL signal is then relayed through another TTL-USB adapter to be interfaced and read by the Linux and Python software.

Data can also be transmitted by use of a Reflective Optical Chopper (ROC). For our purposes, one was generously supplied by Boston Micromachines Corp. The ROC is an external laser modulator that takes in a 3.3V TTL signal and outputs this same signal via FSO. This is done by reflecting a continuous laser source where the reflected laser is the modulated signal. This modulated laser is received by the same photodiode architecture as described above.

3.2 System Implementation

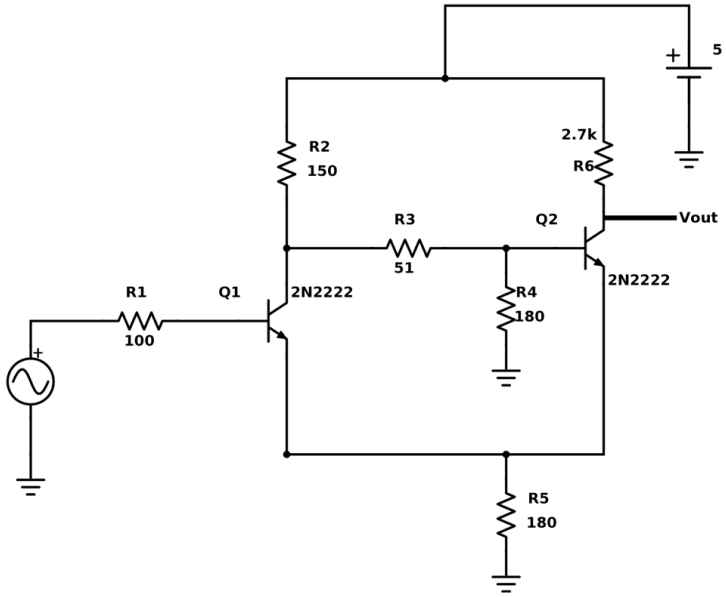

Fig. 3.2.1: Front-End Schmitt Trigger

The front-end Schmitt Trigger is responsible for upconverting the 0 to 3.3 V input data signal from the computer or embedded system to a 0 to 5 V signal to power the laser diode driver. The Schmitt-Trigger limits the system in frequency to 700 kHz.

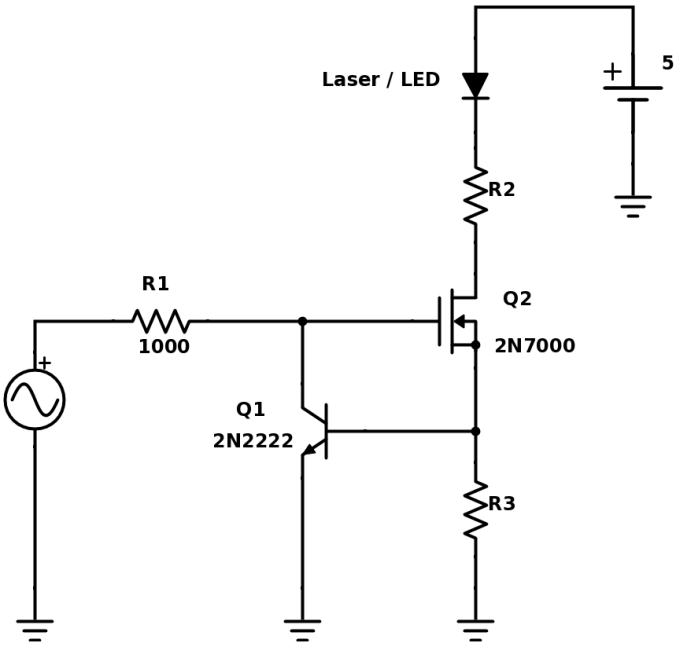

Fig. 3.2.2: Driver Circuit Version 2

The laser diode driver powers the LED and transmits the data stream to the optical receiver.

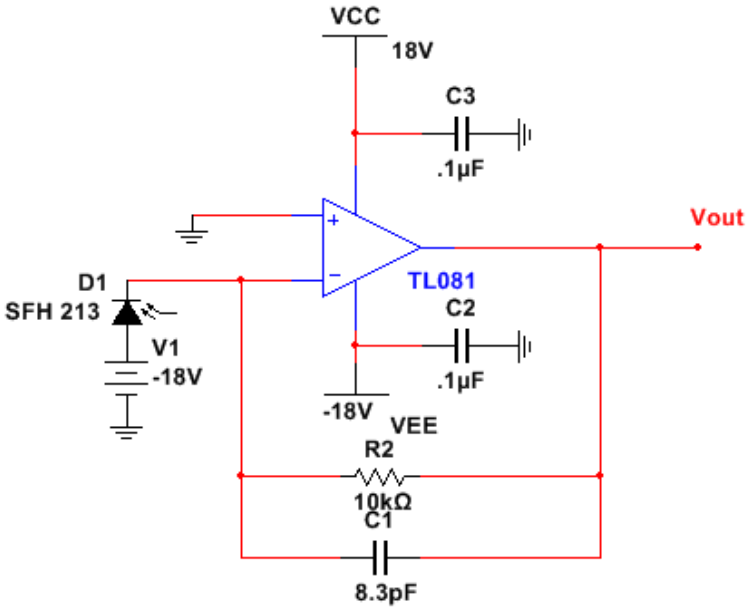

Fig. 3.2.3: Transimpedance Amplifier [Section 5.4.2]

The transimpedance amplifier converts the light signal to an electrical signal. The transimpedance amplifier limits the system in frequency to 1.3 MHz.

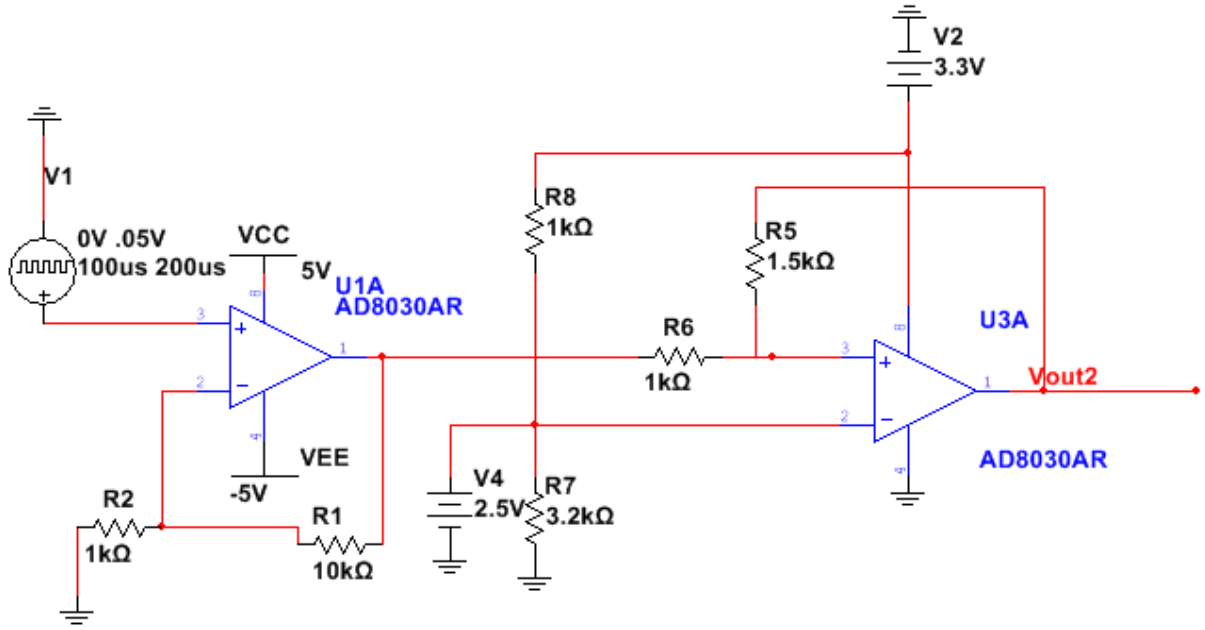

Fig. 3.2.3: Non-inverting amplifier with gain of ten cascaded to non-inverting comparator. [Section 5.4.2]

The non-inverting amplifier amplifies the signal from the transimpedance amplifier by 10 to produce a 0 to 5 V input signal to the comparator. The comparator's reference voltage of 2.5 determines what data bits are high and low. The output of the comparator is a TTL high signal compatible for the USB-Serial Cable.

3.3 System Performance

The intended goal was to stream HD Video. The USB-Serial cables allow a baud rate of 6 MBaud, which is capable of HD streaming. Therefore, the goal was to optimize the RX section, including the transimpedance amplifier, non-inverting amplifier, and comparator at 6 MHz. However the maximum rate we could achieve was 700 kbps. This allowed us to successfully stream audio and send audio files. Due to time limitations, the hardware was not totally optimized for HD Video Stream. However, with the system we have, python code can be drafted to stream video of low quality. Table 3.3 shows the overall performance of each system component and their optimal rate.

Table 3. 3.1 : System Performance

System Component	Theoretical Optimal Frequency	Frequency Achieved	Simulation Reference	Experimental Reference
USB-TTL Chip in Cable	6 MHz	6 MHz		
Schmitt Trigger	N/A	500 kHz	N/A	Section 5.3.2.1
Laser Diode Driver V2, V4	N/A	1 MHz	N/A	Section 5.3.2.4 Section 5.4.2
Transimpedance Amplifier: TL081	GBP = 3 MHz	1.3 MHz	N/A	
Noninverting Amplifier	GBP = 125 MHz	1.3 MHz	Fig. 5.4.3.1 - 5.4.3.3	Section 5.4.4
Comparator	GBP = 125 MHz	1.3 MHz	Fig. 5.4.3.1 - 5.4.3.3	Section 5.4.4

The bottleneck of the system is the Schmitt Trigger, only rated at 500 kHz. If this design could be improved, higher data rates can be achieved on the receive end.

Things to consider:

If the AD8030 was used as a transimpedance amplifier higher frequencies by at least 10 fold can be achieved based off Fig. 5.4.14.a. We would have to design for the gain that allows for this frequency to boost performance. However, based off simulations and our new intended goal of 1 MHz, the simulations correspond to the experimental of the receiver back end as referred to in the table.

Another way to improve performance is to place the TX and RX onto their respective PCBs. Surface mount parts can also be used in place of axial resistors. Bread boards provide too much parasitic capacitance and allows for RF to jump from trace to trace. Other factors effecting the performance of the system is the light intensity of the LED and degree of orientation to maintaining the direct line-of-sight. We noticed when finding the direct line of sight and increasing the intensity of the LED, the signal performance is cleaner and improved. Finding the correct angle of incidence of the photodiode produces the maximum system output. Also, it is important to note that the photodiodes implemented in our design were rated for infrared light, and all of our designs were done with 650 nm visible red light. Choosing the wavelength that correctly partners with the photodiode can improve performance.

3.4 System Design Iterations

Under this subheading all iterations of the design leading up to the final prototype must be formally presented in the form of system block diagrams and sufficient accompanying text so as to describe the necessity for the shift from one design methodology to another.

3.4.1 Driver Circuit

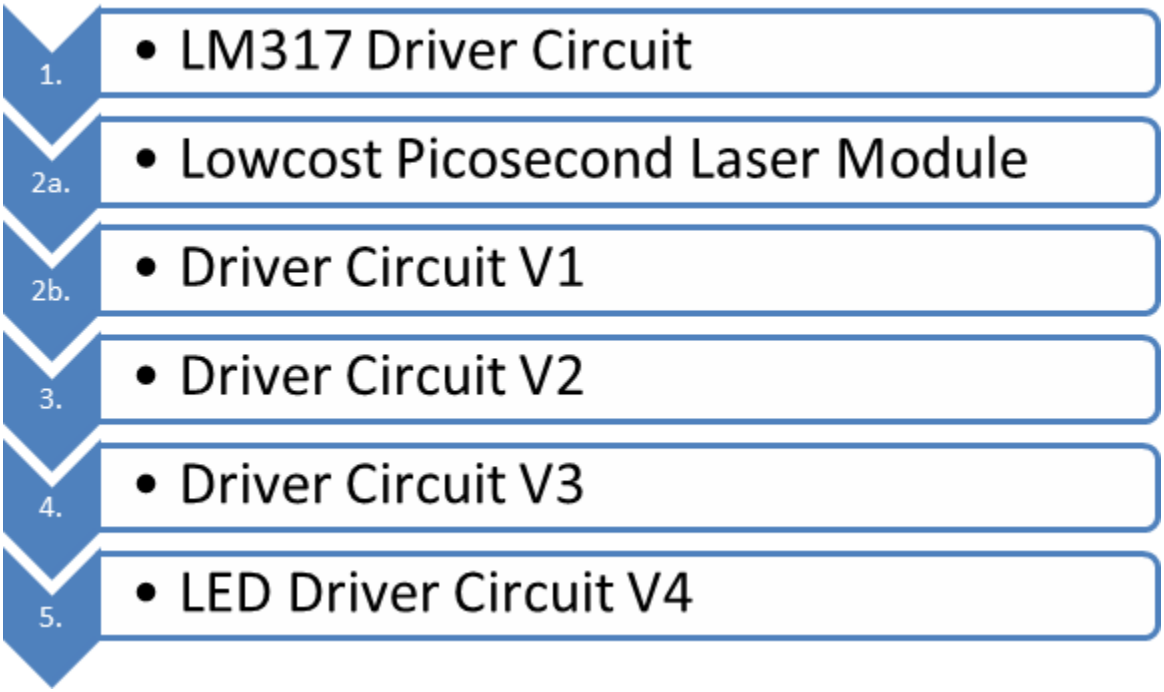

The initial driver circuit was based upon the LM317 linear voltage regulator, a common IC used in hobbyist designs (Fig 5.3.2.2). This driver design was deserted for its inability to transfer recoverable data over 200 kHz. The Low cost Picosend Laser Module design and Driver Circuit V1 were constructed simultaneously(Fig 5.3.2.3, 5.3.2.4). Construction issues were encountered with the Low cost Picosecond Laser Module which led to its abandonment as the Driver Circuit V1 show preliminary signs of success. Driver Circuit V1 was based upon hobbyist designs, but due material constraints in the lab could not be built with suggested parts. The design required use of a MOSFET, and when the 2N7000 FET became available it was incorporated by replacing a single 2N2222 BJT. The new circuit was called Driver Circuit V2 (Fig 5.3.2.7). After testing suspected drop current drop off above 1 MHz led to the design of Driver Circuit V3 which included an additional resistor to decrease the sensitivity of the safety transistor in the design which drew away overloading current through the diode by reducing the amplitude of the input signal (Fig 5.3.2.20). Once it determined that an LED was more suitable for data transmission because of tracking concerns with a laser and photodiode, LED Specific Driver Circuit V4 was created (Fig. 5.3.2.23). The difference between Driver Circuit V3 and V4 was the addition of a

2N7000 transistor in parallel with the previous one in order to handle the higher current draw which the Engin 5W LED could demand. Despite the last two design iterations, Driver Circuit V2 is currently used at the final prototype for data transmission due to miscommunication in the lab due to late incorporation of the design into on going documentation. Driver Circuit V3 is the final prototype version in the laser transmitter which is required by the Reflective Optical Chopper (ROC).

4. Task List and Work Distribution

Under this heading the individual sub-system- and system-level tasks that have been completed must be described in detail. The completed tasks must be representative of all aspects of the design process, from initial background research, to simulations, to the preparation of the final report, and the final project presentation.

Raspberry Pi, Python Interface & Fault-Tolerant Receiving/Transmitting Code:
Wayne Chang 100 %

Computer Vision Tracking System:
Wayne Chang 100%

TX Laser Diode Driver and Schmitt Trigger:
Jonathan Giordano 70%, Kyle Cavorley 20%, Taichi Hirao 10%.

RX Transimpedance Amplifier:
Kyle Cavorley 90%, Wayne Change 4%, Jonathan Giordano 3%, Taichi Hirao 3%

Non-inverting Amplifier, Comparator:
Kyle Cavorley 100%
This includes the RX system as a whole from research, simulation, design, and test.

Receiver Construction, Lens Collimator:
Wayne Chang 50%, Jonathan Giordano 50%

ROC Testing and liaison with BMC:
Taichi Hirao 80%, Jonathan Giordano 20%

Project Poster for Poster Day:
Kyle Cavorley 33.3%, John Giordano 33.3%, Taichi Hirao 33.3%

Mounting Platform/Gimble, Servo Controller:
Wayne Chang 100%

Explored Area: Initial Background Research on FPGA Integration:
Kyle Cavorley 100%
My first task involved researching how to integrate the Altera DE2-115 FPGA boards to handle data transmission in the Free Space Optical Communication link. This required knowledge on how to integrate the USB 2.0 or ethernet, SDRAM, SD Card, and Nios II Soft Core Processor.

Luckily, Quartus II Software provides a QSys tool that provides the ability of linking each component, such as the processor, SDRAM, SD Card, and USB/Ethernet. The tool generates interconnect logic by connecting the IP functions and subsystems. Writing C code for the processor can control the storage of data, buffering it through SDRAM, and transmission via Ethernet/USB. Due to the complexity of creating the FPGA system, the group decided to move to a Raspberry Pi System to handle data processing and transmission, which is handled by Wayne.

Explored Area: Research on Interfacing with Memory on FPGA:
Kyle Cavorley 100%
A variety of through tutorials and IP code of SDRAM, and the SD Card were investigated to develop a comprehensive understanding.

Explored Area: Research on Interfacing with USB and Ethernet w.r.t. to FPGA:
Taichi Hirao 100%

Explored area: Receiver Mosfet amplifier, Mosfet Schmitt Trigger:
Taichi Hirao 100%

Explored area: RF & directional antennas:
Jonathan Giordano 100%

5. Design Project Details

5.1 Computer Vision

Name of team member who designed this sub-system: Wayne Chang
Name of team member who wrote this subsection: Wayne Chang

5.1.1 Theoretical Considerations

A visual feedback system tracking an LED mounted on the receiver is required to point the transmitter in the correct direction. Techniques range from simple "brightest region" detection to complicated methods involving clustering and stereo reconstruction. Additionally, a proposed identification scheme allowed for blinking the receiver LED to broadcast a synced pseudo-random unique identifier. Unfortunately, there was not enough time to evaluate the tracking system because construction of the transmitter and receiver components occupied most of the allotted time.

The goal of using cameras is to provide feedback to the servo controller, tuning the platform to center on the receiver. The camera processing output is modeled as an XY-offset. If the cameras move with the platform, then this offset simply must converge to zero or some other constant position. However, if the camera poses are independent of the platform motion, the XY-offsets must be calibrated to platform position to ensure accuracy. If distance measurements are available to the brightest region, then they may be accommodated for with a linear function with input of distance output of center offset.

5.1.2 Design Procedure

The simplest solution of tracking a brightest region was implemented very quickly. The algorithm searched for the the brightest 9x9 block of pixels and reported the center pixel in the block as the target coordinate. This algorithm ran in order O(mn) time with m as the number of pixel rows and n as the number of pixel columns. Multi-point tracking is possible by keeping track of the k brightest blocks with at least distance d of separation.

It is difficult to identify a single receiver with multiple receivers with lit LEDs. Therefore, a proposed solution is to blink the receiver LEDs with unique and updating identifiers so that the transmitter may differentiate between the multiple receivers. This blinking can occur at a theoretical 30 bps due to the Nyquist frequency of the camera which has the maximum framerate of 60 fps. A buffer is used to store the previous states of blinking blocks in the same location, accommodating for slight shifts in position. Fortunately, this blinking is slow enough to be orthogonal in frequency to the high-bandwidth FSO communications.

Lastly, stereo vision is a viable option for obtaining distance measurements. Using simple geometry and convex optimization techniques, poses between two camera views can be established. This allows extrapolation of 3D data from multiple views of the same scene. This technique can be used to provide the aforementioned distance data for a bright cluster of pixels. Unfortunately, there was not enough time to implement and test this approach due to complications in receiver design.

5.1.3 Simulation Results

The simulated brightness tracker functions as expected, drawing a circle around the brightest 9x9 cluster of pixels. The very simplistic code did not have opportunity for improvement due to time constraints.

5.1.4 Observed and Measured Results

Due to time constraints, this section was not completed.

5.2 Computer/Embedded System Interface

Name of team member who designed this sub-system: Wayne Chang
Name of team member who wrote this subsection: Wayne Chang (Python), Kyle Cavorley (FPGA)

5.2.2 Design Procedure

The system interface is required to send and receive arbitrary data across the FSO link. It bridges the gap between the transmitter/receiver circuitry and higher-level devices that send/process information. The USB interface was chosen for the higher-level device side due to widespread adoption, low cost, and high availability. TTL serial was chosen as the circuit-level interface due to single transmit and receive lines and compatibility with USB via low-cost converters. The Prolific PL-2303HX USB-to-TTL-Serial converter[20] was chosen to interface with any USB-compatible hardware. The converter supports a baud rate of up to 6 megabits and cost $10 each. Two converter-laptop pairs were used during implementation and testing: one pair for transmitting and one pair for receiving.

A stop bit is embedded as the last bit per byte for frame synchronization. This allows for only 7 out of 8 bits of information, resulting in a 12.5% reduction in transmission efficiency. However, the stop bit is important for clock synchronization and differentiation between a stream of ‘0’ and an idle data line. The inclusion of a stop bit is the default configuration for most serial communications, but this can be changed.

Python was chosen as the implementation programming language due to available serial libraries and ease of use. Because Python is a high-level scripting languages, care had to be taken when

handling byte-level amounts of data at high bitrates. For example, at one megabyte per second, the computer would have to process one byte every microsecond. A Python call requiring 20 microseconds per byte due to system call overheads would not be sufficient. Therefore, many bytes must be processed at once (in blocks) to reduce overall overhead and attain high data rates.

A repeating test sequence that generated a square wave (0x54a952a) was used to evaluate the communications channel. The value was determined after factoring in the effects of the stop bit, thereby leaving the desired sequence of 0101 0100 1010 1001 0101 0010 1010. Reliable generation of a square wave at the actual TTL voltages was essential for testing and implementation of the FSO circuitry. Varying frequency to test response was convenient using the Python serial communications module.

For transmission and receive to operate on file levels, a simple communications protocol with a preamble and postamble was implemented. The preamble was a chosen codeword of a 0x55 byte repeated a specified amount of times followed by a zero byte. The postable was a 0x55 byte repeated an arbitrary amount of times. Future iterations should have a more unique code word along with specification of bytes to receive, thereby eliminating the necessity of a postamble. An MP3 streaming service was built on top of this protocol, and is described in Section 5.2.4.

5.2.3 Simulation Results

For simulations, the two TTL interfaces were directly connected, bypassing the FSO communications framework. Both devices performed to specification, as seen in the table below:

Baud Rate (Mbps)	BER
1	0
3	0
6	0

As mentioned in the design phase, a test sequence was used to generate a square wave. The square wave was very sharp when inspected and allowed testing of the system without an additional function generator.

5.2.4 Observed and Measured Results

First, a 1024 kilobyte text file with the contents of a repeating byte (0x56) was sent across the constructed data channel. Discrepancies in received data are grouped into two categories: dropped or error. Dropped bytes are bytes that were not picked up by the receiver during expected receive time, and error bytes are bytes that were modified (not 0x56) upon receive.

Frequency (kHZ)	Bytes Sent	Dropped Bytes	Error Bytes	BER
100	1048576	0	0	0
500	1048576	0	0	0
700	1048576	0	0	0
750	1048576	218235	0	0.21
800	1048576	293822	0	0.28
850	1048576	800492	0	0.76

The table above demonstrates that error bytes were not an issue, but dropped bytes were pervasive as frequency increased above 700 kHz. The dropped bytes result from a disfigured comparator output waveform. The USB-TTL converter requires a clean 3.3 V TTL signal to receive data; with attenuated or deformed signals, data recovery is not possible. This phenomenon can be explained by a reduction in receiver front-end amplifier gain due to higher frequencies, and the instability of the receiver backend comparator at higher frequencies, accentuated by the former effect. To achieve higher speeds, faster parts are needed. Higher frequency transistors should be considered for the comparator, and the front-end receiver should be constructed from discrete high-frequency transistors as well. As the simulated results show, the USB-TTL converter can easily handle data rates up to 1 MHz.

Lastly, digital audio streaming software was constructed upon the simple communications protocol described in previous sections. Python was used for streaming transmissions while Unix shell scripting was used for receiving transmissions, both techniques utilizing the already-constructed serial communications protocol. The Python streaming transmission script read an audio file and split it into chunks for partial transmission. The receiving Unix shell script runs the receiving code and queues received partial audio files for playing. With correct buffering, the transition between partial audio files is seamless.

Unfortunately this simplistic technique of transmission introduces significant overhead:

Purpose	Overhead per audio slice (bits)
Preamble and Postamble	400 bytes
0.3 Second Transmit Pause	0.3 * rate bytes

A 0.3 second pause is introduced to allow the Unix shell script receiver to ready the system for another slice. With the overhead, different slicings transmit with different efficiencies. For example, assuming an audio file with the maximum MP3 bit rate of 320 kbps:

Slice Size (kbits)	Seconds at 320 kbps	Efficiency @ 700 kHz
64	0.2	0.23
320	1	0.60
1600	5	0.88

As the slices become larger, the efficiency of transmission is improved. With improvements in the serial receiving code to support an "always on" mode, this system can become efficient for even small slice sizes. At 700 kHz, the highest quality MP3 streaming can be achieved and modest video streaming is also possible. Reasonable D1-quality video streaming can nearly be achieved at this rate:

Video Size Type	Video Size	Total bit rate (Kbps)
QCIF	176x144	48
CIF	352x288	300
D1	640x480	800
HD	1280x720	1736

5.3 Transmit Section

Name of team member who designed this sub-system: Jonathan Giordano
Name of team member who wrote this subsection: Jonathan Giordano

5.3.1 Theoretical Considerations

Any transmitter of the optical link will require some type of mechanism which emits photons. In the case of this design project, these mechanisms have been chosen to be either Light Emitting Diode (LED) or Light Amplification by Stimulated Emission of Radiation (Laser). Both of these modules tend to continually draw current until they either burn out of damage the power supply. These diodes therefore require not only a regulatory systems which maintains a relative constant current draw, but is also capable of fast switching time (> 1 MHz).

5.3.2 Design Procedure

5.3.2.1 Schmitt Trigger

Because the initial data stream is released by USB, the voltage levels are set to standard TTL levels of 0 to 3.3 Volts for low and high respectively. The initial purpose of the Schmitt Trigger was on the receiving end, but upon realization that it could be quickly used as a front-end voltage amplifier adjustments to the circuit were made so that output voltages levels were 1.25 to 5 Volts for low and high. The hysteresis is set to a negligible amount so that history of past inputs has little control over the output.

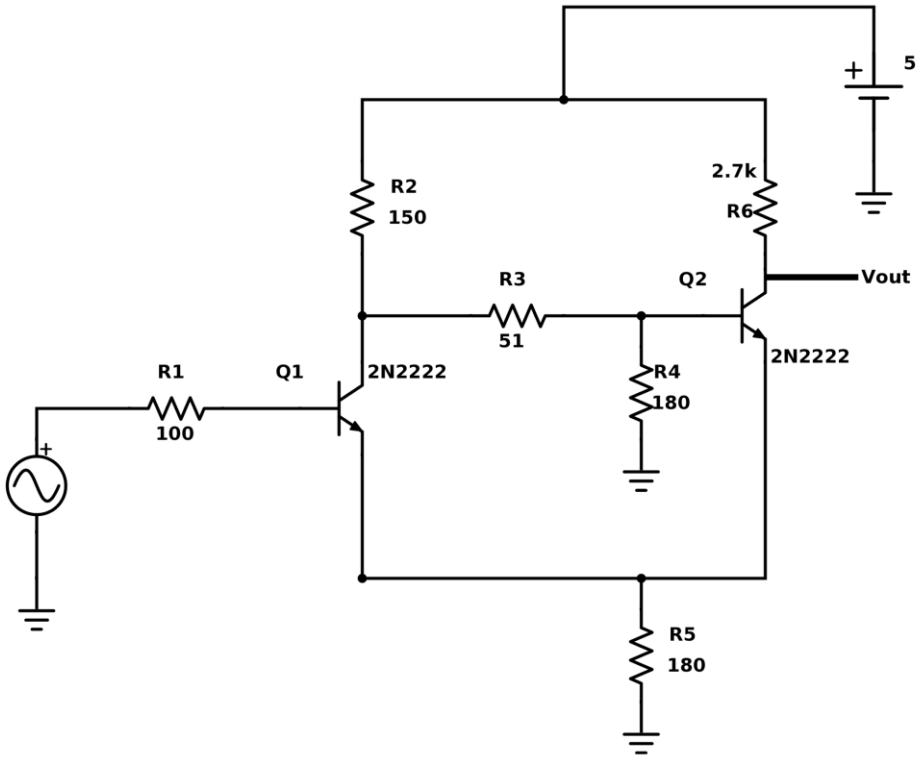

Fig. 5.3.2.1: Front-End Schmitt Trigger

Testing for the Schmitt Trigger proved to indicate that the system was a bottleneck for the transmit side. This was discovered late into the projects lifetime. Fig 5.3.2.2 show the output of the Schmitt Trigger with an input waveform from the USB port of a PC producing a signal of 0x55 repeatedly (101010…) at 500 kHz. At this frequency there is notable degradation at the output of the Schmitt Trigger particularly a long rise time. This proved to be somewhat fatal to higher transmission speed, as the Schmitt Trigger was necessary as a voltage amplifier for the TTL output from the USB port in order to turn on the driver circuit, and thereby the laser or LED diode. Future work would include replacement with a faster front end amplifier.

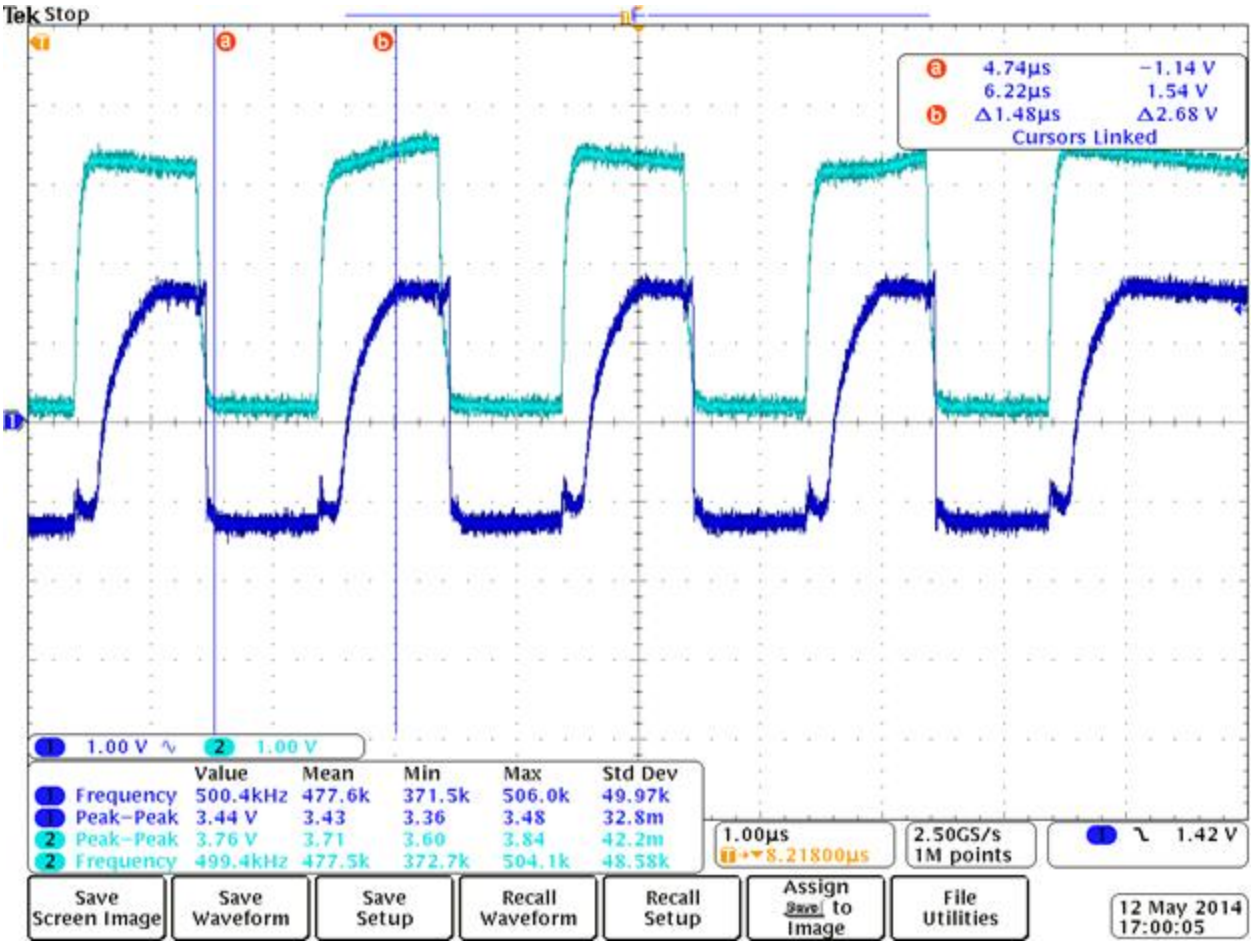

Fig. 5.3.2.2: Schmitt Trigger Output (1) and PC USB Ouput of 0x55

5.3.2.1 LM317 Based Driver Circuit

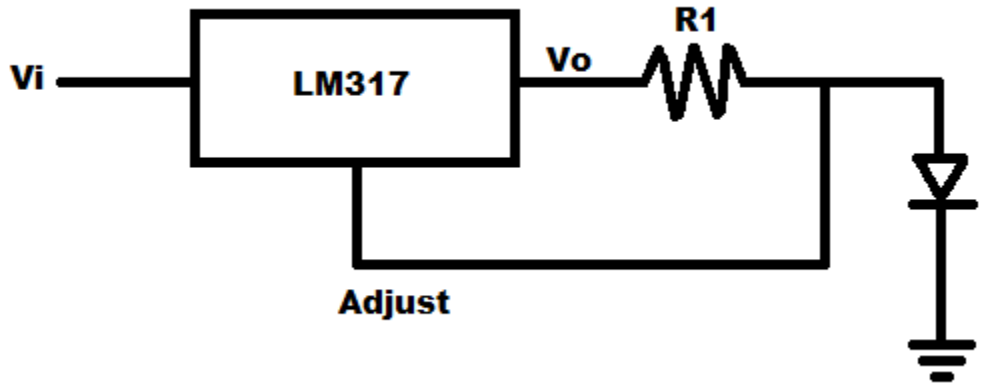

Fig 5.3.2.2: LM317 Based Driver Circuit

The first tested driver circuit was based upon the linear voltage regulator LM317. The complete driver circuit was based upon a popular LED driver used by hobbyists. At the time of

construction the Engin LZ1 5W LEDs were being utilized to transmit the data. The circuit was built around the LED's capabilities and to achieve a 0.8A drive current, an R1 choice of 1.5625 Ω was calculated. This was replicated in the lab through two 3 Ω resistors in parallel. Testing found that the LM317 could easily power the 5W LED but switching frequencies above 200 kHz were found to be unfeasible. At the time of testing no other appropriate receiver front-end had been constructed and due to the complexity of the LM317 circuit, it was deemed to be too slow to handle higher switching frequencies.

5.3.2.2a Low-Cost Picosecond Laser Module

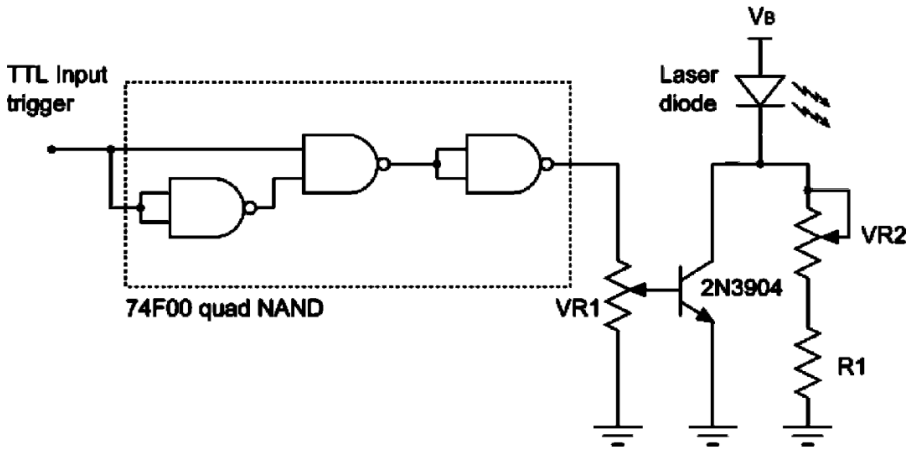

Fig 5.3.2.3 Low-Cost Picosecond Laser Driver Circuit

The Low-Cost Picosecond Laser Module was constructed early during the projects lifetime together with Driver Circuit Version 1. It was constructed off of designs by Lucio Pancheri and David Stoppa as detailed in their paper "A Low-Cost Picosecond Laser Module for Time-Resolved Optical Sensing Applications". Unfortunately possible setup issues were encountered, and because the circuit was built upon the same prototype board as another circuit, it had to be partially deconstructed while another other circuit was tested. The observed problem was a constant current through the circuit with an input at 0 V along with an accidental short. Further investigation and testing was not performed because the Laser Driver Circuit Version 1 had been constructed and showed promising results and time constraints did not allow for any more development.

5.3.2.2b Driver Circuit Version 1

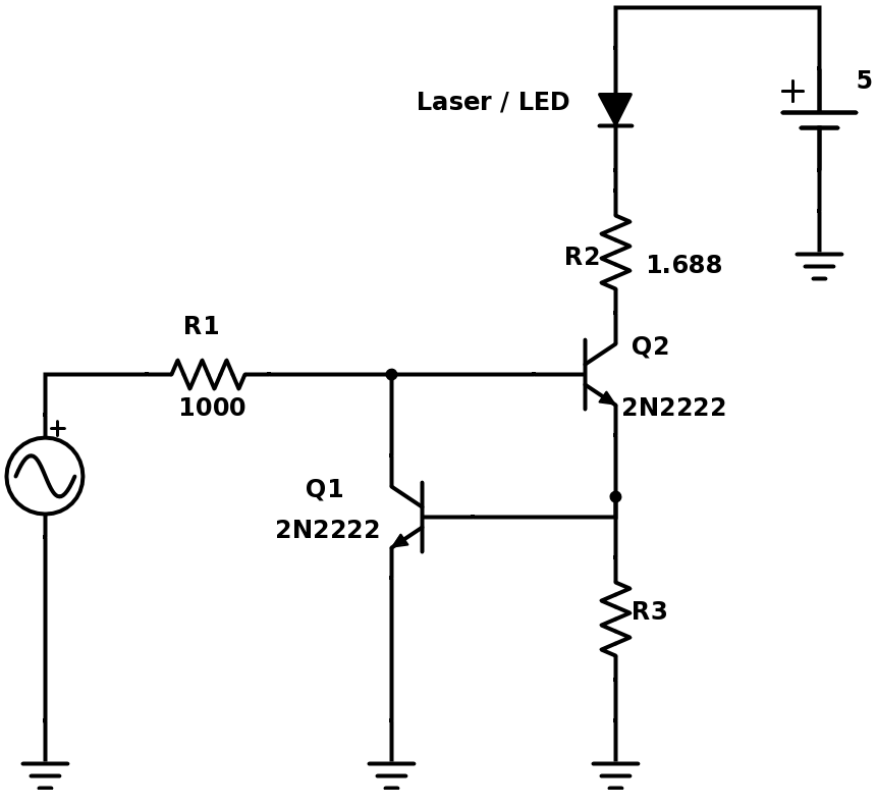

Fig 5.3.2.4: Driver Circuit Version 1

A second driver was constructed based again on hobbyist designs, but from a minimal bottom up approach. Initial transistor supplies were limited so despite design call for a MOSFET, a BJT was used in place at Q2. Depending if the circuit was being tested with Engin LZ1 LED or a laser diode, R3 was modified to regulate the maximum current. R2 was in place in order to measure current passing through the Laser/LED module.

In the following test, a 1mW 650nm laser diode was used in placed with R3 = 3 Ω. Input voltage was adjusted from 0 to 5 Volts, and the voltage across R2 was measured. During this same experiment, the 720-SFH213 photodiode was tested by placing it as close as possible to the laser output and measuring their response voltage. SFH213 was placed in parallel with a 150kΩ resistor during this measurement.

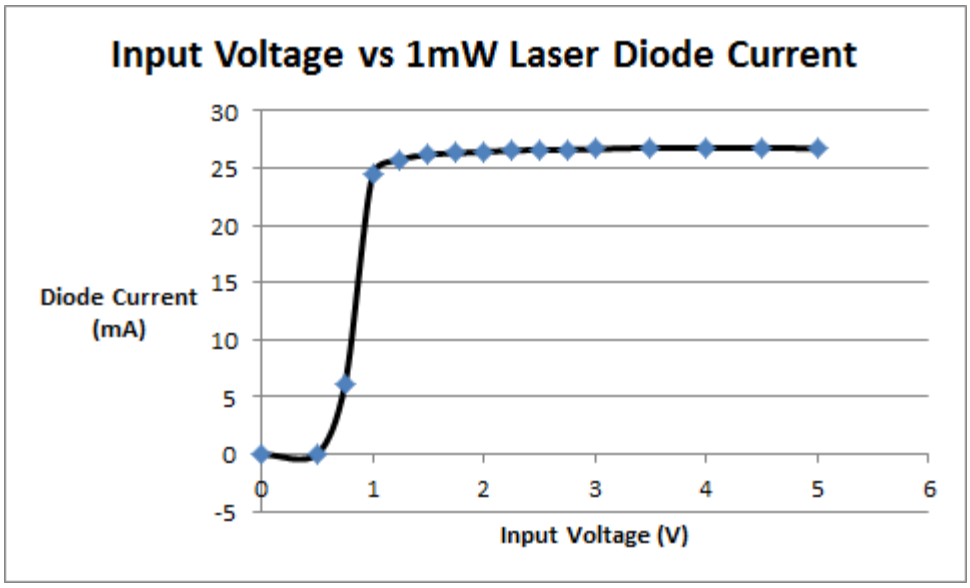

Fig 5.3.2.5: Input Voltage vs Laser Diode Current for Driver Circuit 1

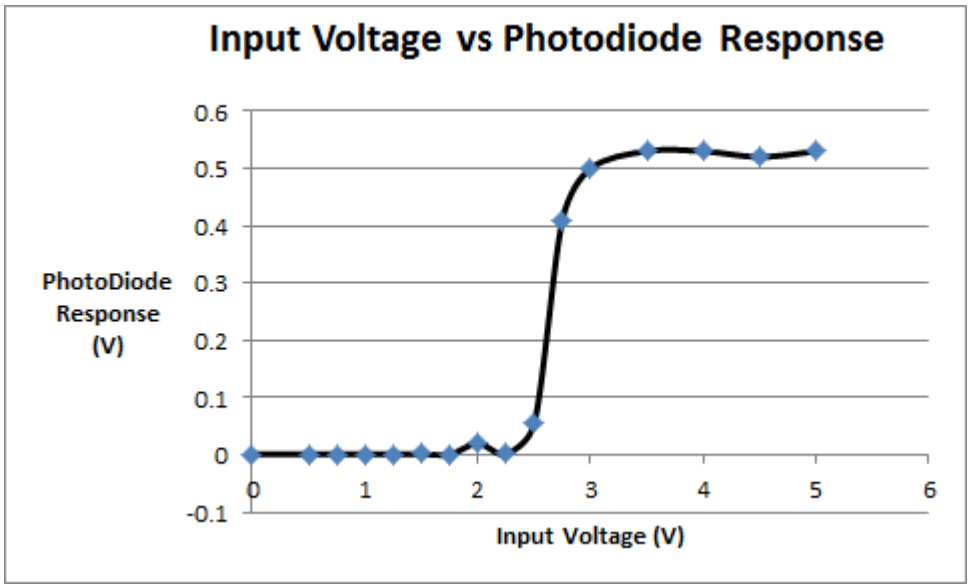

Fig 5.3.2.6: Input Voltage vs Photodiode Response for Driver Circuit 1

5.3.2.3 Driver Circuit Version 2

Upon the availability of the 2N7000 FET transistor Q2 was swapped out to incorporate the change.

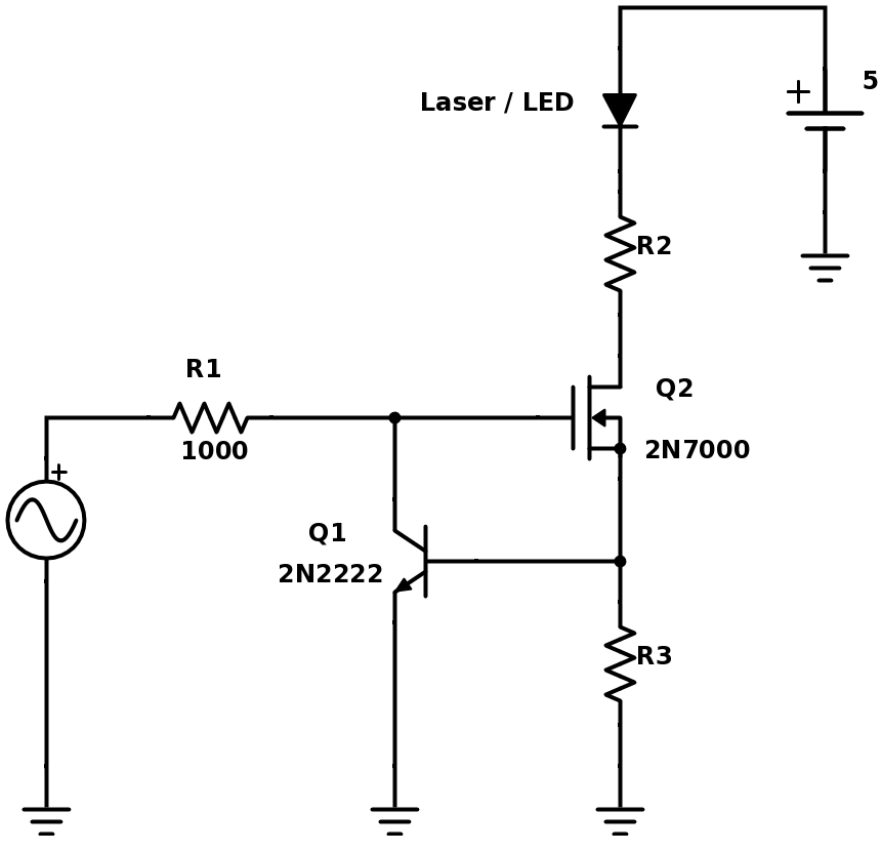

Fig. 5.3.2.7: Driver Circuit Version 2

The same testing performed on Driver Circuit V1 was repeated with no other changes. R2 = 1.688 Ω and R3 = 3 Ω.

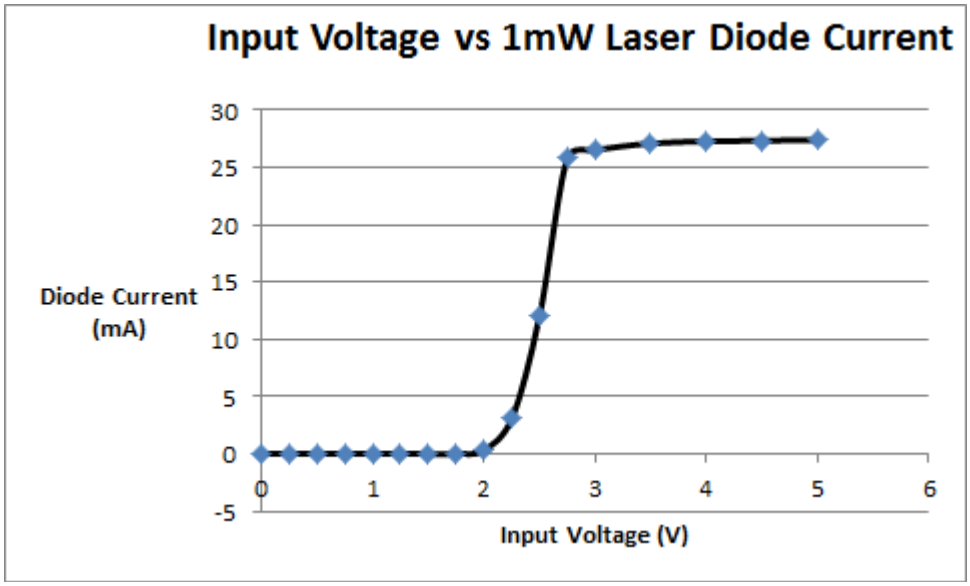

Fig. 5.3.2.8: Input Voltage vs Laser Diode Current for Driver Circuit 2

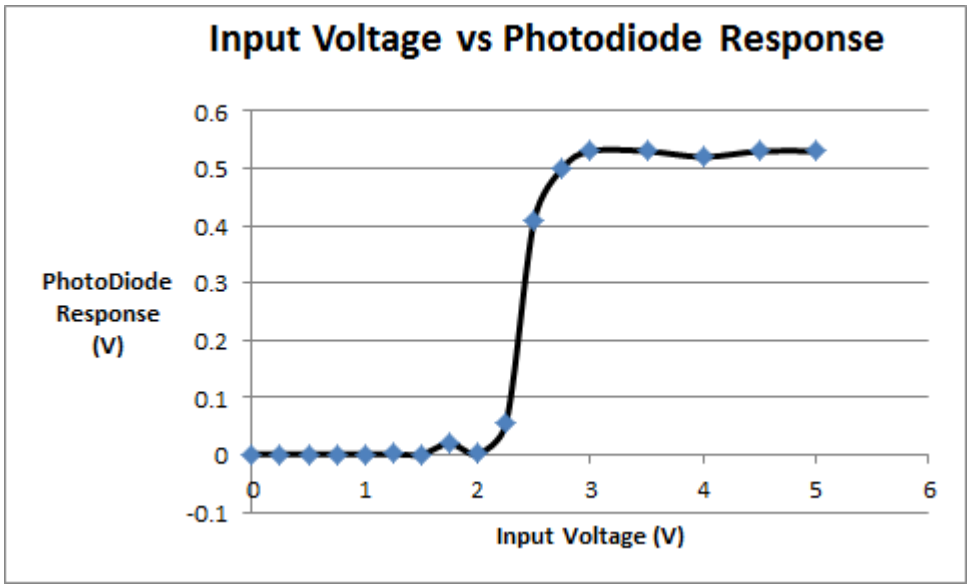

Fig. 5.3.2.9: Input Voltage vs Photodiode Response for Driver Circuit 2

Driver Circuit Version 2 became preferred over Version 1 for two factors. The switching time on the 2N7000 is superior to that of the 2N2222, and the driver has a higher voltage threshold before drawing current through the diode. This can be seen in Fig. 3.4.4 compared with 3.4.7 where the threshold for Version 1 is ~1V and Version 2 ~2.75V. Because of this higher value the Schmitt Trigger did not have to be modified to lower its low output voltage.

In our testing three 1 mW laser diodes burnt out which was believed to be caused by the module receiving too much current. Modifications were made to the design. R2 and R3 values were adjusted to lower the possible maximum current. Furthermore, the laser module was replaced with a 270 Ω resistor as an approximation. This was done for frequency testing on the laser driver circuit so that no lasers could be damaged. An LED was not put in place for the laser for there was concern at the time that the switching times of the LED was significantly lower than the driver circuit could provide, thereby bottlenecking the results.

In the following experiment a frequency plot was tested on the Driver Circuit Version 2,with the input held at 5 V P-T-P, with the low being 0 Volts, and the frequency ranging from 100 Hz to 5 MHz. The voltage was measured across R2. Voltage measurements were made with the Agilent 34401A Digit Multimeter, and frequency measurements made with the Tektronix DPO 4082 Oscilloscope. The reader should note that the input was measured even though it was held at a constant level on the function generator.

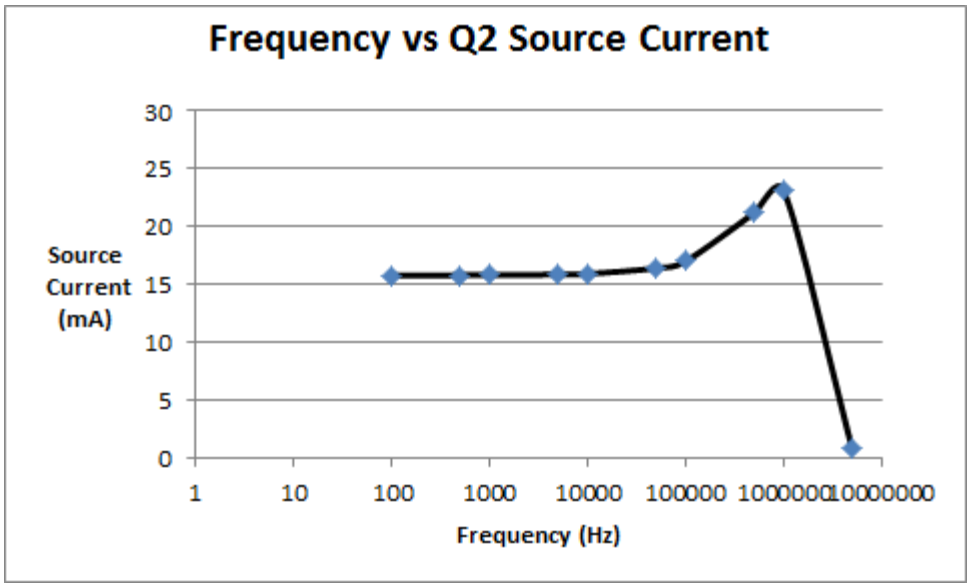

Fig. 5.3.2.10: Frequency vs Q2 Source Current for Driver Circuit Version 2

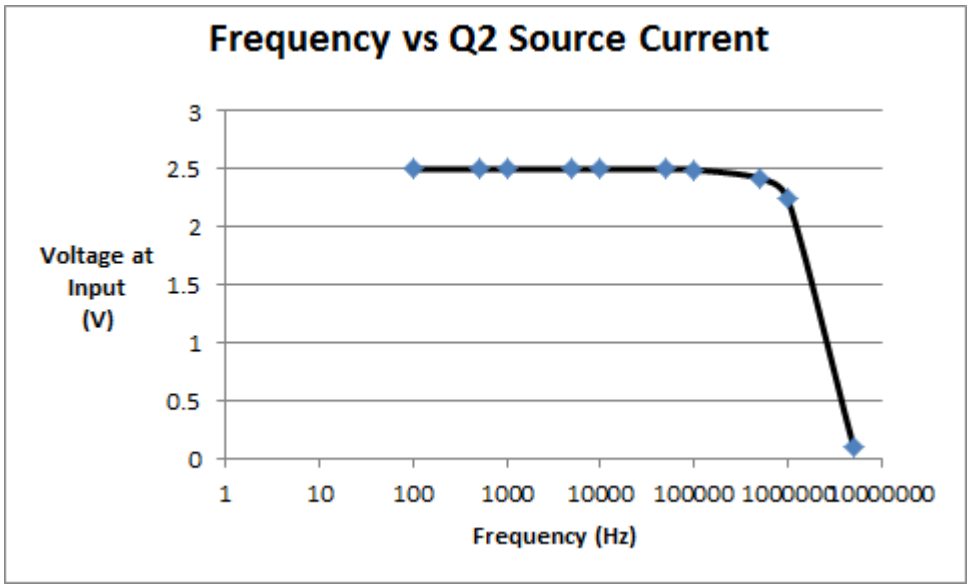

Fig. 5.3.2.11: Frequency vs Voltage at Q2 Source Current for Driver Circuit Version 2

From this experiment several concerns developed. The first issue was the decline of voltage at the input as the frequency of the input signal increased. There was question as to whether the function generator was having difficulty driving the output at the higher frequencies or that the safety transistor Q1 was draining much of the input at the higher frequencies. There was also concern about Agilent multimeters capability to measuring HF accurately, which was supported by oscilloscope measurements from the top of R2 to ground.

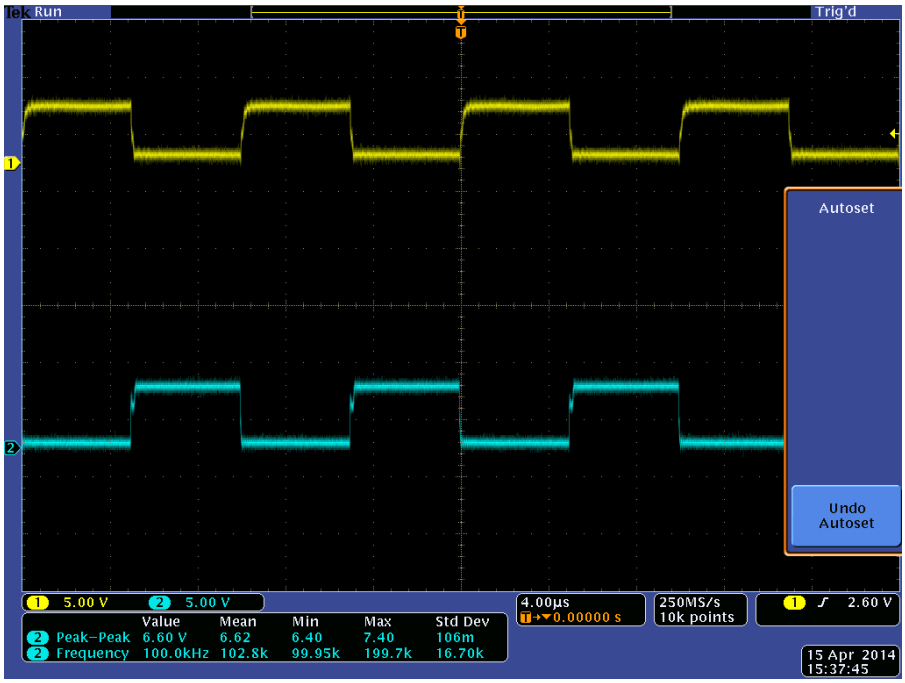

Fig 5.3.2.12 Voltage Measurement of LED Driver Version 2 at 100 KHz

Channel 1 (Yellow) displays the response measured from the top of R2 to Ground at 100 KHz. Channel 2 (Cyan) is the output of the function generator. The reader will note that the oscilloscope gives a value of 6.60V even though the function generator was set to 5V, confirmed by the Agilent Multimeter. Increasing the scale increased the accuracy of the measurement, but did not bring it close enough to 5 V to be considered accurate.

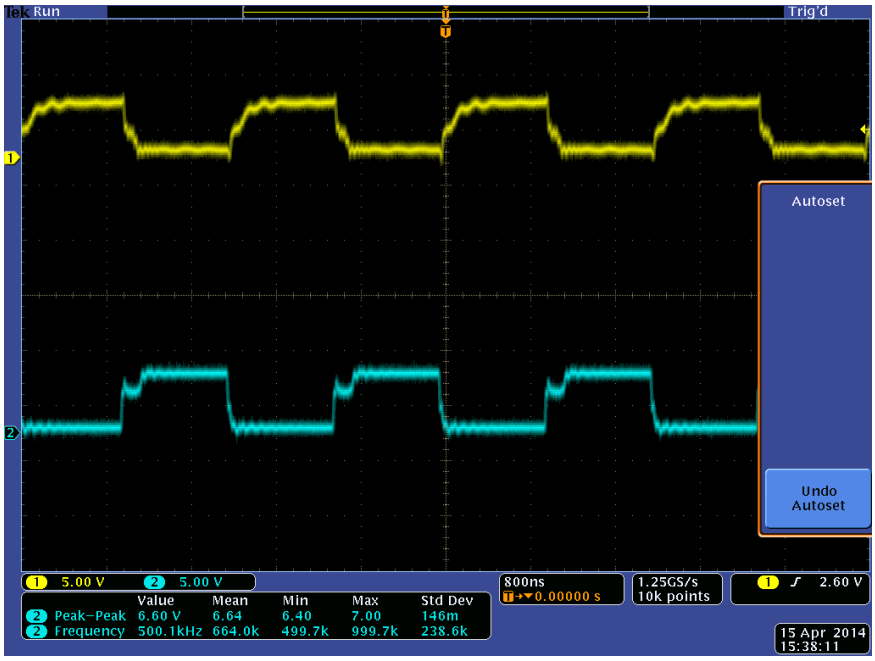

Fig 5.3.2.13 Voltage Measurement of LED Driver Version 2 at 500 KHz

Channel 1 (Yellow) displays the response measured from the top of R2 to Ground at 500 KHz. Channel 2 (Cyan) is the output of the function generator. The waveforms from both the function generator and the show distortion.

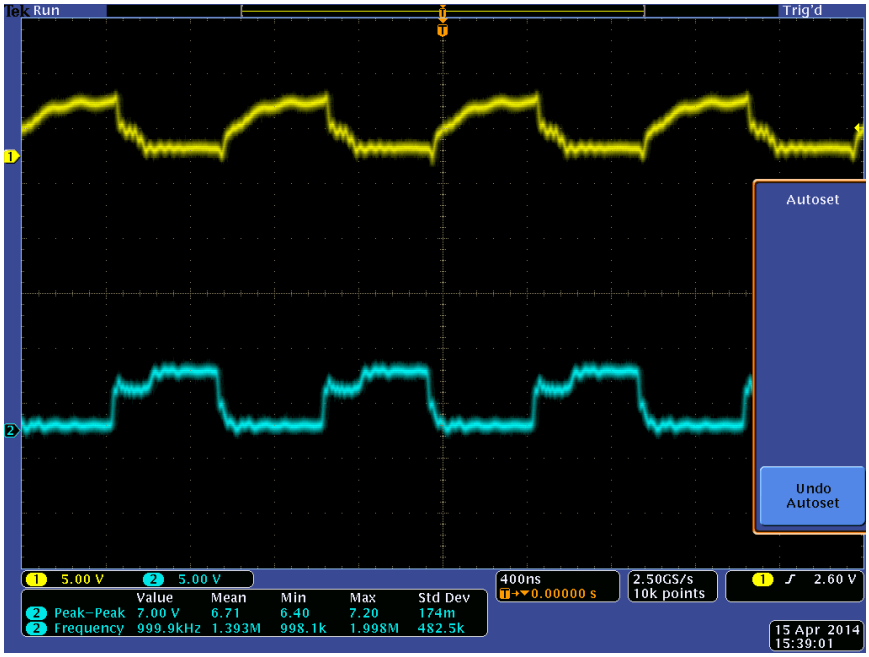

Fig 5.3.2.14 Voltage Measurement of LED Driver Version 2 at 1 MHz

Channel 1 (Yellow) displays the response measured from the top of R2 to Ground at 1 MHz. Channel 2 (Cyan) is the output of the function generator. There is significantly more distortion to the driver waveform at 1 MHz.

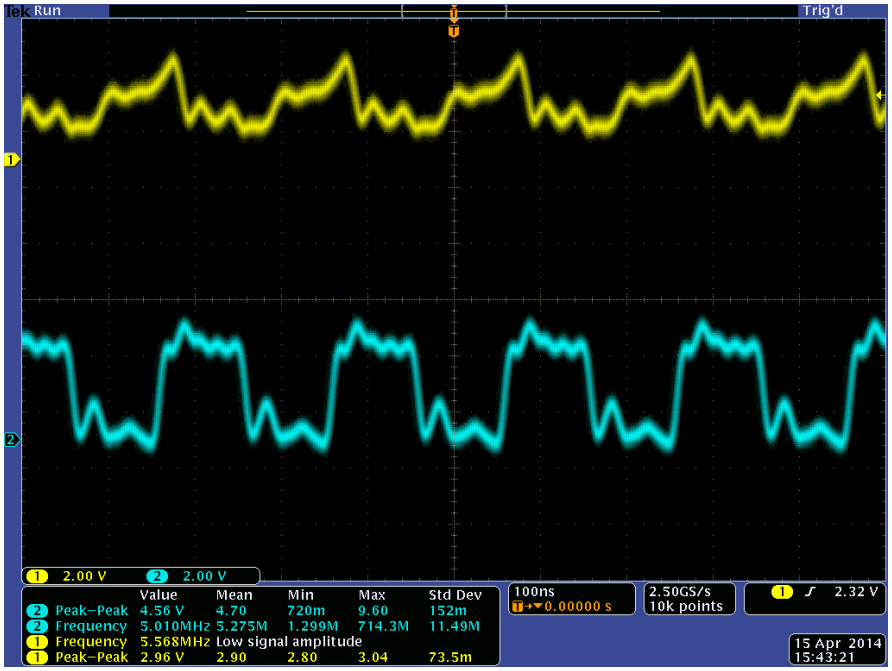

Fig 5.3.2.15 Voltage Measurement of LED Driver Version 2 at 5 MHz

Channel 1 (Yellow) displays the response measured from the top of R2 to Ground at 5 MHz. Channel 2 (Cyan) is the output of the function generator. The distortion is severely damaging to the driver circuit output waveform. However, even the output of the function generator is grossly distorted. This oscilloscope screen shot also indicates that the Agilent Multimeter has difficulty reading the voltage at such high frequencies as the voltages listed for them are 3000 greater according to the oscilloscope.

A second experiment was performed to test the effects of the current by adjusting the R3 value in the circuit from 3 Ω to 47 Ω. Input voltage was kept at 5 V P-T-P, measured by the Agilent 34401A Multimeter, and the input frequency kept at 100 KHz. The measurement was over R2. The Laser/LED was replaced by a 270 Ω resistor and R2 set to 3.34 Ω.

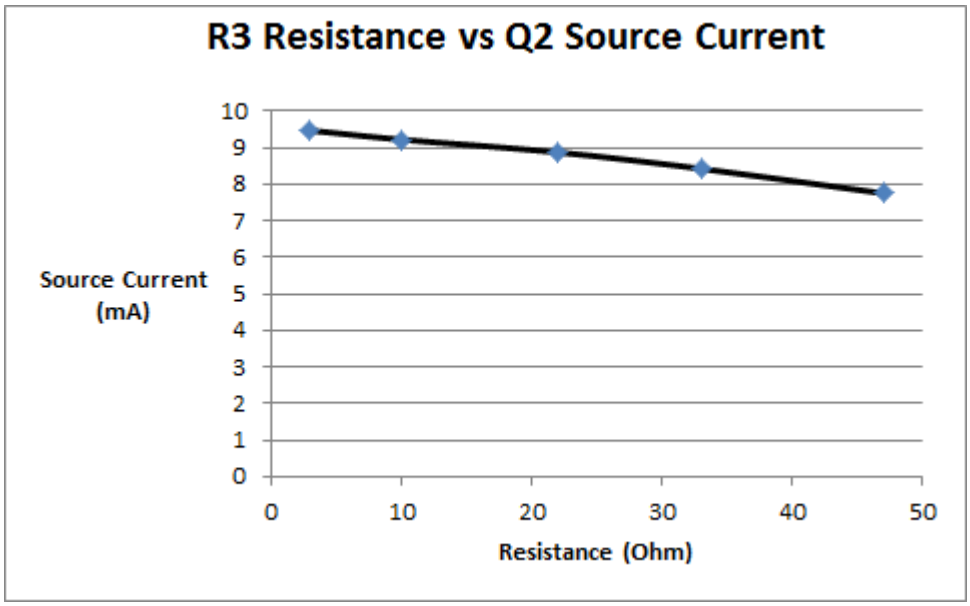

Fig. 5.3.2.16: R3 Resistance Value vs Q2 Source Current for Driver Circuit Version 2

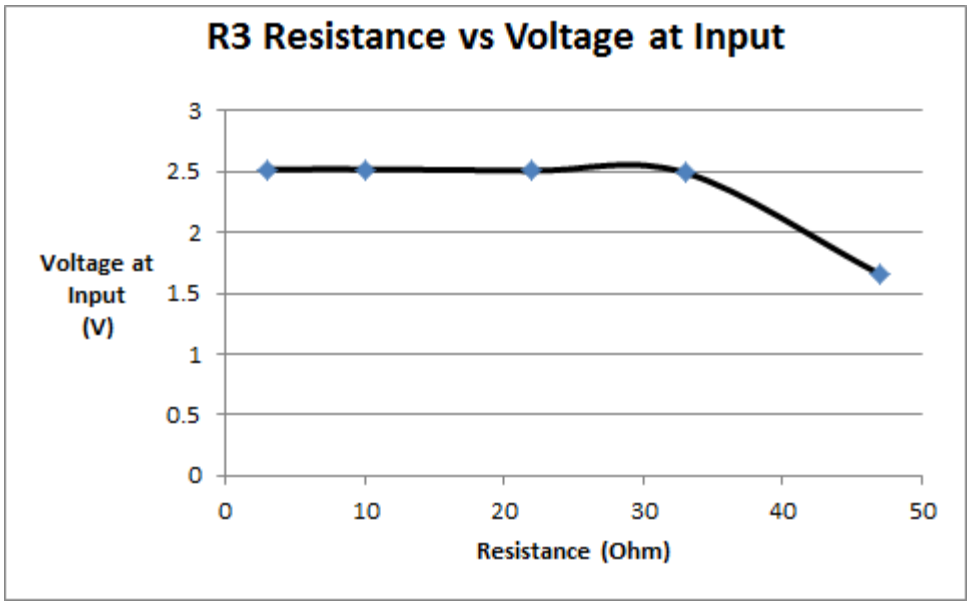

Fig. 5.3.2.17: R3 Resistance Value vs Voltage at Input for Driver Circuit Version 2

A third experiment was performed to test the effects of the current by adjusting the Laser/LED substitute resistor value in the circuit from 10 Ω to 270 Ω. Input voltage was kept at 5 V P-T-P, measured by the Agilent 34401A Multimeter, and the input frequency kept at 100 KHz. The measurement was over R2. R2 was set to 3.34 Ω and R3 set to 33 Ω.

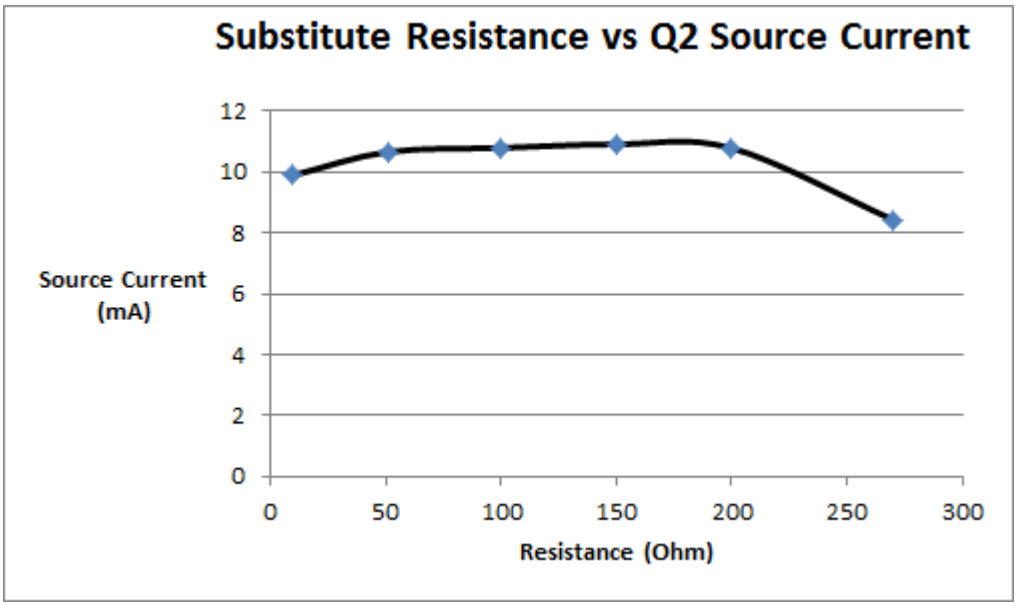

Fig. 5.3.2.18: Substitute Resistance vs Q2 Source Current for Driver Circuit Version 2

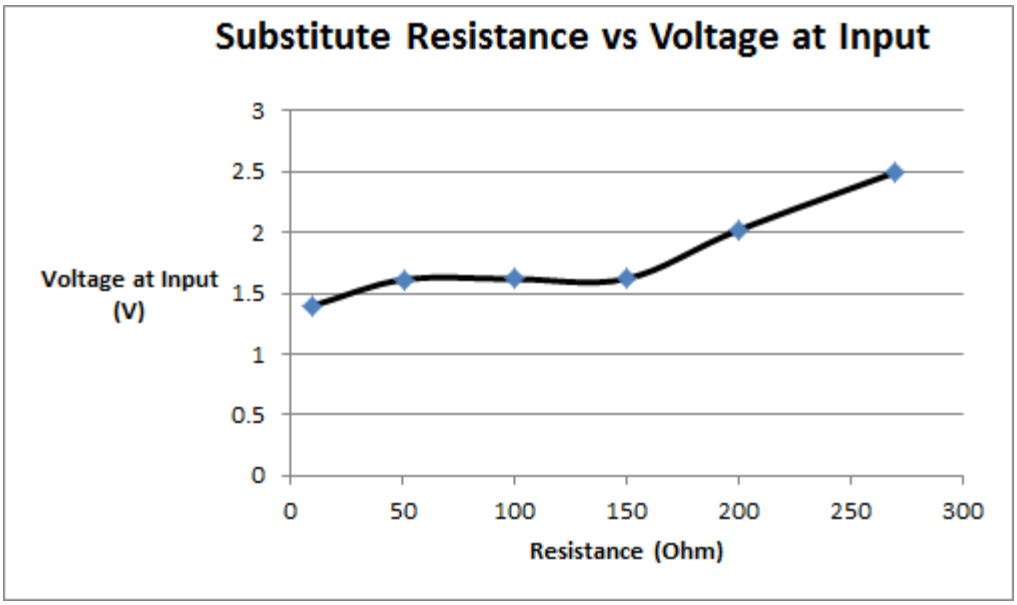

Fig. 5.3.2.19: Substitute Resistance vs Q2 Source Current for Driver Circuit Version 2

5.3.2.4 Driver Circuit Version 3

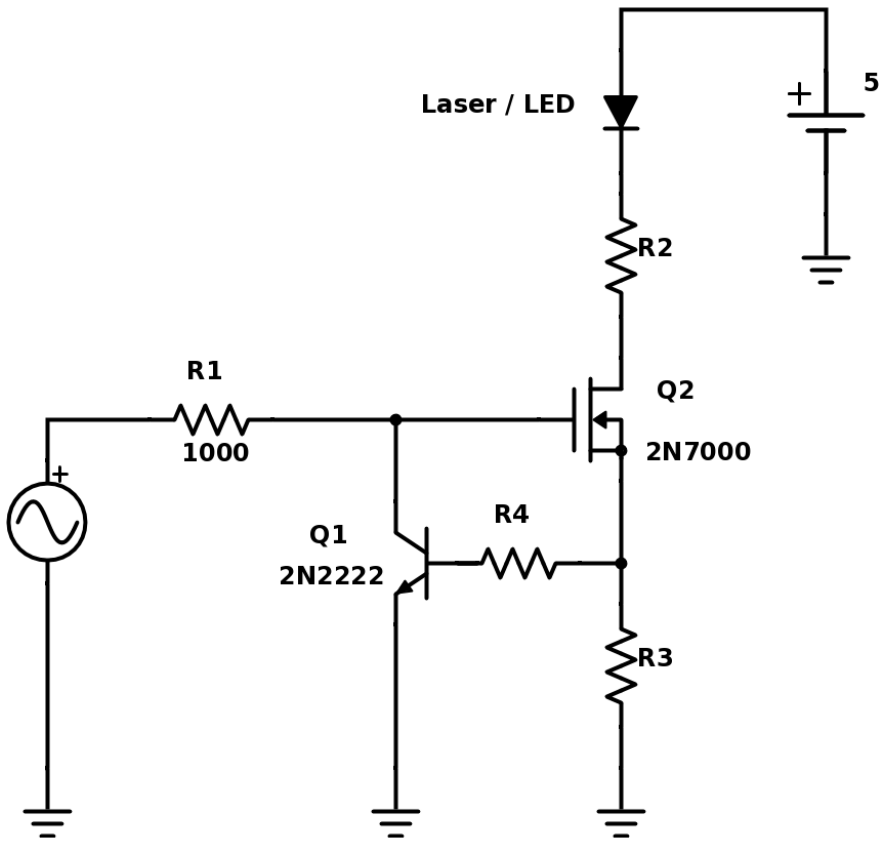

Fig 5.3.2.20 Driver Circuit Version 3

In the belief that high frequency circuits were causing Q1 to turn becomes overactive resistor R4 was added to decrease this possible problem. Initial testing with both 5 mW 670 nm and 10 mW 650nm laser diodes demonstrated a lagging DC current after a high input, causing the laser to turn on. The problem was discovered to be a series of damaged 2N7000 transistors.

Frequency testing of the Driver Circuit Version 3 revealed interesting effect with the 10 mW 650 nm laser and Engin 5W LED in place. The circuit was able to effectively operate at 1 MHz, but there were interesting effects believed to be caused by the diodes which appear as some kind artifact representative of amplitude modulation at very high frequencies. In the case of the laser diode, the modulation was at 27 MHz (Fig 5.3.2.21), and the LED display frequencies of 20 MHz (Fig 5.3.2.22). Measurements were taken over diodes. The discrepancy between the overlaid frequencies support the idea that the effect is responsible from the diodes as is the testing in Driver Circuit Version 2 where a substitute resistor was utilized in their place and the effect went unobserved. Because of the modulating frequency is ~20-27 times greater than the message signal it is believed that the effect does not have significant impact upon reception, and lab tests do not show damaging impact as well.

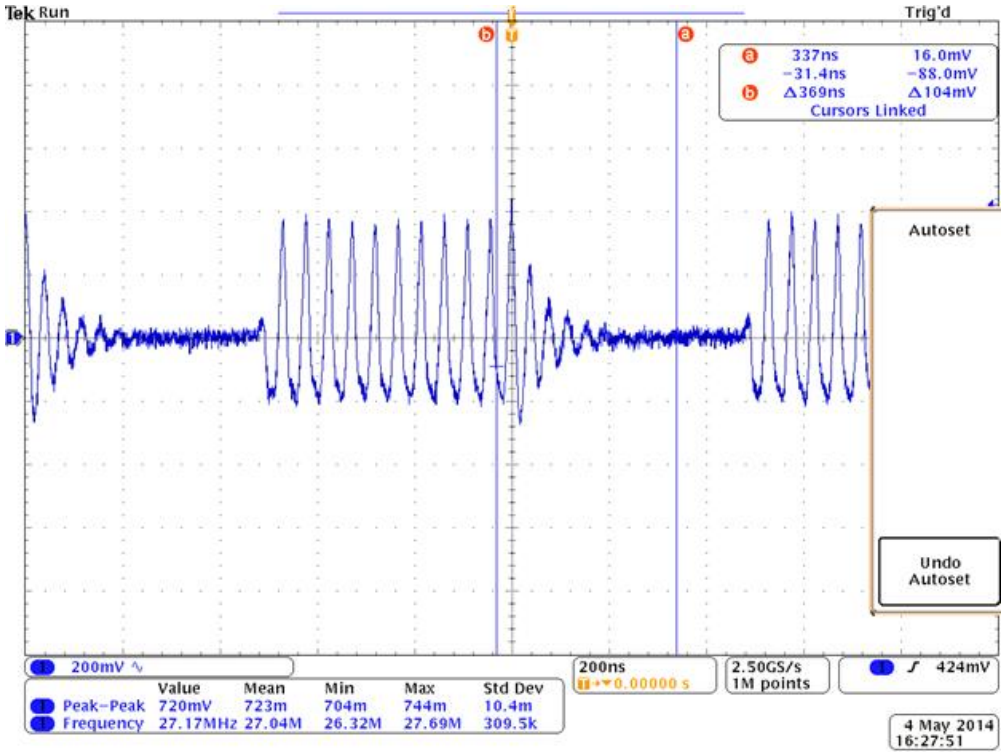

Fig. 5.3.2.21: 10 mW 650 nm Laser output of Driver Circuit Version 3 showing modulation artifact at ~27 MHz

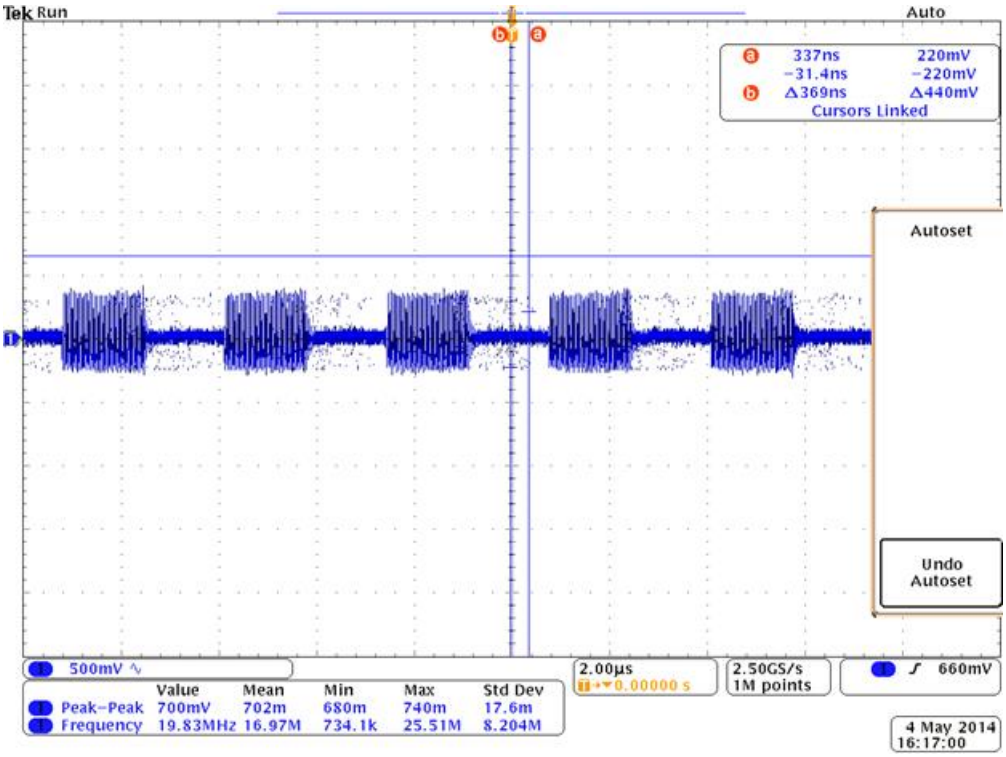

Fig. 5.3.2.22: Engin LED output of Driver Circuit Version 3 showing modulation artifact at ~20 MHz

5.3.2.4 LED Specific Driver Circuit Version 4

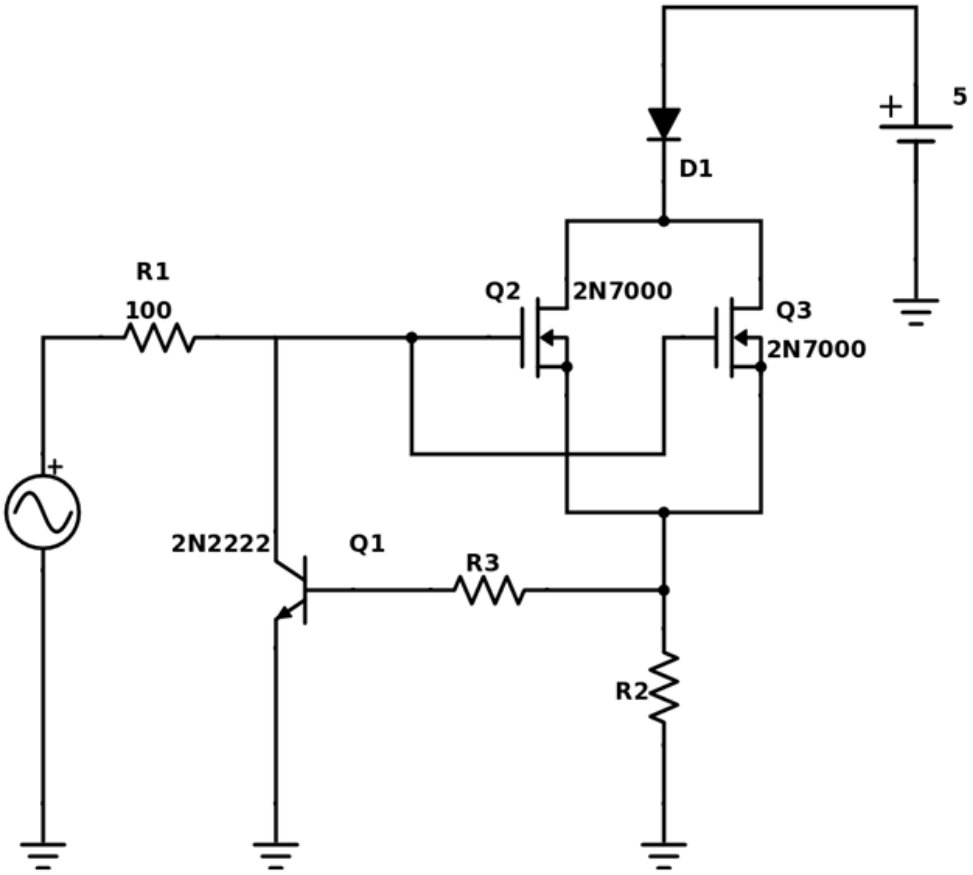

Fig. 5.3.2.23 LED Specific Driver Circuit Version 4

A fourth driver circuit was designed with the LED in mind. During this time of this time of the project, concerns were raised regarding the ability of the pan-tilt platform and computer vision system to be accurate enough to connect the modulated laser beam on to the photodiode receiver. With the LED problems with accuracy would less severe. The 2N7000 is limited to 0.2 mA of continuous current draw while the LED is rated for 1.2 A. Because the LED was desired to be at the highest safe brightness possible an additional 2N7000 FET was placed in parallel with Q2 from previous designs to alleviate overdrawn current problems.

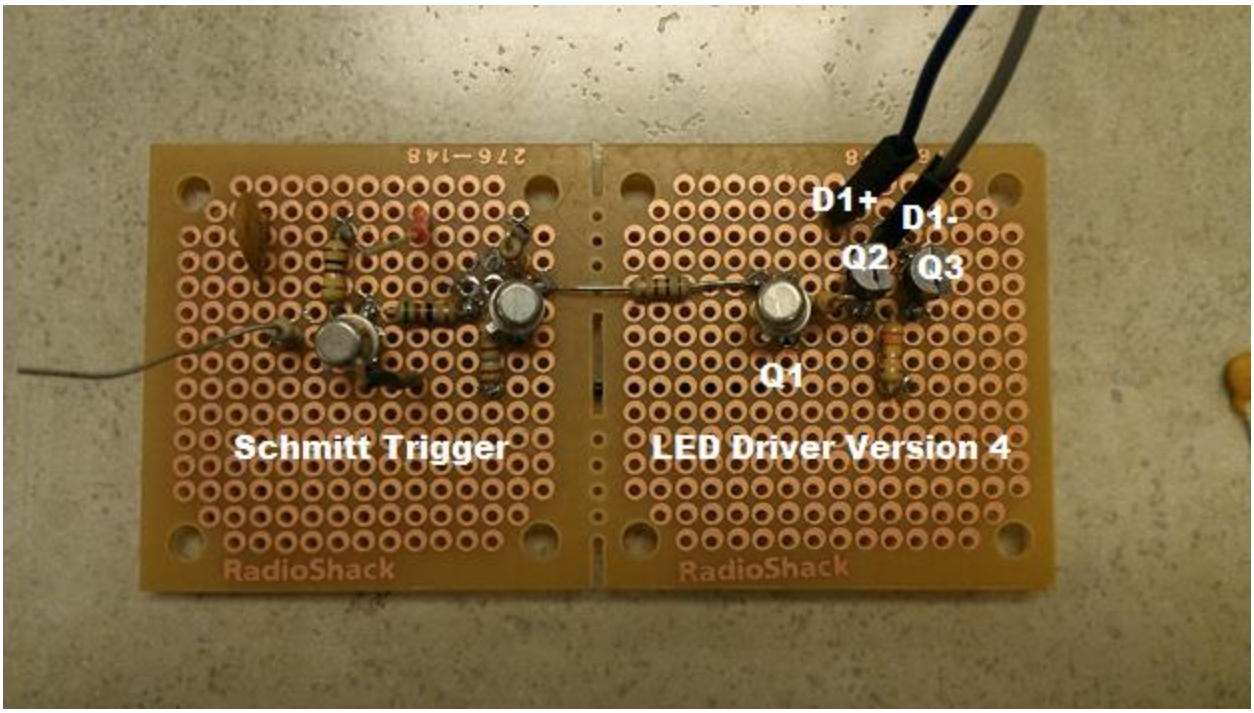

Fig. 5.3.2.24 LED Specific Driver Circuit Version 4 with Schmitt Trigger on Perfboard

In Fig 5.3.2.24 the LED Specific Driver Circuit V4 is displayed on perfboard with a connection to the Schmitt Trigger which was designed for the front end input. Not seen on the board is the LED module. D1+ and D1- display the end of two female-female wire adapters which connected the output pins of the board to the leads on the LED terminals. This is the system used in testing resistor values for a reversed bias diode at 1 MHz as detailed in section 5.4.2.

5.4 Receiver

Name of team member who designed this sub-system: Kyle Cavorley, photoelectric effect theory by Jonathan Giordano
Name of team member who wrote this subsection: Kyle Cavorley

5.4.1 Theoretical Considerations

A photodiode is a reverse biased PN junction diode that can be used to detect light. When a photon of sufficient energy strikes the diode, it creates an electron- hole pair. This mechanism is known as the inner photoelectric effect or impact ionization. If the absorption occurs in the junction's depletion region, the carriers are swept from the junction by the built-in electric field. The holes move toward the anode, and electrons toward the cathode, and a photocurrent is produced. The total current through the photodiode is the sum of the dark current (current that is

generated in the absence of light) and the photocurrent. The dark current must be minimized to maximize the sensitivity of the device.

The photodiode is used to capture the signal emitted by the LED or laser module. When the photodiode is biased near avalanche breakdown voltage, photo-generated carriers are multiplied by the impact ionization in the depletion layer as the electron-hole pairs are carried by the electric field. This process produces a photocurrent of greater magnitude and is shown in Fig.5.4.1 below.

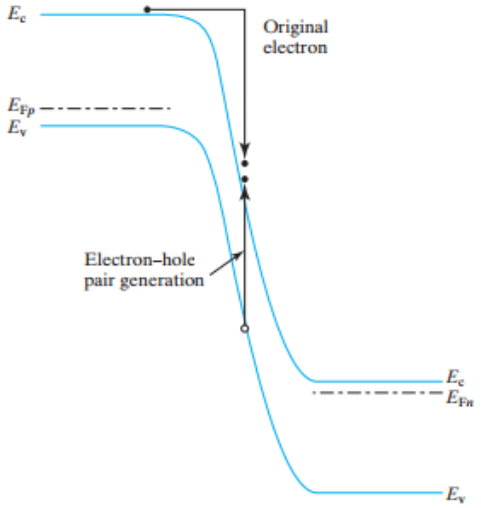

Fig. 5.4.1: Impact Ionization of Photodiode. [13]

Impact ionization occurs in the presence of increasing electric field. With increasing electric field, electrons traversing the depletion layer gain higher kinetic energy. Some electrons have enough energy to raise an electron from the valence band to the conduction band, forming an electron-hole pair as shown in figure above. As reverse bias increases, the potential barrier of the depletion region increases, therefore, decreasing the depletion capacitance (Wdep). The figure below shows the characteristic of the capacitance of the two photodiodes used in our experimentation under reverse bias. Their individual performances agree that an increase in reverse bias reduce the depletion capacitance.

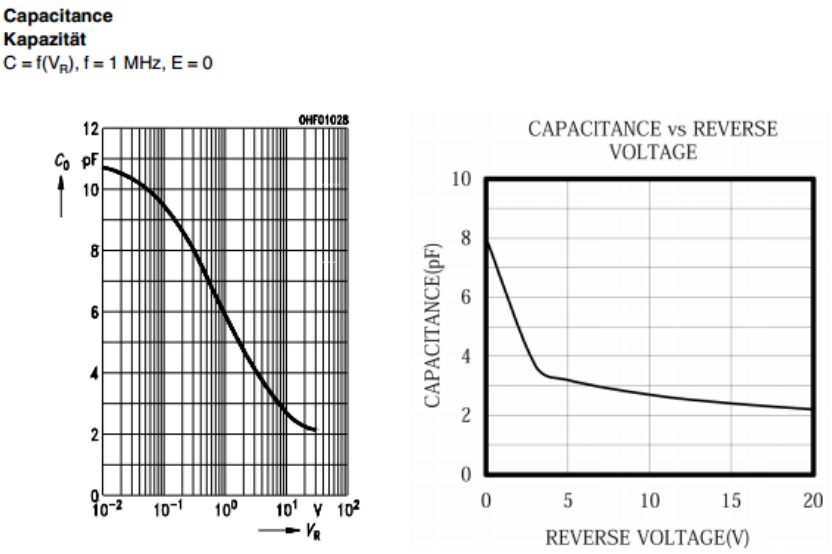

a) SFH-213 Photodiode [14] b) MTD5010W Photodiode [15]

Fig 5.4.2: Capacitance versus Reverse Voltage

This phenomena is represented by the equations below:

$$W_{dep} = \sqrt{\frac{2\varepsilon_s(\phi_{bi} + V_r)}{qN}} = \sqrt{\frac{2\varepsilon_s \times \text{potential barrier}}{qN}}$$

Fig. 5.4.3 : Wdep = Depletion Capacitance, Phi = Built in Potential, Vr = Reverse Voltage, q = charge, N = Number of carriers, and es = permittivity of silicon

$$C_{dep} = A\frac{\varepsilon_s}{W_{dep}}$$

Fig. 5.4.4: Equation to calculate depletion capacitance.

As the depletion region increases by adding reverse bias, the depletion capacitance decreases as shown in Fig. 5.4.4. It can be concluded that when reverse biasing a photodiode, the PN junction conducts negligibly small current. However, at junction breakdown, the critical reverse biased is reached. At this critical reverse bias, the current increases as shown in Fig. 5.4.5 below.

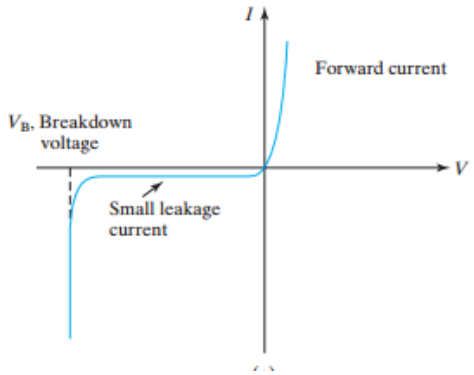

Fig. 5.4.5: Theoretical Current vs Voltage graph of Photodiode [13]

The value of the reverse bias voltage was chosen to satisfy the break down voltage of each photodiode. Not only does the reverse bias voltage chosen at -18 V push the SFH213 photodiode to maximize its system response, but also operates within the reverse voltage range for the MTD5010W photodiode. The maximum reverse bias voltage for the SFH213 photodiode is 20 V. The current produced by the photodiode is proportional to the intensity of the incident light. A transimpedance amplifier can be used to convert the current to a voltage signal.

A transimpedance amplifier is a current to voltage converter, and can be implemented by using an operational amplifier. This circuit is shown below.

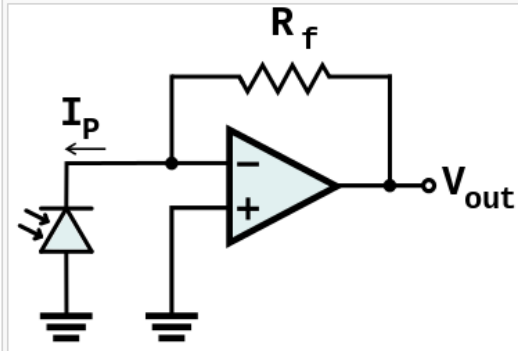

Fig. 5.4.6: Transimpedance Amplifier operating in photovoltaic mode

The transimpedance amplifier presents a low impedance to the photodiode, and isolates the photodiode from the output voltage. Large values of Rf in the MΩs present this isolation. Rf also determines the inverted gain of the signal. Fig. 5.4.6 shows the photovoltaic mode when the photodiode is reverse biased at zero volts. The photovoltaic mode is implemented when using low light levels that require a lot of gain. Since the feedback resistor is so large, the amplifier amplifies the signal the best it can over frequency. However, as frequency increases, the resistance value decreases significantly. Therefore, around 1 MHz, a 1 MΩ resistor behaves as a resistor of a few hundred ohms. This limits the gain. This is why we see the amplification decrease as frequency increases to the point where only the first harmonic is amplified.

A photoconductive mode is more preferred because it operates at higher frequencies. This requires reverse biasing the photodiode at a voltage greater than zero as shown in the figure below. This implementation, shown below, is similar to the final design of the transimpedance amplifier. A greater reverse bias improves the magnitude of the current produced by the photodiode because of a decreased junction capacitance. Higher frequencies are also achieved as a result of lower junction capacitance. In the final design, a feedback capacitor is used for faster switching speed and improved stability of the amplifier. The feedback capacitor also helps eliminate RF.

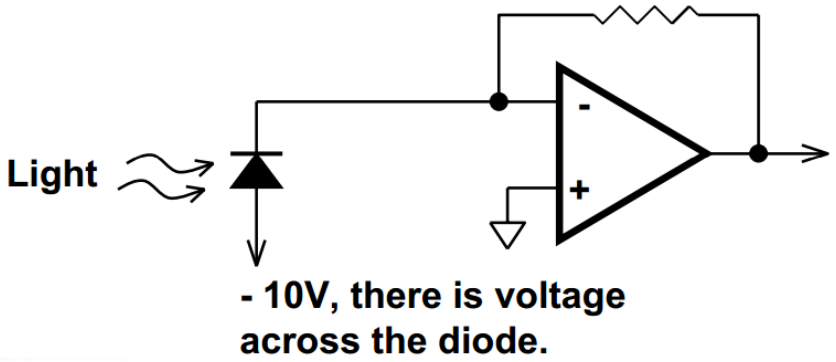

Fig. 5.4.7: Increased Reverse biased photodiode

When designing the transimpedance filter, the relationship below was considered when choosing a feedback resistor.

$$f(-3dB) = \sqrt{\frac{GBP}{4\pi * R_f * C_D}}$$

.

GBP represents the gain bandwidth product of the op amp. The amplifier being used in the transimpedance design is the TL081 which has a GBP of 3 Mhz. This was implemented so that harmonics of the square wave are amplified at operating frequencies nearing 1 MHz.

Recall in Principles of Communication Systems that a square wave is made up of odd harmonics, which are sine waves at the fundamental frequency f, 3f, 5f, and so on. The most power reside in the first, third, and fifth harmonic, which is essential for proper signal amplification. When working with an op amp with a 3 dB GBP of 3 Mhz, the maximum frequency achieved to successfully recreate the data stream is around 1 Mhz. To further amplify the signal generated by the transimpedance amplifier, a non-inverting amplifier is used.

The non inverting shown in the figure below, is used to amplify the signal by a factor Gain = 1 + Rf/Rg.

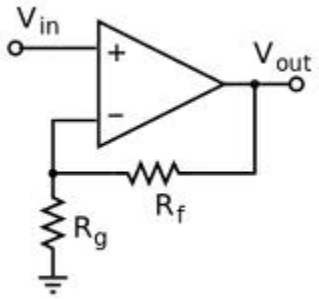

Fig.5.4.8: Non-inverting Amplifier

This design was considered to amplify the signal response from the transimpedance amplifier from 0 to 0.5 V to 0 to 5 V. The noninverting scheme was chosen to prevent the data from being inverted. A signal higher in magnitude is easier to work with in a comparator circuit.

The amplified signal is fed into a comparator circuit to produce a 0 to 3.3V signal compatible with the USB to serial converter chip. Op-amps are push-pull outputs that swing close to the power supply rails as feasible. This is why the comparator designed has a V- = 0V and a V+ = 3.3 V. The functionality behind the comparator, is that it compares two levels as quickly as possible above or below the reference voltage, and outputs a high for voltages greater than the reference voltage, and low for voltages less than the reference voltage.

In our design, the comparator has a positive feedback to introduce a small amount of hysteresis. Without feedback, capacitive strays from the output to an input may cause the comparator to become unstable. Hysteresis provides comparator stability, separating the up and down switching points. When a transition has started, the input undergoes a significant reversal before the reverse transition can occur. Hysteresis also provides for a cleaner pulsed signal. Signals superimposed with noise without hysteresis can provide multiple output transitions as a noisy input signal crosses and recrosses the threshold region. A comparator with hysteresis introduced provides for clean output transition. The design of the comparator in our system is shown in Fig. 5.4.9 below.

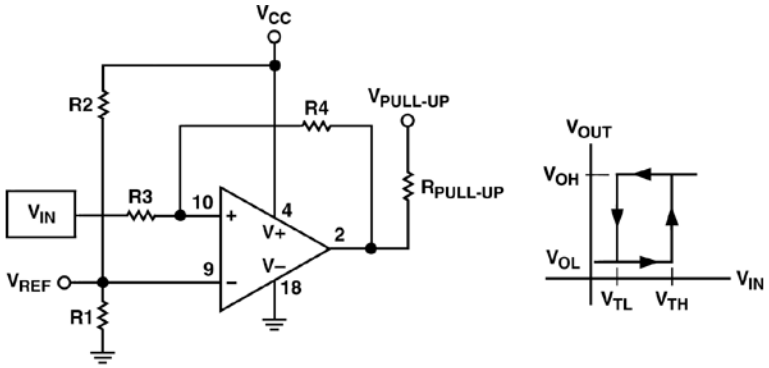

Fig. 5.4.9: Single Supply Noninverting Hysteresis Comparator

The Vth and Vtl is our 5 and 0V input from the signal respectively. By arbitrarily choosing Vref = 2.5 V and Vcc = 3.3V, we can set values for R1 and R2. The Vol and Voh values respectively are 0 and 3.3 V. From this point, we can pick R3 and R4 values to design the circuit. All resistor values calculated are shown in the circuit schematic in Fig. 5.4.16. With this theoretical background, the receive system can be designed.

A side thought experiment developed due to concerns with transmission accuracy and the small receiving area of a typical photodiode. The idea for receiving was based out of usage of the photoelectric effect. The photoelectric effect is the ejaculation of electrons from various types of metal cause by light shining on the metal's surface. This is due to the wave-particle duality of light, and as such not the amount of light. But the energy of the light is what causes the electrons

to be emitted. The energy of the light is due to the lights frequency as seen in the Planck relation:

$$E = h\nu$$

Once the threshold frequency of a metal has been met, it will begin to emit photons, and this emission can be used to develop a charge on the receiving plate. This charge can thus be used to measure a receiving signal.

Calculations were completed for the highest frequency laser which had been purchased. The wavelength as such was 650 nm. Utilizing the frequency-wavelength relation the frequency is equal to $4.615 * 10^{14}$ Hz.

$$\nu = \frac{c}{\lambda}$$

From the Planck relation, the energy of a 650 nm laser is equal to $3.05815 * 10^{-19}$J which equates to 1.9087 electron volts. Based upon the work functions tables of commonly available metals, our highest energy laser would not be enough to cause any electron emission, and therefore unusable for any signal reception. There also existed concerns regarding size of the metal receiving plate and its reactivity to high speed signals.

5.4.2 Design Procedure

The SFH-213 photodiode was selected for its wideband optical bandwidth, low cost, and wide availability. Table 5.4.1 shows six randomly selected SFH-213 photodiodes and their characteristic voltage-current responses under ambient light. It is seen that the measured voltages and currents are stable with respect to the same environment.

Table 5.4.1: Voltage and current values of 6 different Photodiodes showing stability of photodiodes.

Diode Number	Voltage (V)	Current (mA)
1	0.32	0.005
2	0.33	0.005
3	0.35	0.0048
4	0.32	0.0048
5	0.35	0.005
6	0.33	0.005

To test the response of the photodiode, a LED was hooked up to the signal generator. The leads of the photodiode were connected to the oscilloscope to measure the response. As expected, the photodiode was successfully able to detect the signal emitted from the LED. The measured DC voltage of the device when lased ranged between 0.4 to 0.6 V. At a distance of 14 feet, the photodiode produced a reading of 0.5 V across the multimeter. This provided sufficient results for the goal of our project. Table 5.4.2 shows the current measurements of the LED, generator voltage, voltage across photodiode, power of the LED and photodiode, frequency, rise, and fall times of the photodiode when connecting a reverse biased photodiode to a 10 Ω resistor. Table 5.4.2 shows our initial tests. The table shows the power of the LED and photodiode increase with current and voltage across LED and photodiode respectively. These tests were run to find the maximum power of the LED and photodiode we could achieve without a driver circuit. The rise and fall times of the photodiode are stable with increasing power.

Table 5.4.2: Photodiode Response with Red LED and no driver circuit

I (mA) LED	Gen Vpp	Meas. Vpp	I(mA) Photo	Power LED mW	Power Photo (mW)	F	Tr (ns)	Tf (ns)
0.23	8	0.15	7.5	0.92	0.5625	10 MHz	9.5	9.7
0.43	9.6	0.18	9	2.064	0.81	10 MHz	9.5	10.5
0.63	11	0.19	9.5	3.465	0.9025	10 MHz	10	10.5
0.8	12	0.22	11	4.8	1.21	10 MHz	10	10.9
1.2	14	0.25	12.5	8.4	1.5625	10 MHz	10	10.9
1.6	15.8	0.29	14.5	12.64	2.1025	10MHz	10	10.9
2.7	20	0.37	18.5	27	3.4225	10 MHz	10	10.9

When reverse biasing the photodiode at 5 V in series with a resistor, the current produced from the photodiode builds up a voltage signal across the resistor. The magnitude of the signal depends on the size of the resistor. This is known as photovoltaic mode. Table 5.4.3 shows the effect of increasing series resistances connected to the reverse biased photodiode. At high frequencies such as 10 MHz, the most gain comes from the 20 kΩ resistor. The result of this waveform is displayed in Fig. 5.4.10. However, the response of the photodiode at 10 MHz does

not produce a clean square wave in photovoltaic mode. The schematic is shown in Fig. 5.4.11. This is because photovoltaic mode is rated for frequencies less that 300 kHz.

Increasing the resistance further provides too much distortion for a good reading. These measurements were taken at maximum power emitted by the LED.The table shows the current decreasing at higher resistances, which is intuitive according to Ohm's Law. The rise and fall times also increase as higher resistances are added. This is a result of the photodiode seeing such a high impedance.

Table 5.4.3: Driver Circuit Photodiode response with Red LED

I (mA) LED	Gen Vpp	Meas. Vpp	I(mA) Photo	Power LED mW	Power Photo (mW)	F	Tr (ns)	Tf (ns)	R Ω
2.7	20	0.3	1.5	27	0.225	10 MHz	2	1	100
2.7	20	0.78	0.764705882	27	0.298235294	10 MHz	5	2.5	510
2.7	20	1	0.5	27	0.25	10 MHz	6	3	1000
2.7	20	1.15	0.2875	27	0.1653125	10 MHz	8	4	2000
2.7	20	1.2	0.0615	27	0.0378225	10 MHz	6.6	4	10000
2.7	20	1.2	0.03	27	0.018	10 MHz	6.7	4.5	20000

Fig. 5.4.10: Response of reverse biased photodiode with 20 kΩ resistor at 10 MHz in photovoltaic mode.

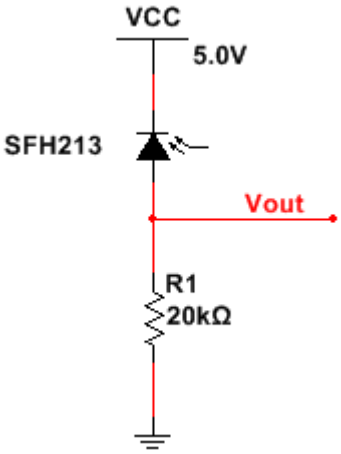

Fig. 5.4.11 Photovoltaic method original design

As shown Fig. 5.4.10, the response of the photodiode is somewhat distorted and does not represent the clean square wave at 10 MHz. This is because the photovoltaic method cannot produce a clean response at high frequencies.

Photovoltaic frequency response of a reverse biased SFH213 photodiode was tested by using the LED Driver Circuit V4 with the Engin 5W LED to transmit a 1 MHz square wave. The diode was reversed by +5 V. It was found that 150 Ohm resistor produced the strongest non degraded signal out of all resistor values. The resistor was in series with the photodiode.

Table 5.4.4: Photodiode with variable resistor at 1MHz with LED

Resistor Value (Ω)	Voltage of Diode (mean P-T-P V)	Average Rise (ns)	Average Fall (ns)	Signal Condition (arbitrary)
51	0.2	385	215	Ok
100	0.4	180	140	Good
130	0.48	170	155	Good
*150	0.58	160	120	Good
172	0.6	170	140	Good
180	0.63	180	145	Ok
300	1	180	160	Ok
470	1.4	190	200	Ok
1000	2.22	220	300	Bad

*Best Result

Before completely abandoning the photovoltaic mode, it was desired to test the photovoltaic mode with an op-amp to increase the gain. The TL081 and AD8030 are the op-amps considered with gain bandwidth product of 3 MHz, and 125 MHz respectively. The op-amps are shown below in Fig 5.4.12.

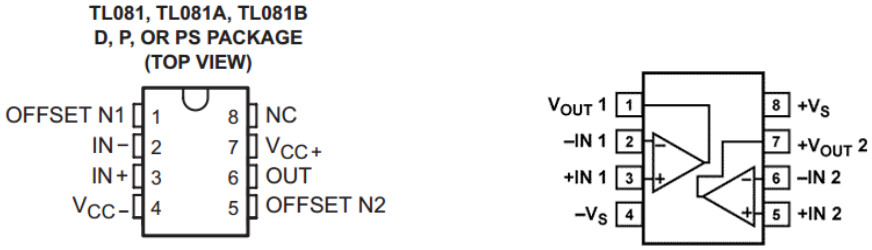

a) TL081 b) AD8030

Fig. 5.4.12: Op amp pin outs.

The TL081 op-amp was provided by Rutgers University and the AD8030 dual-package op-amp was provided by Triad RF Systems. Fig. 5.4.13 shows the AD8030 op-amps used in the design.

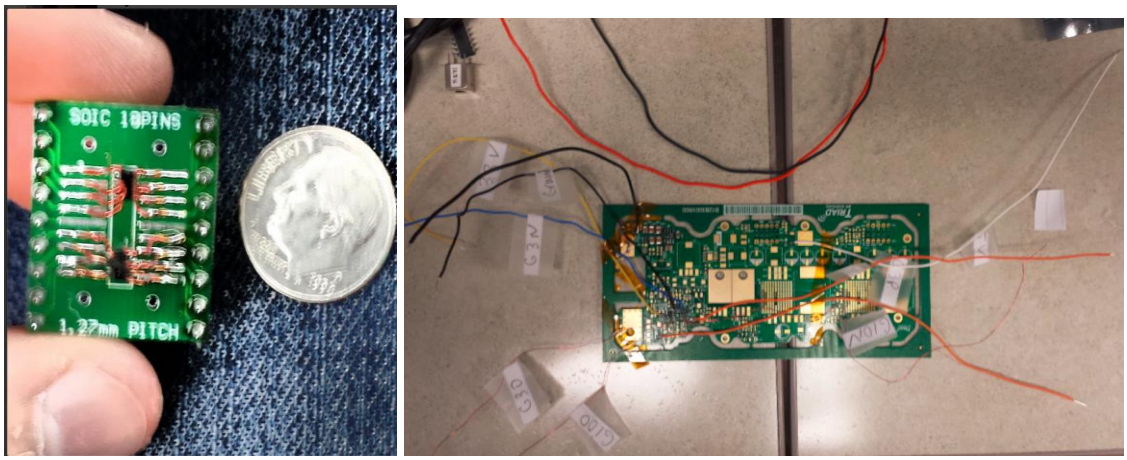

Fig. 5.4.13: AD8030 on Schmart Board and Triad RF board

Fig. 5.4.6 shows the design of the op-amp used in photovoltaic mode. The feedback resistor is 1MΩ to amplify the response. The design itself using the TL081 is shown in Fig. 5.4.14 below. Please refer to the Dropbox shared links below to see the experiment in action!

https://www.dropbox.com/s/4dsm5awcg0ih64r/20140419_123819.mp4

https://www.dropbox.com/s/sa2lnlqk2bxvvxz/20140419_123737.mp4

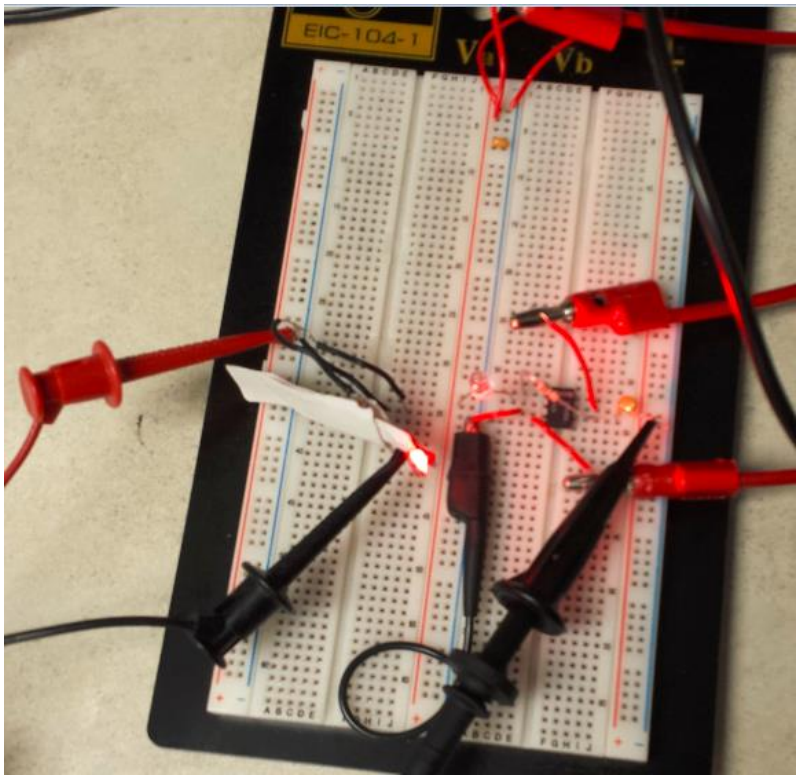

Fig. 5.4.14 Photovoltaic mode with TL081 op amp.

The response shown in the videos is very distorted. The work around to this method is using the photodiode in photoconductive mode. The figure implemented is shown in Fig. 5.4.7 and includes a reverse biased photodiode. This was constructed with both the AD8030 op amp and TL081 op amp. There gain response for the op-amps over frequency are shown below.

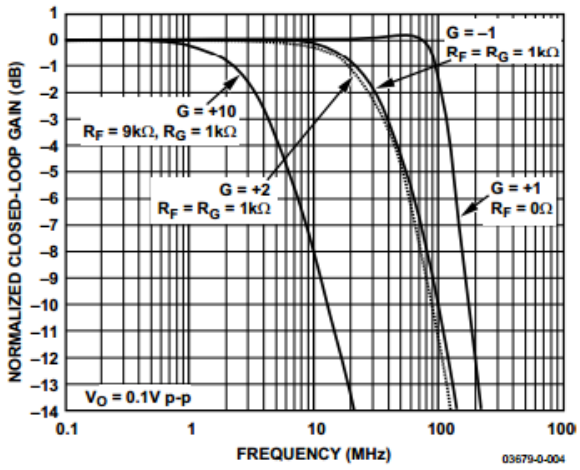

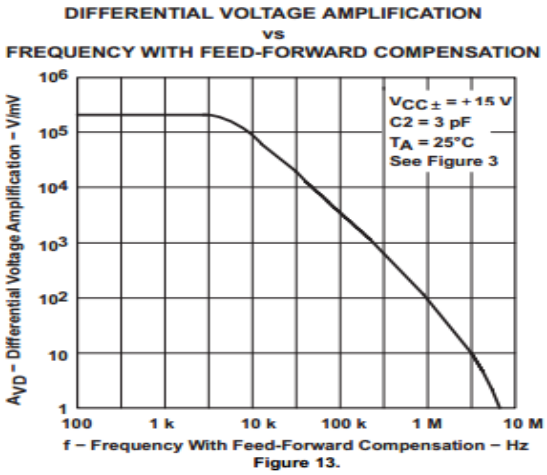

[a]Frequency response of AD8030 op-amp. [b] Tl081 frequency response

Fig. 5.4.15: Frequency response versus gain.

The AD8030 has a higher GBP than the TL081 as shown in Fig. 5.4.15. When referring to Fig. 5.4.15.a, the best frequency response of the AD8030 is achieved at a GBP of one. The chart also shows that our gain is limited to ten when trying to achieve high frequency.

Amplifiers are necessary to amplify the signal from the photodiode. The high frequency op-amps are essential so that all odd harmonics of the data transmission are amplified within the GBP of the op-amp. The AD8030 is prefered because it operates at higher frequencies. The TL081 serves as a bottleneck when amplifying signals of frequency greater than 700 kHz.

Before constructing the transimpedance amplifier in photoconductive mode, it was decided to build the noninverting amplifier. The noninverting amplifier amplifies the signal from the transimpedance amplifier before entering comparator circuit. A noninverting amplifier was built because of the measurements taken when lasing a photodiode in photovoltaic mode. The mode produced a signal that ranged from 0.4 to 0.6 volts. Amplifying this signal by ten would make it easier for the comparator to act as a decision maker because a higher reference voltage can be used. The figure below shows an amplifier with a gain of ten, to produce a large enough intput to the comparator. This noninverting amplifier precedes the comparator circuit shown in Fig. 5.4.16.

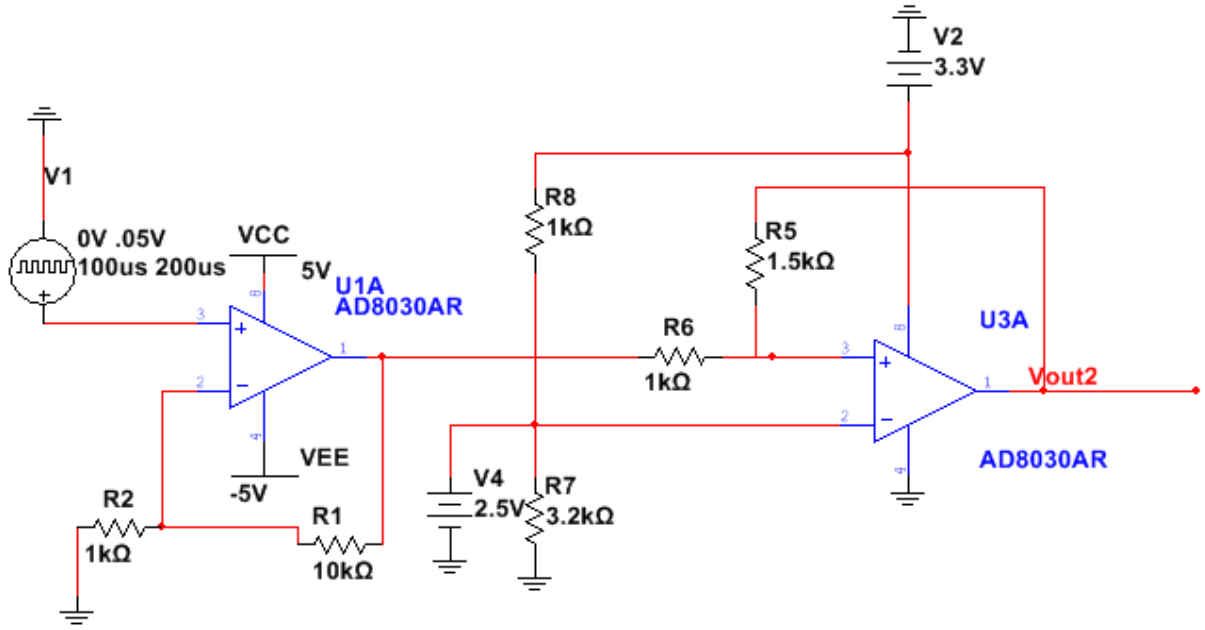

Fig. 5.4.16: Noninverting amplifier with gain of ten cascaded to non-inverting comparator.

The design of the comparator with noninverting hysteresis was determined from Fig. 5.4.9. As mentioned before, Vth and Vtl is 5 and 0V input signal respectively. This signal is produced from the noninverting amplifier. I chose the Vref voltage as 2.5 V because it is the average voltage of the signal. With a functioning comparator, anything above the reference voltage will result as an output high of 3.3V and anything below as 0 V. Vcc was set to 3.3V because this is the high value desired for the output signal. Using the equations shown in Fig. 5.4.9 the functioning comparator circuit was designed accordingly. The resistor values are computed below:

$$\text{Vref} = \text{Vcc}\left(\frac{\text{R1}}{\text{R1} + \text{R2}}\right)$$

$$2.5 = 3.3\left(\frac{\text{R1}}{\text{R1} + \text{R2}}\right)$$

$$\text{R1} = 3.125\ \text{R2}$$

After finding the ratio of R1 to R2, the values R2 = 1 kΩ and R1 = 3.125 kΩ were chosen arbitrarily. The hysteresis voltage is equal to the Vth minus Vtl, which is 5 V. With the hysteresis voltage known, R3 and R4 can be determined. These resistances are computed below:

$$\text{Hyst} = \text{R3}\left(\frac{\text{Voh - Vol}}{\text{R4}}\right)$$

$$5 = \text{R3}\left(\frac{3.3}{\text{R4}}\right)$$

$$\text{R4} = (3.3/5)\text{R3}$$

After finding the ratio of R4 to R3, the value of chose R4 as 1kΩ and R3 as 1.5 kΩ were chosen arbitrarily. The calculated resistances are depicted in Fig. 5.4.16 comparator circuit. When swapping R3 and R4 in the simulations, the comparator seemed to function better. The simulation for the noninverting amplifier and comparator circuit is shown in the simulation section 5.4.3. The simulations produce the correct waveforms desired.

Figure 5.4.3.1 displays the simulated response of an amplifier cascaded with a comparator designed for hysteresis. The first stage amplifier takes in a signal from 0 to .5 V at 5 MHz (red). This was chosen to replicate the response of the photodiode. This signal is amplified by ten producing a signal from 0 to 5 V at 5 MHz (green). The cascaded comparator circuit turns the 0 to 5V signal into a 0 to 3.3V signal rated for the USB to serial converter chip by Ardafruit (blue). When the incoming signal to the comparator is above 2.5V the comparator outputs a 3.3V, and when the signal is below 2.5V, the comparator outputs a 0V. Please refer to Fig. 5.4.3.1 through Fig. 5.4.3.3 for further simulation analysis. The simulations correspond with the experimental data shown in Fig. 5.4.4.1 through Fig. 5.4.4.3 in 5.4 Observed and Measured Results section. Please refer to the video "Comparator" on the Vision Based Free Space optical YouTube channel to show the experimentation. [11]

At frequencies above 1 MHz, the time when high and low differ. To correct this so that the time when high and low are equal at high frequencies, the reference voltage was lowered. The reference voltage was lowered because the time high was less than the time the signal was low. The preamplifier and comparator circuit function up to 1.3 MHz. The front end Schmitt Trigger and TL081 used as a transimpedance amplifier bottleneck the receive circuitry.

When finishing the comparator circuit, the design of the transimpedance amplifier was started. In this final design, both the MTD5010W and SFH213 were tested. The rise and fall times of the MTD5010W and SFH213 photodiodes are 1ns and 5ns respectively. Their max reverse bias voltages are 30 and 20 V respectively. Therefore a reverse bias voltage of -18V was chosen to operate in the safe region. Both diodes produce the same results. The rise and fall are unnoticed by the oscilloscope because the maximum frequency the system can achieve is limited by the TL081 and Schmitt Trigger at 700 kHz. The working and final system transimpedance amplifier is shown in Fig. 5.4.17 below.

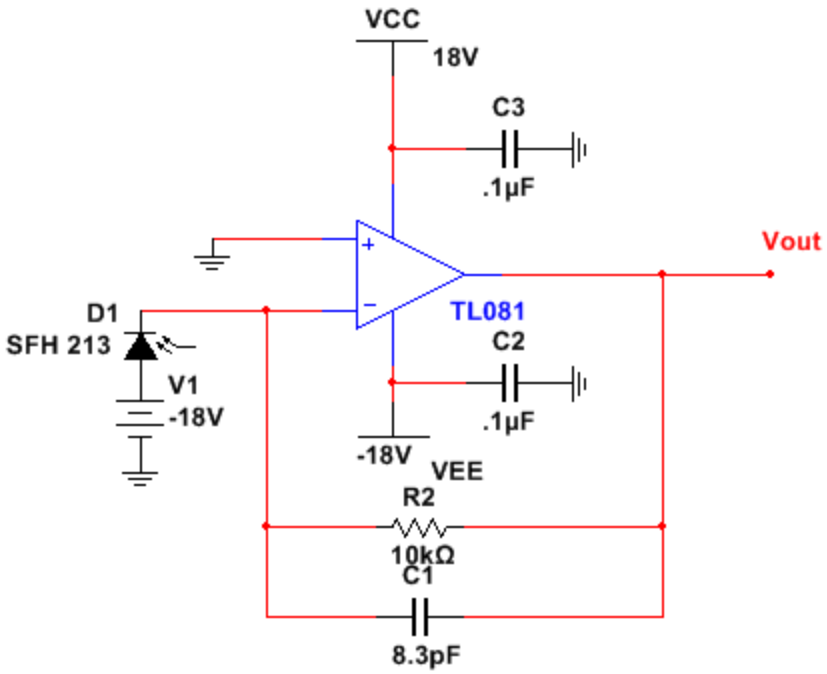

Fig. 5.4.17: Transimpedance Amplifier

The feedback resistor of 10 kΩ was chosen to amplify the response of the photodiode by 10. The 8.3 pF capacitor was installed to eliminate any RF above 2 MHz. The corner frequency of this system is 1.9 MHz. This is found from the relation

$$f = \frac{1}{2\pi(Rf*Cf)}$$

where Rf and Cf are the feedback resistor and capacitor respectively. Please refer to the video "System with LED" on the YouTube channel to demonstrate the Receive Component in full.

The final receive response is documented in Fig. 5.4.4.6 to Fig. 5.4.4.7. The images display the signal that enters the system from the signal generator, to the Schmitt Trigger, to the LED Driver Circuit, to the Transimpedance Amplifier, to the noninverting amplifier, and finally to the comparator. The darker blue waveform represents the signal from the signal generator as input to the transmitter, and the cyan colored waveform represents the output of the receiver. Like the simulations, as frequency increases, a phase delay is introduced because the op-amps are working harder to switch faster. However, these images demonstrate the success of the system.

5.4.3 Simulation Results

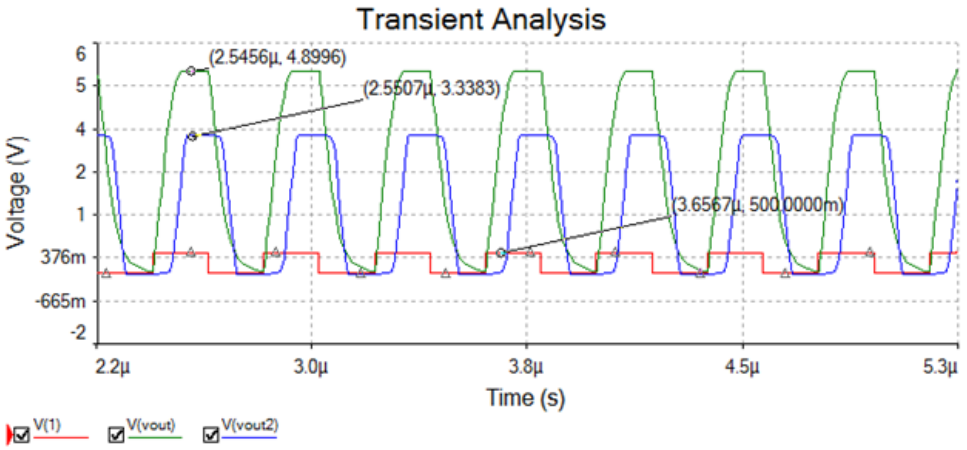

Fig. 5.4.3.1: 0 to .5V 5 MHz signal amplified in first stage of Fig. 5.4.16 to 0 and 5 V, and sent through a comparator to produce a 0 to 3.3 V signal.

From the simulation, one can notice a phase delay in all three signals. When operating at high frequencies, we are really driving the hardware to produce the gain we desire. However, the phase delay is irrelevant to our system and will have no effect.

If for whatever reason the signal generated by the photodiode is 50 mV, another noninverting amplifier preceding the comparator can be used to multiply the input signal by 100 for proper comparison. This simulation is shown in Fig. 5.4.3.2 below. The system takes in a signal 50 mV and turns it into a 0 to 3.3V signal. The red 50 mV signal is amplified to the green 0.5V signal. The 0.5 signal is amplified to the 5V signal, than passed through the comparator to produce the 0 and 3.3 V output.

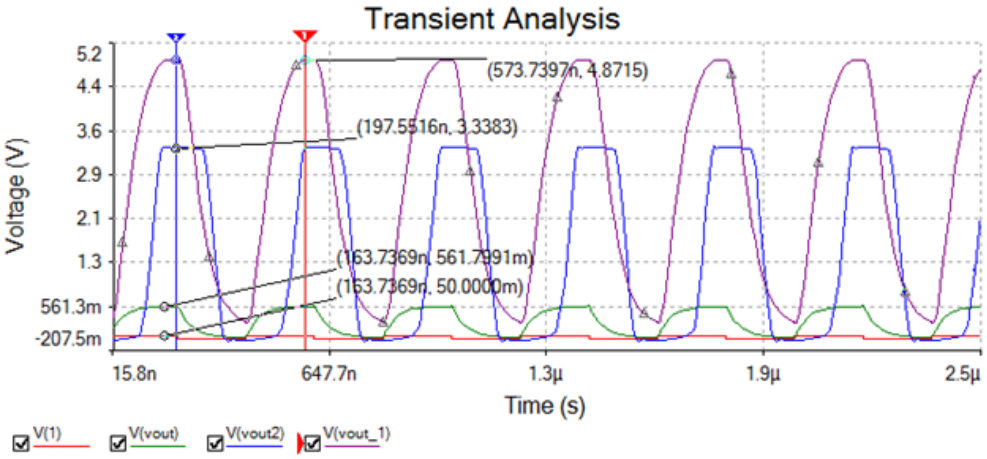

Fig. 5.4.3.2: Two stage amplifier with a gain of ten before entering comparator circuit at 5 MHz.

As we decrease the frequency of the system, the phase delay reduces tremendously. This is

because the rise and fall times are orders of magnitude smaller than the frequency of the system.

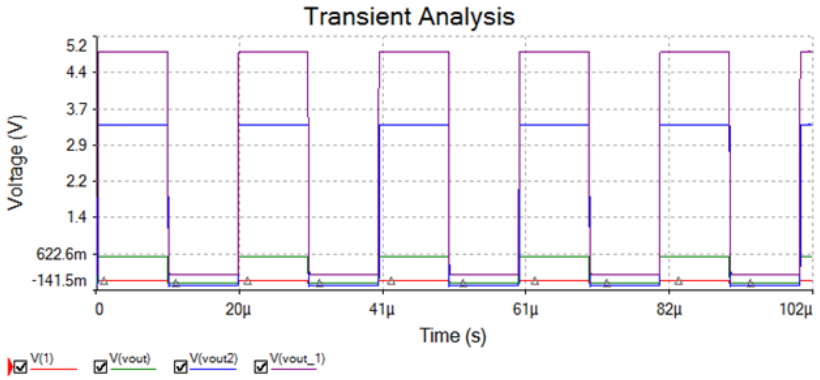

Fig. 5.4.3.3: Simulation of 50 mV at 100 kHz input signal entering two stage amplifier feeding into comparator circuit.

5.4.4 Observed and Measured Results

Shown below is a figure that takes in a 0 to 0.5 V signal and amplifies it to a 0 to 5V signal. This is stage two of the receiver.

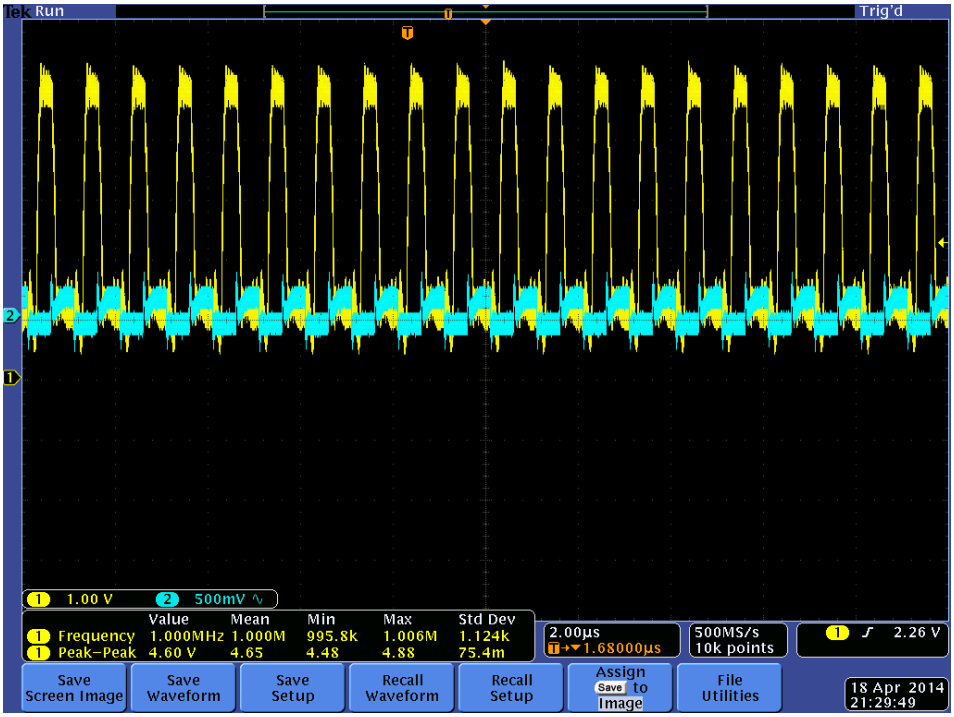

Fig. 5.4.4.1: Amplification Stage 2. Note that the blue signal is the 0.5 V input signal, and the yellow is the 5 V output signal at 1 MHz.

The signal is then fed into a comparator circuit, and produces a peak voltage of 3.3V. This output signal is shown in Fig. 5.4.4.2 below, and agrees with the simulation. Note that the peak to peak reading reads 3.76V because the oscilloscope is measuring noise. The clean rising and falling edges are accounted for from the hysteresis introduced to the comparator.

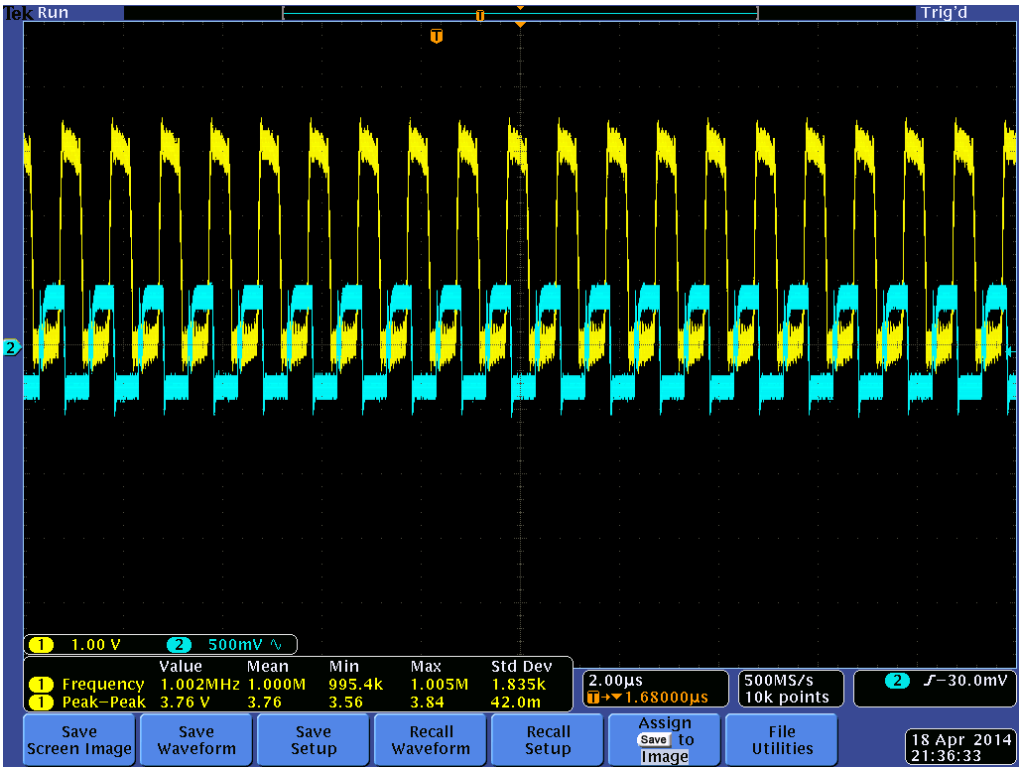

Fig. 5.4.4.2: Note the blue signal is the 0.5V input signal from the signal generator. After amplification and going through the comparator circuit, a 3.3 V signal is produced.

As we decrease the frequency of the signal, the phase delay is decreased as shown in figure 5.4.4.3 below. This also agrees with the simulation . The components in the AD8030 do not have to work as hard at lower frequencies, therefore, the phase delay is reduced.

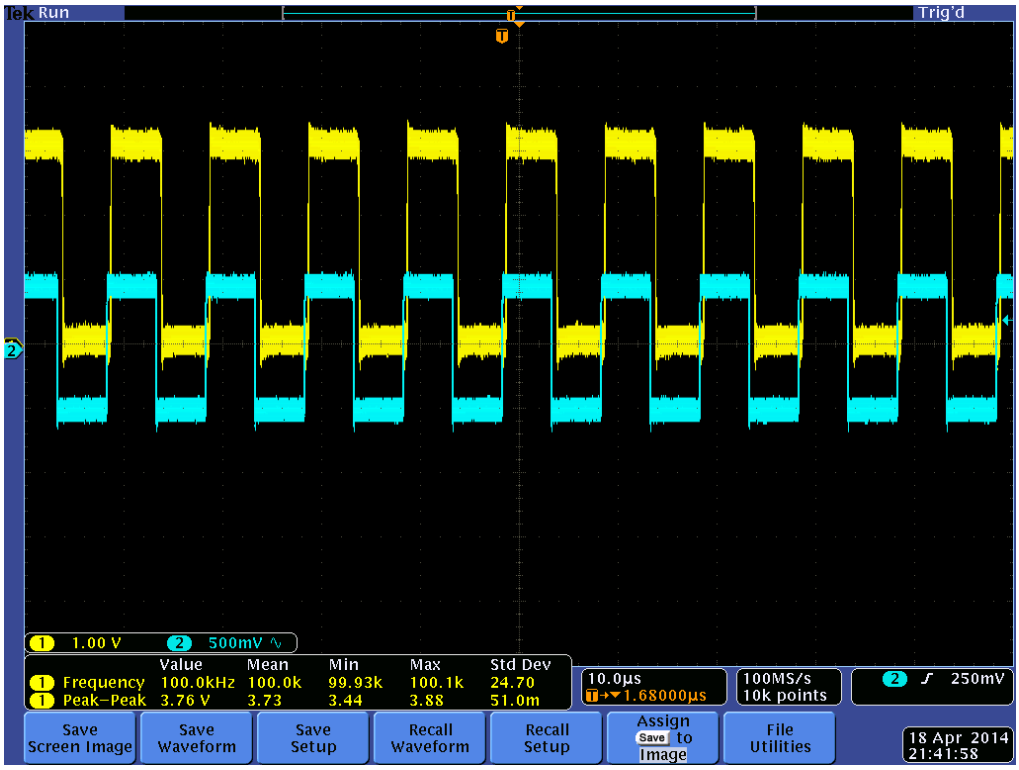

Fig. 5.4.4.3: Phase delay reduced as frequency of the signal decreases. The blue signal is the input signal to the system, and the yellow is the comparator output at 100 kHz.

The final receive response is documented in Fig. 5.4.4.6 to Fig. 5.4.4.10. These images display the received signal that has passed from the signal generator, to the Schmitt Trigger, to the LED Driver Circuit, to the Transimpedance Amplifier, to the noninverting amplifier, and finally to the comparator. These images demonstrate the success of the system.

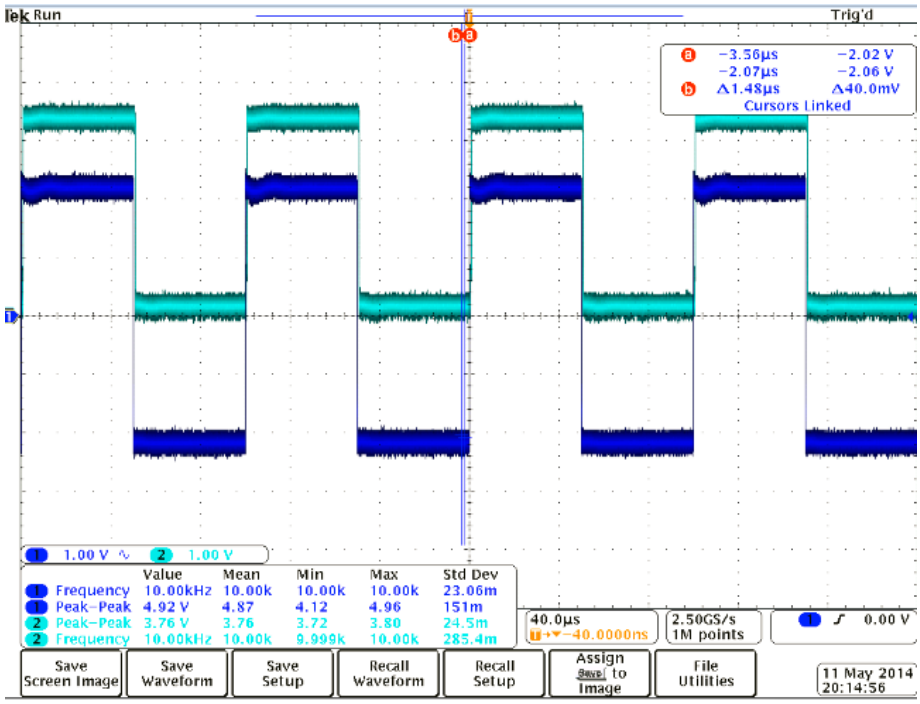

Fig. 5.4.4: System at 10 kHz. The darker blue waveform represents the signal produced by the signal generator to TX system. The Cyan colored waveform represents the output of the RX system.

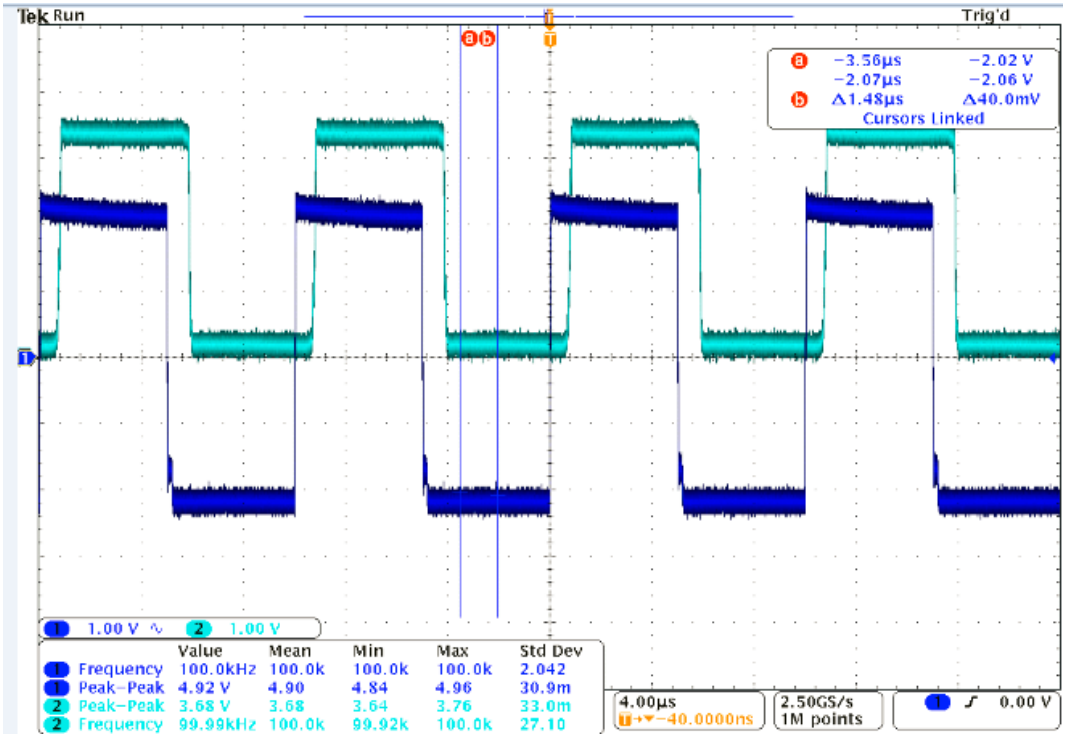

Fig. 5.4.5: System at 100 kHz. The darker blue waveform represents the signal produced by the signal generator to TX system. The Cyan colored waveform represents the output of the RX system.

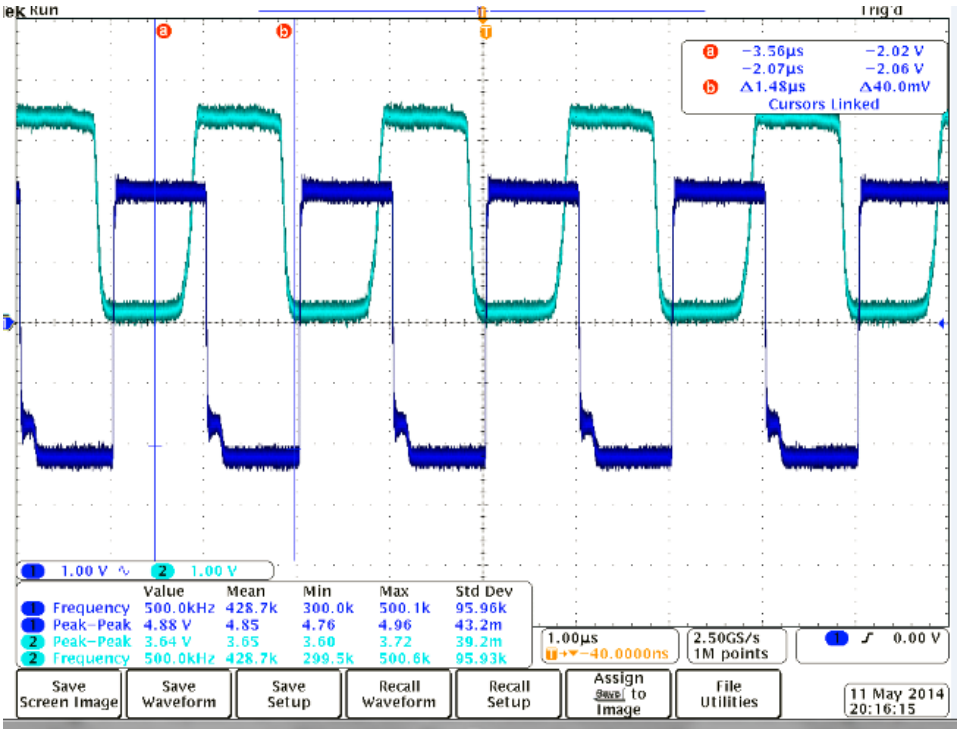

Fig. 5.4.6: System at 500 kHz. The darker blue waveform represents the signal produced by the signal generator to TX system. The Cyan colored waveform represents the output of the RX system.

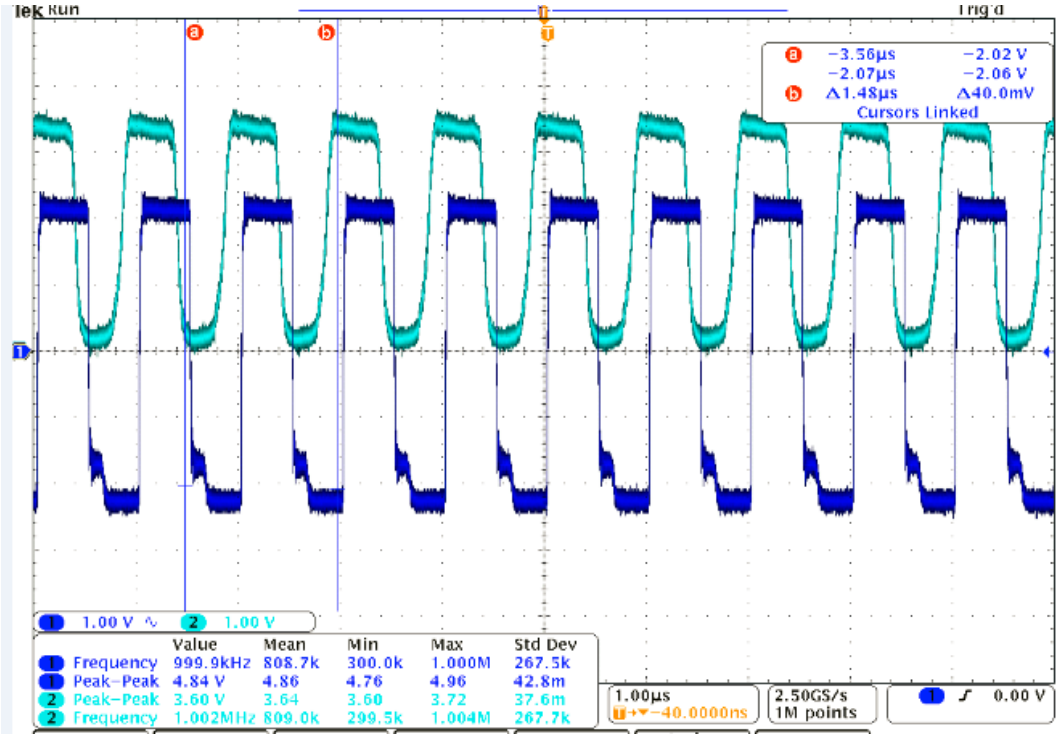

Fig. 5.4.7: System at 1 MHz. The darker blue waveform represents the signal produced by the signal generator to TX system. The Cyan colored waveform represents the output of the RX system.

5.5 Retro Optical Chopper (ROC)

Name of team member who designed this sub-system:

Taichi Hirao, John Giordano (testing and driver), Kyle Cavorley (receiver architecture), Wayne Chang (software)

Name of team member who wrote this subsection:

Taichi Hirao

5.5.1 Theoretical Considerations

The Reflective Optical Chopper works by "chopping" a continuous beam. This chopped signal is a reflected laser and is modulated by on-off keying according to a 3.3V TTL input signal (up to 5V TTL is acceptable). The modulated signal is reflected off of the ROC mirror at the angle of incidence of the continuous laser. This external laser modulator utilizes an electrically controlled reflective diffraction grating to characterize the signal. The reflective diffraction grating is controlled by an electric field that is induced and switched on/off by the precise and sharp cut-off voltage controller, which is supplied by the included driver box. Most likely, some type of liquid crystal technology is utilized, layered and/or oriented in a way that surfaces and aligns in a way for it to function as a diffraction grating when an electric field is applied. Diffraction gratings are optical components with a periodic structure which allows them to split or "diffract" light into several directions. Reflective gratings have a 'zero-order mode' where light is reflected with no dispersed effect and so acts like a regular mirror. The ROC switches between an 'off' state of 'zero-order' mirror mode and an 'on' state where the surface disperses light and inhibits reflection.

External optical modulators, such as this ROC, are used as much as direct optical modulators (i.e. varying current to a laser diode) because both have their pros and cons. People who opt for external optical modulators typically do so to avoid the "chirping" effect of lasers that results from switching them via current. External optical modulators get rid of this problem because the laser merely has to stay on at a continuous signal strength.

One of the results we ended up using an LED was because our driver circuit design was able to get a higher frequency response from it than the laser. It was not until very late into our project that we found out that the main cause of our data rate bottleneck was due to our laser not being able to switch fast enough, or switch effectively. The frequency response of the driver circuit with a substitute load cleared 1MHz, and we assumed the laser would handle the speeds as well However, it seems there is a compatability issue whether that results from the impedance of the laser diode or the natural functional limit of the laser that we acquired. Since, there are no datasheets available in regards to our obtained laser diodes, it is difficult to get to the bottom of our problem.

One hypothesis is that the chirping effect of the laser is affecting the frequency response. Frequency chirping is an effect that occurs when lasers are varied in intensity. When lasers are subjected to drastic changes in output, unnecessary harmonics are introduced by the nature of

laser operation, known as the “chirp” effect. It is thought that this chirp effect inhibited our laser switching speeds to a mere 300 kbps. John’s driver circuit was redesigned to account for a current bias through the laser so that there would be a less dramatic varying of the laser intensity, however, the bias current did not seem to have an effect on the frequency response of the laser. The next step would be to explore more into the physics of laser operation and design a driver circuit that would account for the chirp effect so as to provide a higher frequency response.

Since, the LED performed much better, and it was also easier to handle in establishing a link with the photodiode (due to a greater degree of angular freedom resulting from the dispersed LED light, compared to the pinpoint accuracy of lasers), the LED was opted for in our final design, used with the photodiode receiver amplifier designed by Kyle.

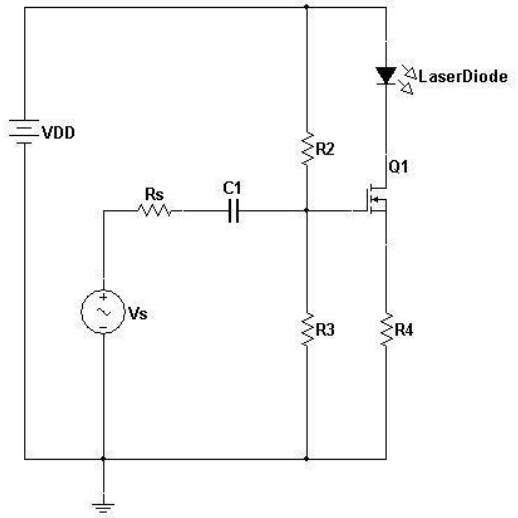

Figure 5.5.1
This simple common source mosfet amplifier is an example of one of the test cases for operating the laser at a current bias to see if the chirp effect could be reduced.

5.5.2 Design Procedure

The main component is the ROC, which was generously supplied by Boston Micromachines Corp. great credits and much appreciation to them, but this sub-system also requires a continuous laser source via the driver (designed by John), the receiver photodiode architecture (designed by Kyle), and the software to process data (designed by Wayne) for the entirety to perform. A wooden platform was put together to serve as a foundation to stabilize the components to maintain steady and accurate line-of-sight links between the laser, ROC modulator component, and the photodiode.

Unfortunately, varying distance measurements between the laser, ROC, and photodiode, could not be tested because our aperture did not have that degree of freedom and one could not be put together in time.

The ROC accepts up to a 5 V TTL signal input via BNC cable to the driver box, which amplifies the signal to the reflective modulator, so data can be channeled directly from a USB port via the Adafruit USB to TTL serial converter. As soon as you send a signal into the driver via TTL signaling, the modulator is already doing its job by switching the reflective mirror on and off regardless of having a laser shined onto it or not.

Here we used the driver circuit version 3, the same one that Johnathan used to directly modulate the laser signal via current, but instead of inputting a modulating signal, we put a DC bias (past the blocking capacitor) to feed the laser with a steady unaltering current so that a continuous beam could be pointed at the ROC.

Once this is set up, the reflected laser off of the ROC mirror is now the modulated signal controlled by the USB input. All that's left is for the photodiode receiver to pick up the signal, the same receiver used the same as described in 5.4.

5.5.3 Simulation Results

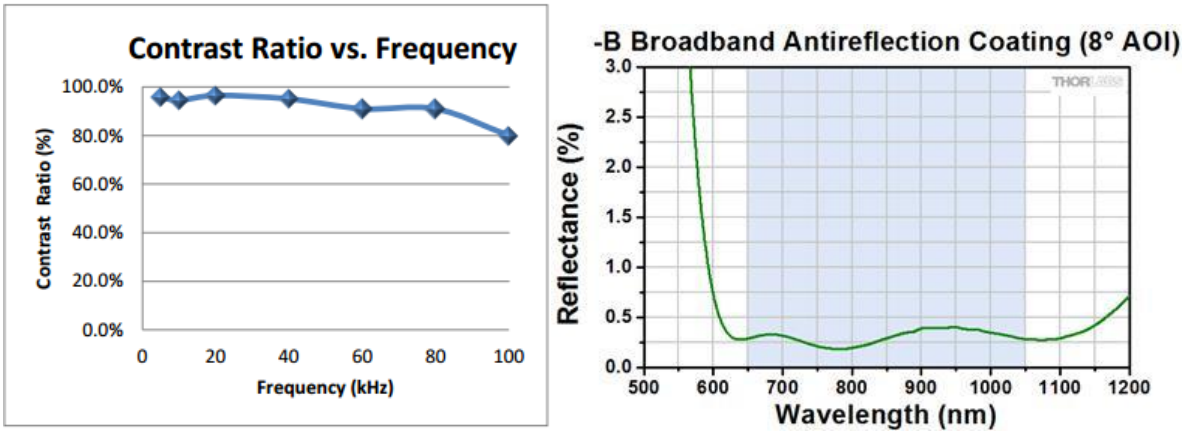

Figure 5.5.2 (a) Contrast Ratio vs Frequency of ROC
(b) Range of permeability for lasers of the AR coasted lens

All ROC simulations were handled by BMC and there is little data available to the public, but the above graph (a) shows the contrast ratio of the ROC across frequencies up to 100 KHz. Of course, we were confident in reaching up to 100 KHz and data transmissions up to 200 KHz, if 2 bits were to be transferred every cycle, but the graph gets cut-off at 100 KHz. We hoped to push the ROC to its limit by increasing the frequency past 100 KHz and battle the declining contrast ratio, which tests our design of the photodiode receiver and software architectures to be able to handle the sensitivity at those response times

Regarding the above graph (b), we were worried that our 650nm laser would not penetrate the AR-coated lens of the ROC, even though it is within the wavelength graph supplied by Thorlabs, because of tolerances existing in the world. However, Thorlabs delivered as specified and the ROC was able to handle our 650nm laser optimally, when compared to our other lasers.

5.5.4 Observed and Measured Results

Test cases

(A)

670 nm 5mW laser

Distance from laser to reflective mirror: 8.75”

(B)

832 nm 5mW laser

Distance from laser to reflective mirror: 8.75”

(C)

650 nm 10mW laser

Distance from laser to reflective mirror: 8.75”

Max data rate observed by oscilloscope:

Test case A: 120 KHz

Test case B: 120 KHz

Test case C: 300 KHz

Max data transmission of audio signal: TBA

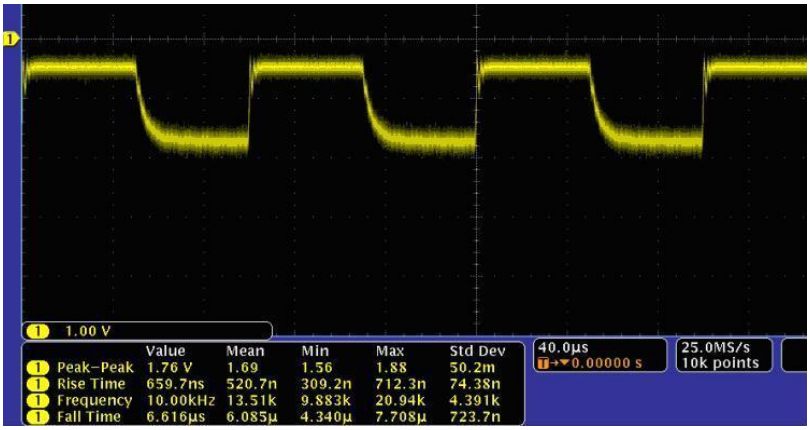

Figure 5.5.3

Test case A at 10 KHz

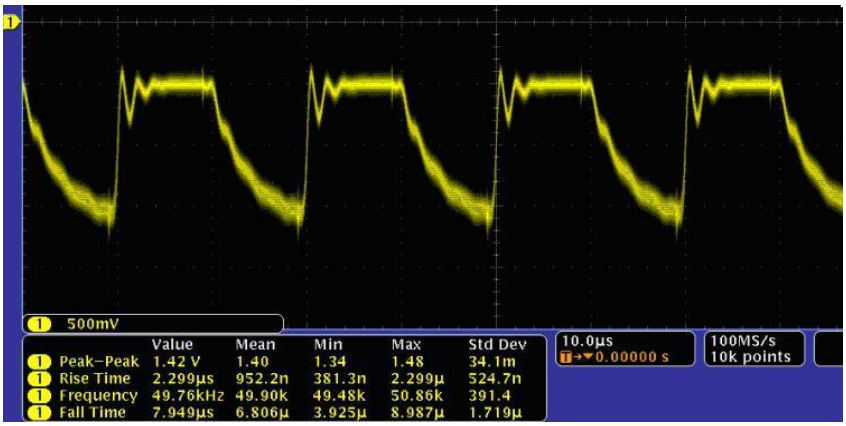

Figure 5.5.4
Test case A at 50 KHz

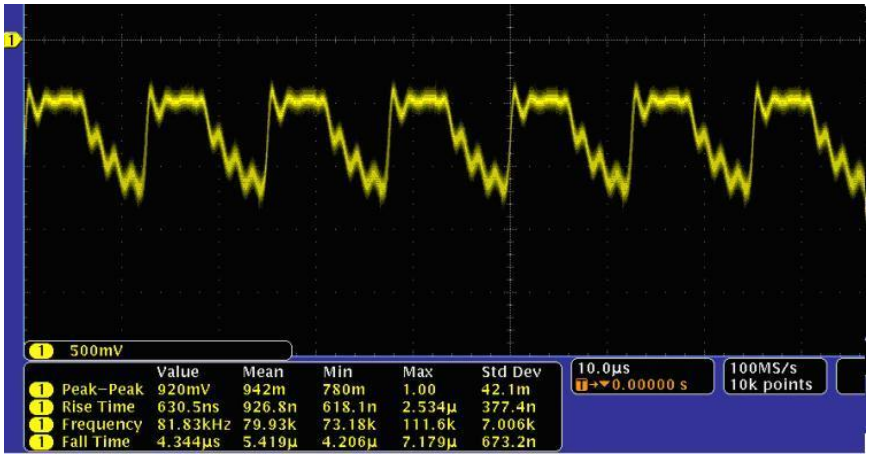

Figure 5.5.5
Test case A at 80 KHz

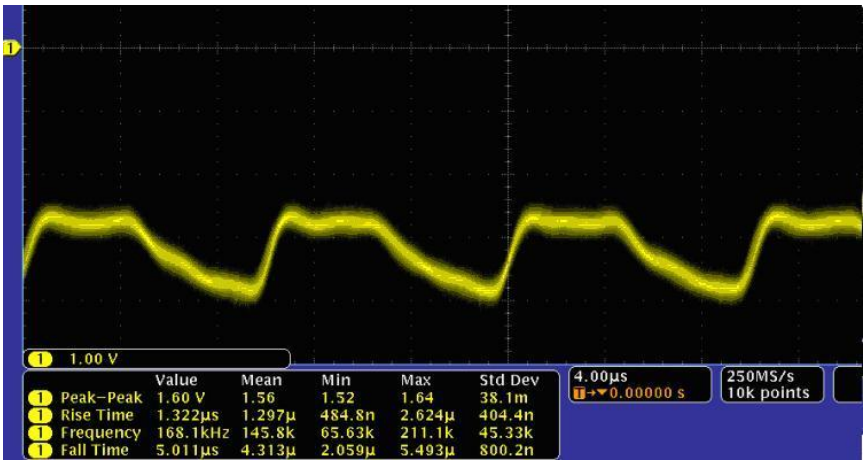

Figure 5.5.6
Test case A at 100 KHz

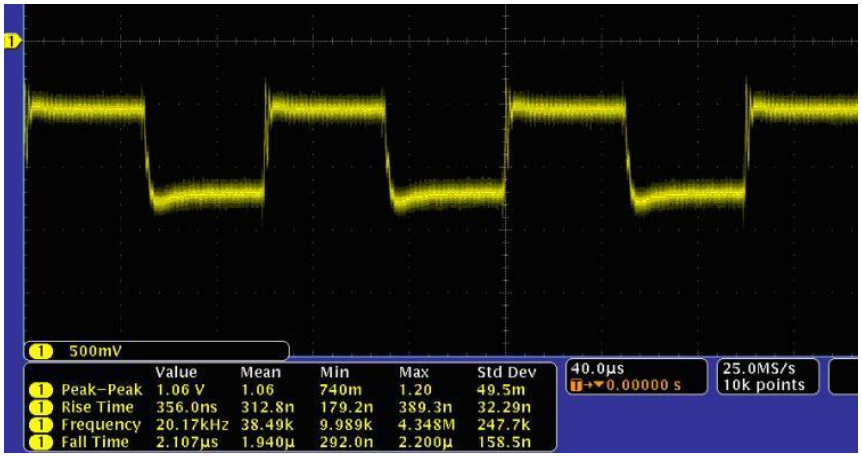

Figure 5.5.7

Test case B at 10 KHz

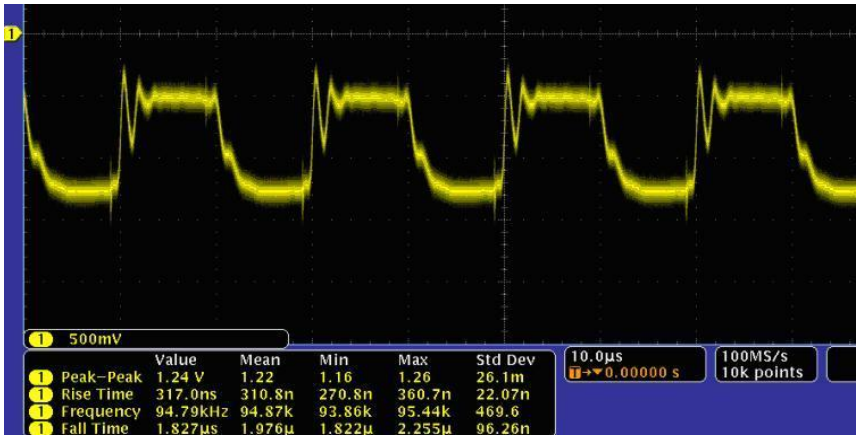

Figure 5.5.8

Test case B at 50 KHz

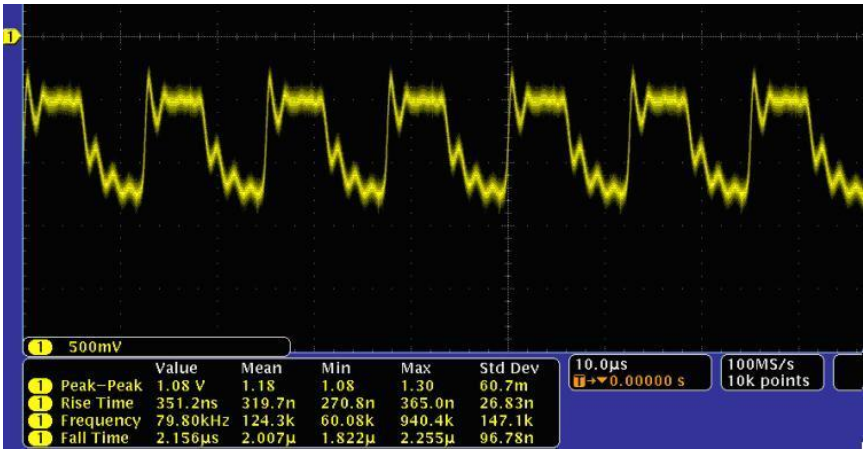

Figure 5.5.9

Test case B at 80 KHz

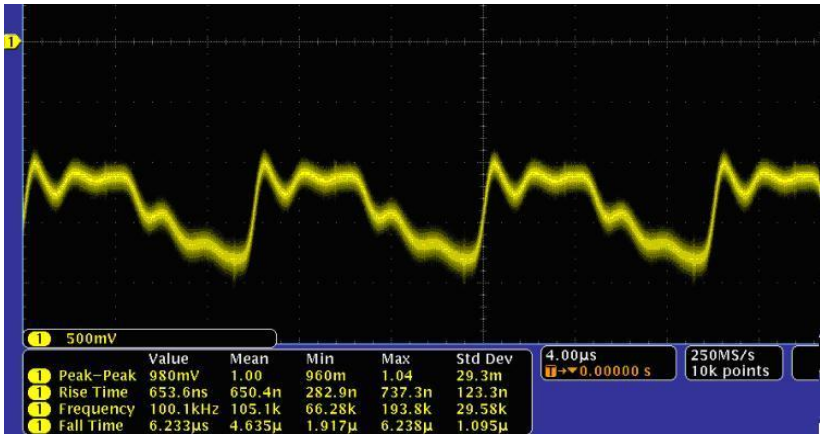

Figure 5.5.10
Test case B at 100 KHz

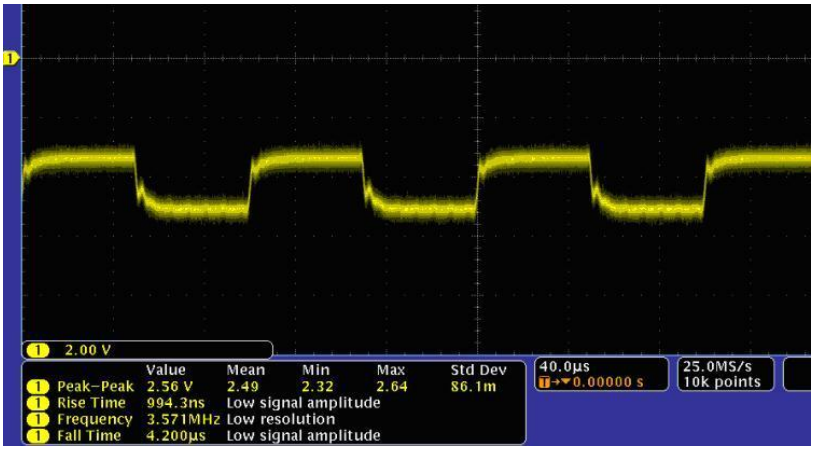

Figure 5.5.11
Test case C at 10 KHz

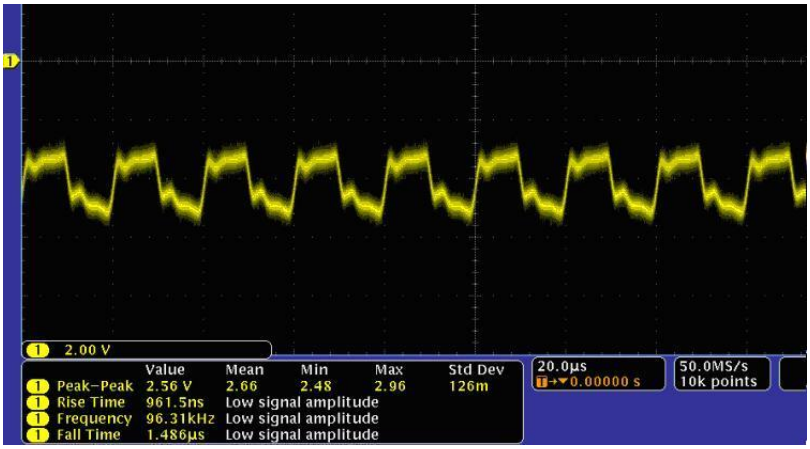

Figure 5.5.12
Test case C at 50 KHz

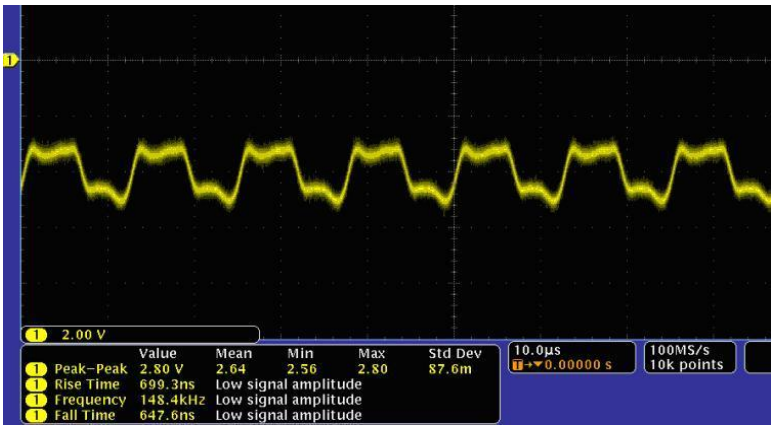

Figure 5.5.13
Test case C at 80 KHz

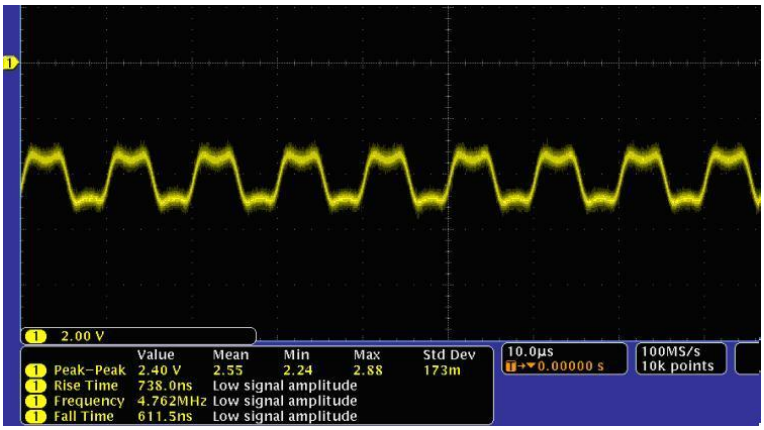

Figure 5.5.14
Test case C at 100 KHz

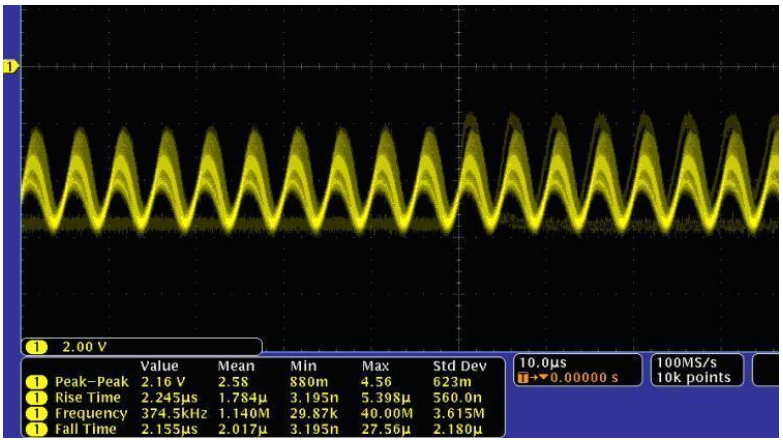

Figure 5.5.15
Test case C at 150 KHz

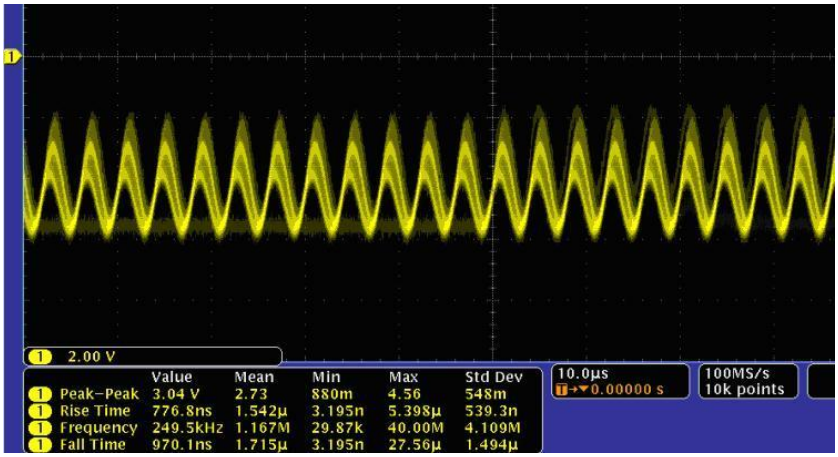

Figure 5.5.16

Test case C at 200 KHz

*Photodiode placement was adjusted so amplitude does not correlate from previous picture.

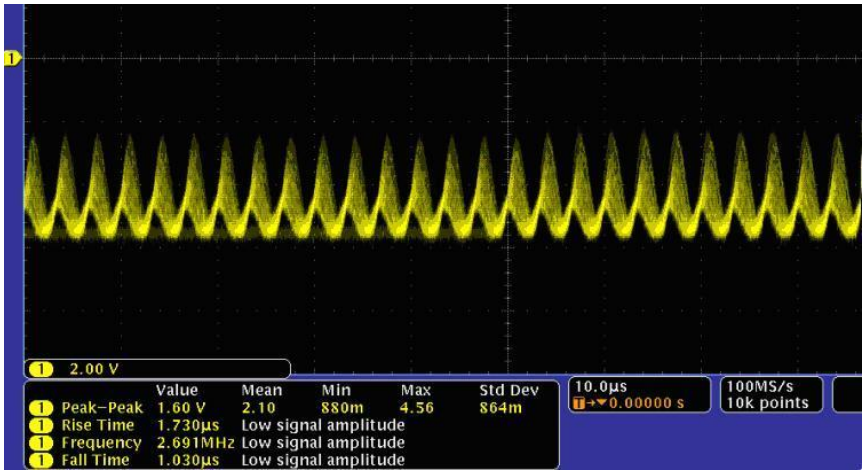

Figure 5.5.17

Test case C at 300 KHz

*Photodiode placement was adjusted so amplitude does not correlate from previous picture.

The frequency readings on the oscilloscopes may not match up with the listed frequencies. This is because the oscilloscope sometimes is not able to properly assess signal shapes that deviate from the ideal sinusoidal shapes.

Voltage readings should also not be counted on to be accurate amplitudes, but the degrading contrast ratio can be reflected upon in these measurement, as well as visualized.

The degrading contrast ratio arises from the gain bandwidth product that results from the frequency response of the ROC component circuitry.

6. Sub-system Integration Considerations

Fortunately, there were not any issues for us when integrating each of the subsystems. The only variable was to carefully match the different voltage levels to maintain compatibility between each stage. However, this was already taken into consideration at the initial design phase.

The maximum and minimum induced current through the photodiode will vary depending on the intensity of the focused light, and the amplifier subsystem has headroom to significantly amplifier those voltage signals, however, the comparator stage is always there to down convert to 3.3V TTL safe voltage signals.

In regards to the ROC, for our intended application, a separate external modulator, the modulating retro-reflector (MRR), would ultimately take place of the ROC because the ROC requires the angle of incidence upon the reflective mirror to be taken into consideration, whereas, the MRR would naturally reflect a modulated signal right back to the origin. Seeing that one of our goals is to embed our system onto mobile UAVs, it would be much more efficient to aim a continuous laser source to a target that will reflect a signal right back to its source without having to calculate the angle of incidence, in relation to distance, as a design variable.

7. Economic Considerations

7.1 Cost Analysis - Prototype

Table 7.1: Project Costs

Item	Quantity	Price ($)	Total ($)
Servos	2	N/A	N/A
Cameras	2	13	26
Platform Materials	N/A	N/A	N/A
38-1030-ND LASER DIODE 850NM 5MW	1	32	32
Reflective Optical Chopper	1	1000-5000	Provided by Boston Micromachines
L21-00R100 High Power LED	3	3.57	10.71
SFH213 Photodiode	50	0.41	20.50
2 GB SD Card Two Pack	1	12.71	12.71
8 GB SD Card Two Pack	1	10.74	10.74
Raspberry Pi Model B	2	35	75
MTD5010W PHOTO DIODE 850NM	2	5.37	10.74
5 mW 670 nm Laser Laser Module	2	6.50	13
L21-00R100 High Power LED	2	5	10
5 mW 832 nm Laser Module	1	16	16

10 mW 650nm Laser Module	1	10	10
Dia: 72 Focal: 118 Lense	2	4.50	9
Dia: 75 Focal: 185 Lense	1	5.35	5.35
AD8030 Op-amp	4	N/A	Provided by Triad RF Systems
Rutgers Lab Materials	N/A	N/A	N/A
Home Depot Supplies	1	48	48

**Taxes and Shipping costs not included

The table above lists all project costs necessary for completing the project. All items purchased were used in experimentation with the system. To prototype the low level communication system, any computer source can be used. Therefore, Raspberry Pi Model B can be excluded from the production cost. Also, the final system implemented uses an LED as shown on our YouTube channel video “Final System”. The different laser modules were purchased for experimentation. Therefore, it is up to the user which device to use, all work well in the system.

Listed below are the laboratory equipment and materials provided by Rutgers University.

TL081 Op-amp, wire, wire cutters, pliers, Tektronix DPO 4082 Oscilloscope and probes,Agilent 34401A Digital Multimeter, Tektronix AFG3021B Function Generator, Lecroy HDO6054 Oscilloscope, BNC cables, BNC connectors, resistors, capacitors, BJTs, MOSFETs, soldering iron, solder

7.2 Cost, Manufacturability and Marketability

While the majority of the parts used in the final prototype are inexpensive it would be ill advised to give theoretical cost estimations based on these values. The current final prototype is still finicky, and does not work near ranges initially sought after it. The highest transmission rate recorded at 700 kbps is at a mere distance of several inches and does not include any connectivity to the computer vision or pan-tilt platform. That sub-system in itself remains unexplored, and additional costs towards the completion of such, including the combination with transmission system are unforeseen. There are further variables which are pertinent, such as the range which the computer vision can theoretically track over which is no more than estimated 25 feet. This in itself makes the tracking program virtually useless in terms of utilization. Other

variables depends upon actions not yet performs, cost-efficiency improvement of using PCB to reduce RF noise, examination of various optical wavelength to determine best signal transfer along with tests for each frequency variation for different atmospheric conditions. Each of these are serious factors which would leave the considered manufacturability and commercialization of the communication system, and without knowing them cost estimation and market feasibility are too unknown to confidently predict.

The marketability for the Vision Based Free Space Optical Communication is extremely limited at this point in time. Current customers of such as system are likely to be either military or space industry. The communication link formed by the system is extremely secure, and would show promise for communication with unmanned military aerial vehicles such as drones. Because of the efficiency of the system compared with RF transmission, this system is ideal for satellites which have limited power supplies. The future may produce a wider market as the explosion of space industry continues along with the corporate and private sector in the development of unmanned aerial craft such as quadcopters. Major companies such as Amazon have indicated interest in the utilization of such mobile craft for the transport of packages.[21] The future may be a place where the skies and lower atmosphere are swarmed with satellites and drones respectively, and with bandwidth already limited, free space optical may be the choice of communication.

8. Individual Discussions of Project

Kyle Cavorley:

The Free Space Optical Communications (FSO) Prototype that we created this semester was a huge success. The system prototype was marketable for utilizing low cost devices to implement a complex communication system of high performance. The value in FSO communications is that it is unlicensed and does not have to meet a particular bandwidth requirement by the FCC. With no environmental obstructions, the FSO can transmit at further distances than RF at an unlimited bandwidth. This optical link is more than capable of reaching fiber like data rates. Although this prototype is limited in frequency, it can still transmit high data rates with a system cost no greater than 30 dollars. Note this cost excludes the embedded system and quality of the cameras for computer vision.

The prototype requires an embedded system to transmit data. The embedded system integrated will inquire the bulk of the cost. A recommended embedded system such as the Raspberry Pi Model B costs $35, and runs on a Linux platform. A more expensive embedded system may be required if the consumer requires memory greater than 16 GB. Increased costs are also placed on the resolution of the cameras involved in the computer vision component. Over extended distances, greater resolution than the $13 Sony Playstation Cameras would be required.

Overall the system provides for an effective and efficient communication system. The reason for choosing to build a low cost FSO system is for its use in the defense industry. The system can be used to communicate with unmanned vehicles. For instance, a base station can transmit instructions to a drone flying overhead to conduct aerial mapping. The transmission rate of the instruction fired from the laser to the drone would be hard for enemies to track location. Using RF would radiate too much power that can be detected. Not only can FSO transmit at rapid rates, the system has unlimited bandwidth because it is unregulated by the FCC. Therefore, a base station can fire gigabytes of data instructions to the drone at fast rates. That is if the hardware for the transmitter and receiver are optimized for higher speeds. At 700 kbps, the enemy will track down the drone overhead when transmitting gigabytes of data.

The Free Space Optical Communication system requires an optical link for data transmission. The transmitter in our prototype is compatible with an LED and laser module. The receiver uses a photodiode to convert a light signal into an electrical signal, which is sent to the receiver circuitry to recover the transmitted signal. To enhance the system, the prototype integrates a computer vision tracking system. Therefore, the FSO transmitter can align itself with a mobile receiver that emits the LED recognition pattern that it recognizes. To design an intricate system, the system must be broken up into multiple sub systems.

The prototype is designed around the embedded system. The first embedded system considered for the FSO system was Altera's DE2-115 FPGA board. The FPGA system can communicate through Ethernet at Triple Speed Ethernet speeds such as 10/100/1000 Gbit/sec. The other viable option for transmission is the USB 2.0 port which is bottlenecked at 12 Mbps.

The integration of data storage, data transmission, and data reception with the FPGA add to the complexity of the project. Integrating an FPGA requires a whole other project in itself that cannot be finished in one semester. A NIOS II Processor is needed to connect the IPs of the components on the board. These components include SDRAM for data buffering, SD card for data storage, USB, and Ethernet. If the system is connected properly with the processor, C code can be drafted to build and integrate the system. However, the stress of this project is based on proof of concept for FSO Communication Systems, therefore the group decided to switch from using the FPGA to the Raspberry Pi Model B.

The Raspberry Pi Model B has a 700 MHz clock, therefore the fastest rate at which it can transmit data is 700 MBaud. The python package pyserial provides for an easy way to transmit and receive data. This data is sent from a USB port and converted to serial data with Ardafruit's USB-Serial converter chip. The code is written so that a preamble is sent from the transmitter to the receiver for recognition. Once the receiver recognizes the preamble, it begins to receive data until the file is fully transmitted. This process is defined for system organization.

The front end Schmitt Trigger receives the 0 to 3.3V data stream and upconverts it to a 0 to 5V signal to properly power the laser driver circuit for transmission. This provides enough power to the LED/laser to transmit over a range of 14 feet. Ultimately, the goal of the project is to achieve maximum distance at high data rates.

On the receive end, a reverse biased photodiode is used to detect the light signal and convert it to an electrical signal. The reason for reverse biasing the photodiode is to reduce the junction capacitance, and push the device to higher frequencies. The electrical signal from the photodiode is converted to a voltage from a transimpedance amplifier. The operating frequency of the transimpedance amplifier is limited to 1.3 MHz because the GBP of the TL081 op-amp is limited to 3 MHz. A non-inverting amplifier is used to amplify the signal before it is sent to a comparator, that sets any bits above the reference voltage of 2.5 V to 3.3V and any bits below to 0V. The comparator is designed with a positive feedback to introduce hysteresis into the system. Hysteresis reduces the noise of the system by stabilizing the comparator to the intended frequency rate. These data bits are then sent to the computer on the receive end.

After a semester that required a lot of effort and work put into the system, it was completed. Due to time limitations we not able to achieve our initial intended goal of HD video streaming. However, we can successfully stream audio at a rate of 700 kbps. The system can also transmit a 4.5 MB song to the receiver of great quality. I am very proud of how the system came together in the end.

For future work, the Schmitt Trigger would require tweaking so that it can operate at frequencies greater than 500 kHz. Integrating the system on a PCB to will eliminate stray capacitance and external RF. Better parts can also be purchased to find ways to demonstrate a low level FSO communications system operating at higher frequencies. In the end, I am satisfied with my progress and seeing the system come together.

Jonathan Giordano:

The Vision Based Free Space Optical Communication was the solution to modern concerns of security and bandwidth utilization, with two unique offsets from the typical optical communication systems. Optical communication systems utilizing lasers and more recently, fast switching LED's have the benefit over RF communication systems by being far more energy efficient and capable of high throughput without sacrifices large bandwidth. Major challenges encountered in this optical communication link are that both transmitter and receiver must be spatially aligned in order for the signal to be transferred. Because of this alignment, communication is typically one way as tracking systems would otherwise be incorporated on both ends of the communication link doubling the complexity of the system.

The initial goal for this communication system was a distance of at least 20 feet, with throughput at 50 MHz. This transmission frequency would allow for 50 Mbps transfer rates using On-Off keying for modulation. As virtually all circuits were constructed from Op-Amps and transistors the designs were limited to far less transfer rates. Because of by hand construction other issues including bleeding RF and parasitic capacitances plagued development. Goal transfer rates were lowered during the projects lifetime, and a measured transfer rate of 700 kbps was observed. With further minor correction, 1 Mbps appears at the end of the projects life as near reachable goal.

In order to combat the two major downfalls of optical communication systems the two unique offsets hinted above, automated computer based tracking and a Reflective Optical Chopper (ROC) were incorporated into the system. The computer based tracking depended upon two digital cameras which would find and follow the receiver. This eliminated time consuming, and human error in establishing an optical link. The cameras would detect pockets of bright light in their vision and mark them. These lights would be attached to the receiver, and an initial design idea included blinking of these receiver lights at different rates to transmit the receiver identification. The physical system utilized two Sony PlayStation Eye Cameras. The vision feed would be processed by code running on an accompanying PC. The ROC was a way for the receiver to send data back to the transmission end without requiring a tracking system. This would require the transmission side to have two optical links, one modulated and one unmodulated. The ROC would "chop" the unmodulated signal and reflect it back to the transmitter. The "chopping" would modulate the reflection with encoded data in the same modulation manner as on-off keying. The ROC utilized for this project was loaned by Boston Micromachines with a started modulation rate of 100 kHz. Testing confirmed this number with high intensity laser at 650 nm, 670 nm, and 830 nm.

With these benefits to our system, the Vision Based Free Space Optical Communication was still limited to line of sight communication, and only as good as its optical transmission and reception. The ideal model required two Raspberry Pi's to run code which would transmit and receive the final data and make it usable to the user. On the transmission end, data would leave the USB port of the Raspberry Pi, enter a Schmitt Trigger where TTL voltage levels would be amplified, and this signal led to a driver circuit which would maintain safe current on the LED or laser it was driving. Testing showed that the Schmitt Trigger turned to be a bottleneck in the system and future plans would have this design replaced by a faster amplifier portion. There were many driver circuit drafts but the latter version proved to be capable of transmission up to 1 MHz.

The receiving end began with a photodiode, the SFH213 proving due be not only the

cheapest photodiode, but the most responsive compared to more expensive, "higher-end" models purchased. The photodiode was back biased, and the output led to a transimpedance amplifier, then to a non-inverting amplifier, a comparator circuit to bring the voltage to TTL acceptable levels, and final to the USB port of the receiving end Raspberry Pi. In practice, the Raspberry Pi was never used, but PC's with a Python interface were. The reason for this was ease of use, but if time allowed this small computer would be incorporated into practice. The receiver end proved to be the most difficult set-up for the entire project due to lack of knowledge in photo-electronics, and the too well known difficulty of working with Op-Amps.

Because of time limitation a complete connection of all parts of the Vision Based Free Space Optical Communication was unfeasible. The computer based tracking was never tested, was any physical mounting for the platform built for the receiver or transmitter. There are many difficulties to consider for the incorporation of the ROC into the system, namely its delicate nature, its small aperture size which requires a finely focus adjust laser which in turn demands a finely tuned computer vision tracking accuracy, and the ability to have the reflection sent back to the transmitter and not an offset angle. Data transmission was tested, and achieved a data rate of 700 kbps, but only at a distance of several inches, and even at that distance transmission was likely to develop data errors.

The commercial usage for such application would be either military or in space industry. The Vision Based Free Space Optical Communication project would in no means in its current prototype state be ready for any practical ventures, but the ideas and proof of concepts developed over the past months show promise in having real-world value. With the use of both higher budget, and IC's developed specifically to replace breadboard circuits, higher data rates with lower error could be achieved.

Wayne Chang:

- transmission-end challenges
    - high frequency + high power for the LED
        - we wanted ~2 A of power at MHz frequencies
        - transistors in parallel for more current
        - investigating existing drivers but they only go up to ~150 mA
- receive-end challenges
    - photodiode capacitance
        - resistor value toggling
        - reverse biasing to reduce junction capacitance
    - clean comparator for TTL input at MHz
- microcontrollers
    - FPGA speeds
    - power draw
    - interfaces (settled on USB)
- platform
    - targeting precision must be offset by conical wave diffraction
    - accuracy of servos or use of stepper motors
    - vision code to track multiple targets
- message structure

- preamble (codeword)
- postamble (codeword)
- error correcting codes

Taichi Hirao:

While still in the phase of trying to improve the speed of our system, our team was stuck on the idea that the receiver amplifier was the bottleneck. Below is an exploratory design that was simulated while Kyle was testing his AD8030 op-amp amplifiers. It was never put together, because the AD8030's sufficed. However, as this project continues outside of Rutgers, expanding on this circuit may be a viable option as the next step because the frequency response has enough headroom for promising results (depending on the quality of the actual mosfets).

The transistors are dc biased at Vds >= Vgs - Vt (parameters are dependent of specific transistors models). Vds is increased as much as possible to widen the depletion region and allow greater gain to generate through the cascaded transistors. The increased Vgs calls for a greater Vds. The 20V VDD is used to cope with this headroom. The combination of the greater gain and increased headroom allow the cascade to operate without distorting while meeting our needs.

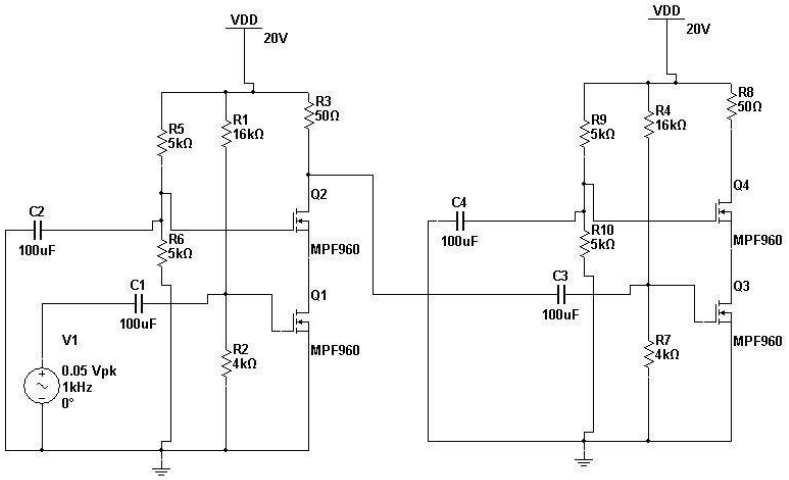

Figure 8.1 (a)
Cascaded Cascode Mosfet amplifiers
Individual gain: 10; Total gain: 100

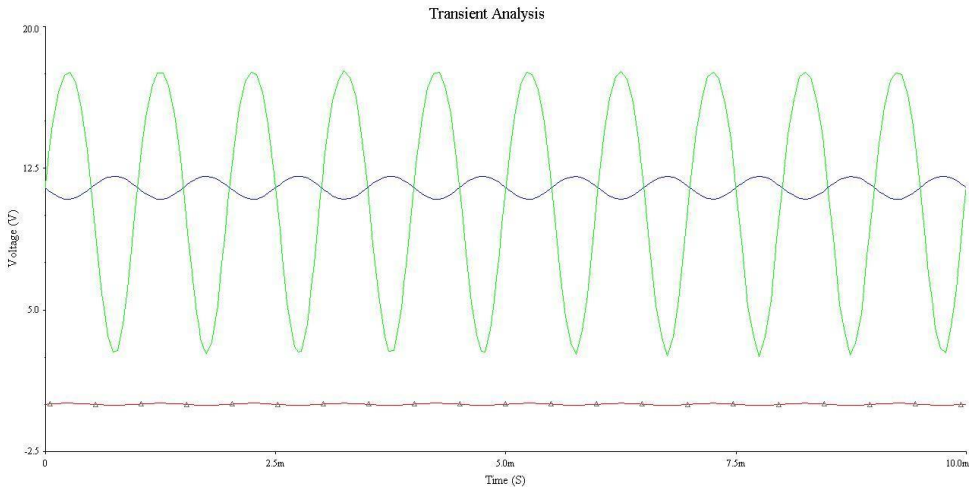

Figure 8.1 (b)
Transient Response
Input signal (red): Vpp 50 mV
First stage output (blue): Vpp 500 mV
Second stage output (green): Vpp 5V

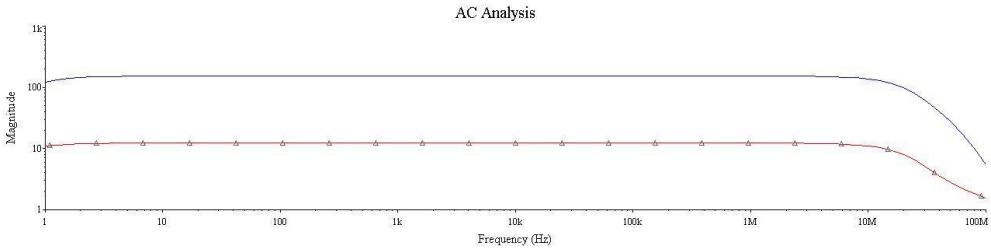

Figure 8.1 (c)
Frequency Response
First stage output (red)
Second stage output (blue)

Below is a variant of the Schmitt Trigger. While Jonathan's Schmitt Trigger utilized BJTs, this design was the result of trying to increase response time of the system by using mosfets. We'll never know the true performance unless it is actually tested, but it may be a worthwhile endeavor if the mosfets can operate at a faster frequency than the BJTs. There is capacitive noise in the output as shown in the Transient response of Figure 8.2 (b), so this area will have to be explored for the advent of out putting clean 3.3 V TTL signals to go into the Adafruit TTL-to-USB converter adapters.

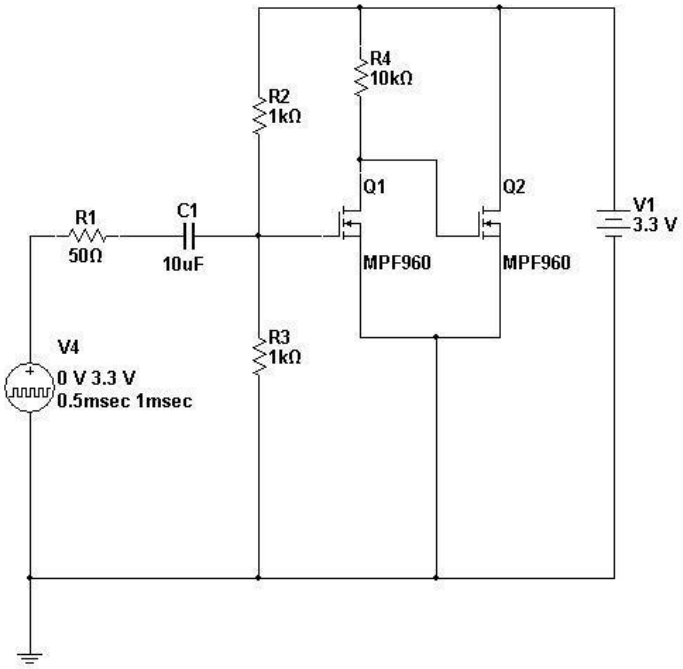

Figure 8.2 (a)
Mosfet based Schmitt Trigger
Gate DC Biased at cutoff voltage of nmos, for it function as a switch : 1.65 V

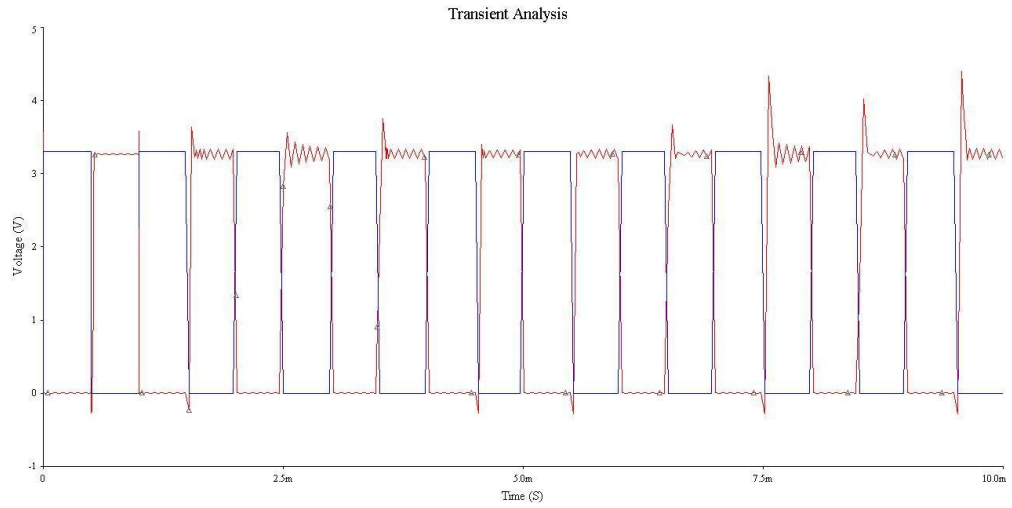

Figure 8.2 (b)
Transient Response
Input (blue): Vpp 3.3V, offset 1.65 V, square wave
Inverted output (red): Vpp 3.3V, offset 1.65 V, square wave

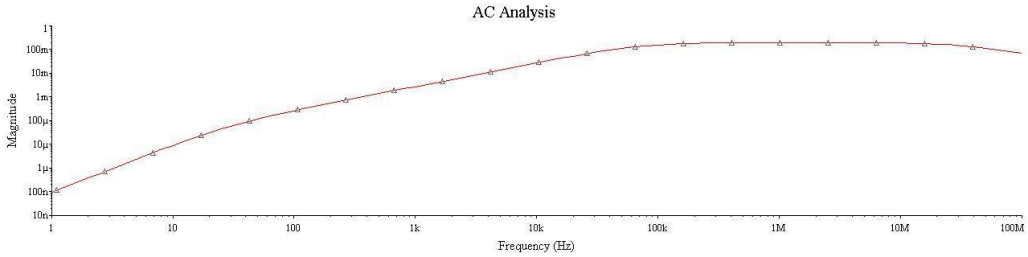

Figure 8.2 (c)
Frequency Response

As this project continues, there are areas for improvement in every aspect of this system design (as with all things). The interface has to be streamlined and simplified to be user friendly, so all people with basic computer knowledge can operate the system.

After optimal frequency response is reached, the next step would be to increase data rates by working on the software architecture to simultaneously transmit multiple data bits. Such as by utilizing different signal strengths of lasers, or using multiple lasers to channel more bits as a time, i.e. the current technology of 1Gbps ethernet protocol.

The visual tracking and targeting software has to increase in artificial intelligence and precision of aiming. The software must be able to distinguish its target from everything else and the motors have to be refined to a greater resolution.

The biggest area of improvement is to research how to operate lasers to optimize their performance parameters, such as frequency response. My interest is in to designing a driver circuit that will compensate the chirp effect by identifying the ideal degree of intensity shift.

The following is the Preliminary Laser Communication Protocol simply to go over the encountered design iterations and reflect on the team's initial goals.

Once tracking is to be successfully defined and demonstrated, on-off keying through laser

communication is one of the methods that is to be explored in wireless transmission. At the early stages of development, the ALTERA DE2-115 FPGA board was investigated to see if it should handle the on-off keying that will control the system. The FPGA was thought to perform all the data processing for transmission and reception and error-correcting codes. However, further investigation resulted in many obstacles, which ultimately led to finding another means: the Raspberry Pi Model-B.

Our initial research was targeted at designing the following Transmit and Receive topologies:

TX

- Data is stored on a SD Card and accessed by the FPGA board.
- Then the data gets buffered onto the SDRAM.
- The Ethernet port will transmit the information from the SDRAM buffer.
- The Tx output from the Ethernet port goes to a differential-input Multi-level decoder
- Output from the decoder goes to an amplifier circuit.
- The amplifier signal will drive the laser diode.

Rx

- Free-space optical stream is captured by an array of photodiodes.
- A comparator is utilized to capture a single stream of data.
- The weak signal goes through an amplifier circuit.
- The on-off keyed data is then put through a multiplexer to be able to communicate with either the multi-level-transmit-three(100BASE) or PAM-5(1000BASE) Ethernet protocol.
- Data is received by the Ethernet port of the FPGA board.
- Buffered into the SDRAM
- Then stored again on an SD Card.

The following are design obstacles, dilemmas and areas for growth that should be explored and utilized for expanding our current final prototype. It is an analysis of the ethernet protocol with the advent of streamlining and synchronizing with FSO technology.

Using a single pair of the 4 pairs of lines in an Ethernet port allows for a mere 25 Mbps data rate on the Altera DE2-115 board using 100BASE and 125 Mbps on 1000BASE. While 100BASE is still faster than using the Fast Speed USB 2.0 port on the same FPGA board (which is capped at 12 Mbps), 25 Mbps is not attractive in today's high-speed world. The reason for wanting to use the 100BASE instead of the 1000BASE is because the 100BASE uses multi-level-transmit 3 whereas 1000BASE uses the 5 level PAM-5 protocol. This will alter the design of our decoder and multiplexer circuits. Decoding a PAM-5 signal will require a decoder twice the speed of the 125 MHz line (250 MHz) to be able to process the two-bit signal and output two separate on-off keyed signals at a time to the laser driver. Using the 100BASE will keep the decoder speed the same 25MHz because it does not output 2 bit signals at a time like the 1000BASE.

It would be interesting to utilize four-lasers, one for each pair of lines of the Ethernet port, to be able to transceiver four bits at a time, essentially 4 x 25 MHz = 100 MHz transmission. Even 4 GHz transmission would be possible with four lasers, if we were able to overcome the design obstacles for 1000BASE.

9. Future Work

- Construction of a new frontend amplifier to replace the Schmitt trigger. This change would remove the transmitter's current bottleneck.
- Completion of the pan-tilt platform in conjunction with the computer vision tracking.
- Construction of a receiving structure with ROC. This would consist of a house which would protect the delicate components, as well as mange the reflect light so that it is directed back towards the receiver. This case would also contain the receiver's front end, and a bright light source for the computer vision tracking to lock on to.
- Further testing of the ROC with varying light frequencies and intensity. This would also incorporate the testing of data transmission using the ROC.
- Fabrication of PCB for Transmission and Receiving circuits to reduce RF noise and parasitic capacitances.

References

[1]: "Pointing, Acquisition, and Tracking Systems for Free-Space Optical Communication Links:" http://drum.lib.umd.edu/bitstream/1903/6734/1/umi-umd-4210.pdf
[2]: "Mobile Free Space Optical Communication System"
http://digitalcommons.calpoly.edu/cgi/viewcontent.cgi?article=1100&context=eeng_fac
[3]: "Development and Implementation of a Pointing, Acquisition and Tracking System for Optical Free-Space Communication Systems on High Altitude Platforms"
http://www.en.pms.ifi.lmu.de/publications/diplomarbeiten/Bernhard.Epple/DA_Bernhard.Epple.pdf
[4]: "An FPGA-based Optical Transmitter Using Real-Time DSP for Implementation of Advanced Signal Formats and Signal Predisortion"
http://citeseerx.ist.psu.edu/viewdoc/download?doi=10.1.1.123.4224&rep=rep1&type=pdf
[5]: "A Real Time Embedded FPGA Interface for An Ethernet Based Line Laser"
http://dspace.uta.edu/bitstream/handle/10106/11545/Ramaswamy_uta_2502M_11904.pdf?sequence=1
[6] Antenna Theory: Analysis and Design - Constantine A. Balanis

[7] http://www.analog.com/static/imported-files/data_sheets/AD8029_8030_8040.pdf

[8] http://ecee.colorado.edu/~ecen4827/hw/hw1/PhotodiodeAmplifers.pdf

[9] "Circuits for using High Power LEDs" http://www.instructables.com/id/Circuits-for-using-High-Power-LED-s/

[10] http://www.analog.com/library/analogdialogue/archives/34-07/comparators/

[11] YouTube. (2014, May) Vision Based Free Space Optical [Video file]. Retrieved from https://www.youtube.com/channel/UCLcOockgnsydlnRXT7J9wwg .
[12]Sedra Microelectronic Circuits 6th Edition
[13]Modern Semiconductor Devices for Integrated Circuits, Chenming Calvin HU, 2010 chapter 4
[14] SFH213 data sheet http://www.osram-os.com/Graphics/XPic5/00101689_0.pdf/SFH%20213%20FA,%20Lead%20(Pb)%20Free%20Product%20-%20RoHS%20Compliant.pdf
[15] mtd5010w data sheet
http://www.marktechopto.com/pdf/products/datasheet/MTD5010W_2011_07_20.pdf
[16] http://en.wikipedia.org/wiki/Transimpedance_amplifier
[17] Direct and External optical modulator & chirping effect
http://web-files.ait.dtu.dk/cpeu/download/34129_E2009_CPEU_DML_EML.pdf
[18] ROC datsheet
http://www.bostonmicromachines.com/pdf/ROC.pdf
[19]Case Study: Photoelectric Effect. http://chemwiki.ucdavis.edu/Physical_Chemistry/Quantum_Mechanics/Case_Studies/Case_Study%3A_Photoelectric_Effect
[20] http://www.adafruit.com/datasheets/PL2303HX.pdf

[21] “Amazon unveils 30-minute Prime Air quadcopter delivery service, but it’s completely impractical”. http://www.extremetech.com/extreme/171879-amazon-unveils-30-minute-prime-air-quadcopter-delivery-service-but-its-completely-impractical

[22] “Diffraction grating with electrically controlled periodicity” US6188462 B1 Feb 13, 2001 Oleg D. Lavrentovich, Darius Subacius <https://www.google.com/patents/US6188462>

[23] “Direct & External Modulation of Light” Technical U. of Denmark Christopher Peucheret http://web-files.ait.dtu.dk/cpeu/download/34129_E2009_CPEU_DML_EML.pdf

Appendix 1: List of Equipment

Lab Equipment:

Agilent 34401A Digital Multimeter
Tektronix DPO 4082 Oscilloscope
Tektronix AFG3021B Function Generator
Lecroy HDO6054 Oscilloscope
Power Supply
BNC cables
BNC connector clip leads
oscilloscope probes
soldering iron/solder
wire
enamel wire
wire cutters
alligator clips
banana plug wire connectors

Resistors: Digikey
3
22
1 K
1.5 K
3.3 K
10 K

Capacitors: Digikey
0.1 uF
8.3 pF

IC:
LM317
TL081 :Transimpedance Amplifier. Manufacturer: STMICROELECTRONICS
AD8030 : Non inverting amplifier and comparator circuit. Manufacturer: Analog Devices

LED:
LED Engin 897-LZ100R100 5W LED

Laser:

Unnamed 1mW 650 nm Laser
Unnamed 5mW 670 nm Laser
Unnamed 5mW 830 nm Laser
Unnamed 10mW 650 nm Laser
38-1030-ND LASER DIODE 850NM 5MW: Manufacturer: US Lasers

Photodiode:
SFH213 : Transimpedance Amplifier. Manufacturer: OSRAM OPTO SEMICONDUCTORS
MTD5010W : Manufacturer: Marktech Optoelectronics

Transistors:
2N2222
2N7000

MISC:
Lenses: Receiver
PBC: Receiver
USB-Serial Cable: Responsible for transmission and reception to embedded system.
Manufacturer: Ardafruit
Raspberry Pi Model B: Manufacturer: Raspberry Pi
Altera DE2-115 FPGA: Manufactuer: Altera
Reflective Optical Chopper
Manufacturer: Boston Micromachines
Comes with:
Driver:
Optical Modulator
BNC cable
Power cord
Electrostatic wrist bands
Platform for supporting ROC Modulator, laser diode and photo diode

Appendix 2: Simulations and Program Code

audiostream.py

```
#!/usr/bin/python

import os
import time
from sys import argv
from pydub import AudioSegment

sound = AudioSegment.from_mp3(argv[1])
step = 5000
for i in range(0, int(len(sound) / step)):
    segment = sound[i*step:(i+1)*step]
    d = os.path.dirname(os.path.realpath(argv[1]))
    f = "audio%05d.mp3" % (i)
    path = "%s/%s" % (d, f)
    segment.export(path, format="mp3")
    print("writing to %s" % (path))
    os.system("./pysend.py %s" % (path))
    os.remove(path)
    time.sleep(0.3)
```

pyrecv.py

```
#!/usr/bin/python

from sys import argv

def waitPreamble(ser):
    i = 0
    while True:
        b = ord(ser.read(1))
        if b == 0x55:
            i = i + 1
        elif b == 0x0 and i > 100:
            print("Preamble Received and Verified")
            return True
        else:
            print("Bad Data: 0x%x" % ord(ser.read(1)))

def isPostamble(postfix):
    if len(postfix) < 101:
        return False
    i = 0
    for b in postfix:
        if b == 0x55:
            if i == 100:
                print("Postamble Received and Verified")
                return True
            elif i > 0:
                i = i + 1
        elif b == 0x0:
            if i == 0:
                i = i + 1
            else:
                return False
        else:
            return False

def updatePostfix(postfix, ba):
    wr = []
    extra = (len(postfix) + len(ba)) - 101
    if extra > 0:
```

```
        for i in range(0, extra):
            wr.append(postfix.pop(0))
    postfix.extend(ba)
    return wr

import serial

ser = serial.Serial('/dev/ttyUSB0', baudrate=500000)
print(ser.name, ": RX")

waitPreamble(ser)

outpath = argv[1]

f = open(outpath, "w")
postfix = []
print("Receiving File")
while True:
    ca = ser.read(1)
    ba = ca
    wr = updatePostfix(postfix, ba)
    if isPostamble(postfix):
        break
    wr = ''.join(list(map(chr, wr)))
    f.write(wr)
```

pysend.py

```
#!/usr/bin/python
```

```
from sys import argv

def sendPreamble(ser):
    for i in range(0, 2000):
        ser.write([0x55])
    ser.write([0x0])
    print("Preamble Transmitted")

def sendPostamble(ser):
    ser.write([0x0])
    for i in range(0, 2000):
        ser.write([0x55])
    print("Postamble Transmitted")

def sendFile(ser, path):
    f = open(path, "r")
    while True:
        c = f.read(2048)
        if len(c) > 0:
            ser.write(c.encode("utf-8"))
        else:
            break
    print("File Transmitted")

import serial

ser = serial.Serial('/dev/ttyUSB0', baudrate=1000000)  # open first serial port
print(ser.name, ": TX")

path = argv[1]
sendPreamble(ser)
sendFile(ser, path)
sendPostamble(ser)
```

Appendix 3: Datasheets

Datasheets for the following components are included:

LZ1-00R100
LZ1-MCPCB
2N2222
SFH213
AD8029/AD8030/AD8040
BMC Reflective Optical Chopper